Spectrum-efficient cognitive MIMO relaying : a practical design perspective

Zakaria El Moutaouakkil

UNIVERSITE BRETAGNE LOIRE / MATHSTIC

IMT Atlantique
Bretagne-Pays de la Loire
École Mines-Télécom

THESE DE DOCTORAT DE

L'ÉCOLE NATIONALE SUPERIEURE MINES-TELECOM ATLANTIQUE
BRETAGNE PAYS DE LA LOIRE - IMT ATLANTIQUE
COMUE UNIVERSITE BRETAGNE LOIRE

ECOLE DOCTORALE N° 601
Mathématiques et Sciences et Technologies de l'Information et de la Communication

Spécialité : *Informatique*

Par

Zakaria EL MOUTAOUAKKIL

Spectrum-Efficient Cognitive MIMO Relaying: A Practical Design Perspective

Thèse présentée et soutenue à IMT Atlantique – Campus de Brest, le 12 octobre 2018
Unité de recherche : Lab-STICC
Thèse N° : 2018IMTA0092

Rapporteurs avant soutenance :

Mohamed-Slim ALOUINI	Professeur, KAUST University Thuwal – Arabie Saoudite
Ghaya REKAYA-BEN OTHMAN	Professeur, Télécom ParisTech

Composition du Jury :

Président :	Gilles BUREL	Professeur, Université de Bretagne Occidentale
Examinateurs :	Mohamed-Slim ALOUINI	Professeur, KAUST University Thuwal – Arabie Saoudite
	Ghaya REKAYA-BEN OTHMAN	Professeur, Télécom ParisTech
	Kamel TOURKI	Docteur, Huawei Research Center – Boulogne-Billancourt
	Halim YANIKOMEROGLU	Professeur, Carleton University - Canada
Directeur de thèse :	Samir SAOUDI	Professeur, IMT Atlantique

Résumé en Français

Le relayage cognitif multiple-input multiple-output (MIMO) hérite l'efficacité spectrale de la radio cognitive et les systèmes de relayage MIMO, apportant ainsi des gains prometteurs en termes de débit et fiabilité pour les futures communications des réseaux sans fil et mobiles. Dans cette thèse, nous concevons et évaluons des schémas pratiques d'émetteurs et de récepteurs pour des systèmes de relayage MIMO cognitif qui peuvent être mis en œuvre à moindre coût. Tout d'abord, nous réduisons l'affaiblissement en termes de débit du mode (simple) half-duplex de relayage MIMO non-orthogonale avec du amplify-and-forward (NAF) pour les transmissions large bande avec demande de retransmission automatique (ARQ). Différemment des travaux de recherche existants, le protocole de relayage proposé ne nécessite que la durée de transmission d'un seul paquet sur des canaux sélectifs en fréquence. De plus, nous proposons un récepteur itératif à complexité réduite pour cette classe de protocoles, entraînant ainsi une amélioration significative des performances de transmission de bout-en-bout. Deuxièmement, nous nous concentrons sur les systèmes de relayage cognitive de partage du spectre single-input multiple-output (SIMO) et évaluer l'impact des contraintes d'interférence instantanée et statistique sur la qualité de leur probabilité de coupure. Nos résultats révèlent que l'imposition d'une contrainte statistique sur la puissance d'émission du système secondaire est plus favorable que son adversaire consommatrice de spectre. Troisièmement, nous capitalisons sur notre deuxième contribution pour étudier les systèmes de relayage MIMO cognitifs avec decode-and-forward (DF) utilisant la sélection d'antenne à l'émission (TAS) ainsi que le maximum-ratio combining (MRC) à la réception. Basés sur la maximisation soit du rapport signal-sur-bruit (SNR) ou signal-sur-interférence-plus-bruit (SINR), nos résultats de probabilité de coupure nouvellement dérivés pour les deux stratégies proposées de TAS démontre l'optimalité du système basé sur la maximisation de SINR par rapport aux effets néfastes d'interférence mutuelle dans les systèmes de relayage MIMO cognitifs avec DF.

I. Introduction

L'émergence du business des réseaux mobiles de la voix aux services multimédias aux applications gourmandes en consommation de données a entraîné une forte croissance en consommation de note spectre fréquentiel. Apparemment, la rareté de cette ressource naturelle constituera un défi majeur pour redéfinir la manière dont il est utilisé, encore loin d'être optimale. En parallèle, plus d'effort devrait également être consacré à l'exploitation de toutes formes de diversité dans le canal sans fil afin de garantir une qualité de service

élevée en échange du spectre occupé. Dans cette ligne de raisonnement, la radio cognitive a été introduite en tant qu'interface radio intelligente visant à prendre en charge un grand nombre d'utilisateurs mobiles et d'appareils intelligents mais avec une qualité de service équitable. Aussi, des techniques sophistiquées de traitement du signal et de diversité ont été proposé pour protéger ces utilisateurs et/ou appareils contre les erreurs de transmission sur le canal sans fil. Parmi celles-ci, le relayage coopératif MIMO apparait comme approche pratique et rentable pour atteindre des communications sans fil à haute fiabilité et faible latence pour les réseaux sans fil du 5G et au-delà. Par conséquent, le spectre est à la fois distribué et exploité d'une manière optimale. Dans cette thèse, nous concevons et évaluons des schémas pratiques d'émetteurs et de récepteurs fonctionnant de manière cognitive tout en exploitant les formes de diversité disponibles dans les systèmes de relayage. Tout d'abord, nous rappelons dans ce chapitre quelques notions de base que nous jugeons essentielles pour mieux comprendre les contributions de nos travaux de recherche.

1. *De la MIMO au MIMO Virtuelle:* L'utilisation de plusieurs antennes localisées aux deux extrémités d'une liaison sans fil point-à-point, appelée MIMO, est considérée comme une solution révolutionnaire aux problèmes de communication sans fil causés par l'affaiblissement du signal, les évanouissements dû aux trajets multiples et les ressources limitées en terme du spectre et énergie. En effet [1], il améliore considérablement l'efficacité spectrale et énergétique ainsi que la fiabilité de la communication sans fil grâce aux gains de multiplexage et diversité spatiale qu'il offert. Outre les avantages que nous venons de signaler, la technologie MIMO est efficace en réduction et élimination d'interférences sur le même canal de transmission. Grâce au Beamforming, les antennes de l'émetteur ou du récepteur peuvent diriger leurs faisceaux (c'est-à-dire l'énergie du signal) de manière constructive vers certains utilisateurs ciblés sans interférer avec les autres. Par conséquent, les utilisateurs les plus éloignés de la station de base bénéficient d'une couverture de réseau plus étendue en utilisant judicieusement la quantité totale d'énergie disponible à la station de base. En dépit du fait que la technologie MIMO procure des gains de performance aussi importants, en raison du coût, complexité et/ou autres contraintes, le déploiement de plusieurs antennes au niveau des terminaux mobiles peut être prohibitif. Comme alternative, le relayage coopératif a été suggéré comme générateur de diversité spatiale face aux limitations susmentionnées. L'idée de base de ce genre de communication provient de la nature diffusive de l'environnement sans fil, dans lequel le signal transmis par une

source peut être entendu par autant de nœuds de réception que l'on a. Certains de ces nœuds peuvent jouer le rôle d'un relais qui coopère avec la source afin de former un système MIMO virtuelle menant à la génération de la diversité à l'émission comme à la réception. Il est important de noter que le gain de diversité résultant du relayage peut être transformé en un gain de multiplexage à condition que nous ciblions un compromis plus équilibré entre les deux.

2. *Les Protocoles de Relayage Coopératif:* La référence [4] a offert un cadre d'évaluation des performances unifié dans lequel plusieurs protocoles de relayage ont été introduits pour les réseaux sans fil assistés par des relais. Ces protocoles peuvent facilement être étendus au cas de coopération multi-relayage MIMO. Ils peuvent être classés en trois protocoles half-duplex nommés protocole I, protocole II et protocole III donnant lieu à des modèles de système homologues aux schémas traditionnels des systèmes MIMO, SIMO et MISO, respectivement. Selon le protocole I, la première phase de transmission est dédiée à la source pour diffuser son message pendant que le relais et la destination écoutent. Au cours de la deuxième de transmission, le relais et la source transmettent au nœud de destination. Les protocoles I et II sont identiques dans la première phase, mais seul le relais qui émet son message lors de la deuxième phase de transmission vers la destination. Le protocole III est essentiellement similaire au protocole I, sauf que le nœud de destination n'est censé recevoir que lors du premier slot de transmission. Notez que le protocole I réalise le maximum des degrés de diffusion et collision qui se génèrent pendant les deux phases de relayage. Ici, nous distinguons deux types célèbres de traitement du signal au niveau du relais: le DF où le relais tente de décoder la réplique du signal reçu, puis le transmettre à la destination et le AF où le relais ne transmet qu'un signal normalisé de ce qu'il a reçu. Quel que soit le traitement qui se fait au niveau du relais, tout protocole de relayage half-duplex doit appartenir à l'une des trois catégories que nous venons de décrire. Le relayage full-duplex est en dehors du sujet de notre étude.

3. *Couplage du MIMO avec les Diversités Temporelle and Fréquentielle:* En plus des formes de diversité qu'un système MIMO peut nous offrir, il existe également d'autres types de diversité qui peuvent être couplés avec les systèmes MIMO traditionnels ou virtuels. Par exemple, l'utilisation des diversités temporelles et fréquentielles avec MIMO a conduit à l'invention des codes espace-temps et espace-fréquence (voir [2] et

les références qu'il contient). D'autant plus, la conception conjointe des protocoles de retransmission ARQ avec le système MIMO entraîne une augmentation substantielle de la fiabilité de la transmission [2] en transformant les rondes du système ARQ, c'est-à-dire le nombre de retransmissions, en un gain de diversité. Ainsi, le relayage coopératif MIMO avec ARQ pourrait apporter des améliorations intéressantes à la qualité de transmission sur le canal sans fil. Dans certaines situations, les relais peuvent jouer le rôle d'émetteurs de paquets, donnant lieu à la généralisation des mécanismes classiques du protocole ARQ. Cela procure une augmentation substantielle du gain en diversité par rapport à un ARQ conventionnel, en particulier sur un canal ARQ quasi-statique qui ne change qu'à long terme. En général, il est assez difficile d'exploiter toutes les formes de diversité simultanément à cause des exigences et des contraintes du système des fois conflictuelles. Néanmoins, une combinaison de certaines formes de diversité peut suffire pour atteindre nos objectifs de conception en termes de latence, fiabilité et de couverture.

4. *Vers un Compromis Latence-Fiabilité plus Balancé:* Selon le principe du relayage simple MIMO half-duplex, le gain en fiabilité de la transmission est obtenu au prix d'une perte en latence à cause de la contrainte half-duplex au niveau des relais. Différentes méthodes ont été proposées pour récupérer cette perte. Par exemple, un relayage successif utilisant un codage répétitif a été introduit dans [5] pour les canaux à évanouissement plat en fréquence. Dans [67], des méthodes de sélection des relais ont également été proposées pour une communication coopérative avec un relayage de type DF. Une alternative intéressante à la réduction de la perte de débit au niveau des relais half-duplex consiste à combiner le mécanisme de retransmission ARQ et le relayage. Cette approche réduirait considérablement la perte de multiplexage en mode half-duplex en activant l'ARQ pour les paquets de données décodés et jugés erronés, lorsqu'ils se produisent. Les approches ciblant la conception conjointe d'ARQ et le relayage dans un protocole commun ont suscité plus d'intérêt (voir par exemple [7, 8]). Motivé par ce raisonnement, nous étudions des techniques de transmission coopératives à efficacité spectrale élevée, dans lesquelles l'ARQ et le relayage sont conçus conjointement.

II. Le Relayage MIMO AF Large Bande avec ARQ

Dans ce chapitre, nous nous concentrons sur les transmissions coopératives larges bande MIMO uni-porteuse avec relayage AF. La plupart des travaux de recherche effectués dans ce domaine ont été mené sur les canaux non-sélectifs en fréquence. Seulement quelques contributions qui ont considéré le relayage sur les canaux sélectifs en fréquence (voir par exemple, [10, 11, 12]). Donc, nous proposons en premier lieu un protocole de relayage de type AF à efficacité spectrale élevée qui opère sur les canaux sélectifs en fréquences. En particulier, la perte en gain de multiplexage due à la contrainte de transmission half-duplex est réduite tout en garantissant des performances en termes du taux d'erreurs et débit très intéressantes. Nous introduisons deux nouveaux protocoles de retransmission ARQ à base du relayage AF afin que le temps total nécessaire à la transmission d'un seul paquet soit réduit par rapport aux méthodes de relayage classiques. Nous évaluons également la probabilité de coupure de notre système et l'efficacité spectrale moyenne des schémas proposés, et nous montrons qu'ils surpassent celles des schémas existants de relayage MIMO coopératifs. Dans ce chapitre, nous proposons également une conception pratique de récepteur itératif turbo qui prend en compte les considérations susmentionnées tout en allégeant la charge de calcul pouvant survenir lorsque le nombre de rondes ARQ augmente. Inspiré du concept de combinaison turbo de paquets reçus, initialement introduit par Ait-Idir et al. [52] puis étendu dans [14] pour les systèmes MIMO avec ARQ sélectifs en fréquence avec la présence d'interférence co-canal, nous proposons d'effectuer une combinaison de sous-paquets au niveau signal au nœud de destination conjointement sur les deux slots de relayage et les multiples rondes du protocole ARQ. Ensuite, nous introduisons une implémentation récursive pour cette stratégie de combinaison, ce qui réduit considérablement sa complexité de calcul. Par rapport aux protocoles de relayage coopératifs classiques basés sur ARQ, le schéma de récepteur turbo proposé est évalué en termes de débit moyen et sa supériorité est tout à fait remarquable sur toute la région du SNR.

III. Une Analyse Exacte de la Probabilité de Coupure des Systèmes de Relayage SIMO DF Cognitive

Nos contributions dans le troisième chapitre sont organisées comme suit. Tout d'abord, nous partons de l'idée de simplifier le schéma d'émetteur du fait qu'il est mono-antenne et nous voyons comment est-ce qu'on peut bénéficier de la diversité que notre système peut garantir. Premièrement, nous présentons un modèle de puissance d'émission à condition que la probabilité de coupure du système primaire reste inférieure à un certain maximum.

Ensuite, deux scénarios d'acquisition du CSI du canal d'interférence sont considérés pour le système secondaire au niveau de l'émetteur et les relais de type DF en fonction d'une connaissance soit complète ou partielle du canal d'interférence radio cognitif. Selon chaque scénario, nous fournissons la CDF du SNR instantané reçu à chaque nœud secondaire réceptrice pendant les deux phases de relayage. La structure récursive des expressions dérivées les rendent très compactes et faciles à manipuler lorsqu'elles sont utilisées pour dériver ensuite la probabilité de coupure du système secondaire de bout-en-bout en une expression exacte et fermée. Nous notons que sans ces expressions faciles à manipuler, il devient très difficile d'avancer dans nos dérivations d'expressions analytiques. En outre, nous fournissons l'analyse asymptotique de la probabilité de coupure du système secondaire. Par conséquent, nous calculons le compromis de diversité et multiplexage de notre système cognitifs à base du partage de spectre sous une contrainte d'interférence fixe ou proportionnelle.

IV. Les Stratégies TAS pour le Relayage MIMO Cognitive

Le quatrième chapitre enrichit les contributions du chapitre précédent en considérant que l'émetteur est équipé de plusieurs antennes mais en activant seulement une via le machisme TAS et selon une contrainte d'interférence statistique. Nos contributions se distinguent par-rapport à chaque phase de relayage. Premièrement, nous dérivons la probabilité de coupure exacte du système TAS piloté par la maximisation du SINR reçu, en plus de mettre les travaux antérieurs sur le système TAS piloté par maximisation du SNR dans le même cadre de formulation. Ici, nous avons apporté des éclaircissements sur l'hypothèse sous laquelle les résultats dans [47, 48, 49] ont été obtenus et nous démontrons qu'ils mènent seulement à une analyse approximative de la probabilité de coupure du système secondaire. À titre préliminaire, nous dérivons de nouvelles expressions fermées du CDF et PDF du SINR reçu à la sortie du combineur MRC pour la stratégie TAS piloté par SINR. Ensuite, nous validons nos résultats à l'aide de simulations Monte-Carlo et montrons de manière intéressante que l'hypothèse d'indépendance des SINR reçus par antenne émettrice aura plus de crédibilité quand le nombre d'antennes déployées au niveau du récepteur secondaire est élevé. Nos résultats de probabilité de coupure concernant la liaison directe (c.-à-d. la première phase de relayage) montrent l'optimalité de la stratégie TAS piloté par SINR dans divers situations et scénarios d'adaptation de la puissance. De plus, l'analyse de la probabilité de coupure de notre système de bout-en-bout est également abordée. Par rapport à la deuxième phase de relayage, nos résultats sont nouveaux et peuvent être résumés comme suit. Nous évaluons les performances en cas de panne du système secondaire utilisant une

stratégie de TAS piloté par SNR. Dans ce cas, nous déduisons de nouveaux résultats sur le type de corrélation que la combinaison MRC engendre sur les variables de système MIMO cognitif nouvellement établi. Ensuite, nous adaptons la stratégie de TAS piloté par SINR relayage de type DF où le SINR combiné est maximisé conjointement sur les deux phases de relayage. Malgré la complexité héritée quant à la dérivation de la probabilité de coupure de notre système de bout-en-bout, nous l'exprimons sous une forme mathématique plus perspicace. Dans le cas d'une seule antenne de réception, nous parvenons à évaluer avec exactitude nos expressions dérivées d'une manière générale pour la stratégie de TAS piloté par la maximisation du SINR. Enfin, nous comparons nos résultats pour les deux stratégies TAS selon une stratégie d'allocation de puissance statistique et adaptative aux différents paramètres du système, et nous confirmons leur exactitude par simulations de Monte-Carlo révélant toujours l'optimalité du TAS piloté par SINR par rapport à son homologue piloté par SNR.

V. Conclusion

Dans cette thèse, nous avons conçu des schémas de transmission et réception pour le relayage MIMO cognitif à efficacité spectrale élevée en adoptant une perspective pratique. Nous soulignons trois contributions majeures dans notre étude. Premièrement, nous avons proposé un mécanisme de retransmission ARQ conjointement avec le relayage AF sur les transmissions MIMO coopératives à large bande. Pour lequel, nous avons abordé la charge de calcul du récepteur itératif proposé via une implémentation récursive et efficace réduisant considérablement son coût. Deuxièmement, nous avons étudié l'impact de l'acquisition de CSI du canal d'interférence dans un système de relayage SIMO cognitif avec partage de spectre. De plus, en fonction de la contrainte d'interférence (statistique ou instantanée) imposée par le système primaire, nous dérivons une analyse exacte et asymptotique de la probabilité de coupure du système secondaire. Nous déduisons ainsi que le relayage coopératif et le déploiement de plusieurs relais et antennes au niveau du récepteur primaire et secondaire sont deux facteurs importants pour améliorer les performances d'un system cognitif de partage de spectre où leur déploiement de plusieurs antennes au niveau de l'émetteur est contraignant. Capitalisant sur ces résultats, en troisième lieu, une analyse exacte de la probabilité de coupure du relayage DF incrémentiel pour les systèmes MIMO cognitif avec TAS/MRC a été menée avec succès. Pour deux types de TAS, piloté par la maximisation soit du SNR ou SINR après MRC, nos résultats d'analyse et de simulation révèlent l'exactitude de nos développements et l'optimalité du TAS pilotée par SINR.

Acknowledgement

First and foremost, I am thankful to the Almighty God for all the blessings and steadfastness He has given me to surmount all the challenges I faced during the course of my PhD.

I have had the great pleasure and honor to being accepted and received at IMT Atlantique (formerly Télécom Bretagne) by my doctoral advisor Prof. Samir Saoudi whose continuous confidence, support and aim of research excellence had given new horizons of fruitful collaboration in my PhD. I am especially thankful to my thesis supervisors Prof. Halim Yanikomeroglu (Carleton University, Canada) and Dr. Kamel Tourki (Huawei Technologies, France) for their diversified help, continuous encouragement, and generosity while hosting me at Carleton University for 1 year and at Texas A&M University at Qatar for 4.5 months, respectively. Besides their insights on my research, Pr. Halim's inclination towards scholarly work along with the scientifically enriching follow-ups with Dr. Kamel have always been a source of knowledge culmination, motivation and enthusiasm to me.

Many thanks are due to my doctoral committee, Pr. Mohamed-Slim Alouini (KAUST, KSA), Pr. Ghaya Rekaya-Ben Othman (Télécom ParisTech, France) and Pr. Gilles Burel, (Université de Bretagne Occidentale, France) for their interest in my research work, reviews and/or remarks that indeed helped in improving its quality of presentation.

I would also like to thank Dr. Tarik Ait-Idir, Dr. Hatim Chergui, and Prof. Houda Chafnaji, being all PhD graduates of IMT Atlantique, for their knowledge transfer on the concept "turbo", support and initial collaboration first during my undergraduate studies at INPT (Rabat, Morocco) up to my first PhD registration at IMT Atlantique. Many thanks also go to my friends Said Lmai and Mehmet Cagri Ilter along with Tamer Beitelmal for helping me out in settling down in Brest and Ottawa, respectively, for my first visits.

Last, but not least, I am grateful to my parents Malika Abou-EL-Aibada and Mohamed El-Moutaouakkil, my grandparents, my wife Ibtissam Zaidi, my brother El-Mehdi and sister Fatima-Ezzahra, for their incredible love, endless support and care.

Abstract

Cognitive multiple-input multiple-output (MIMO) relaying inherits the spectrum usage efficiency from both cognitive radio and MIMO relay systems, thereby bearing promising gains in terms of data rate and reliability for future wireless and mobile communications. In this dissertation, we design and evaluate practical transmitter and receiver schemes for cognitive MIMO relay systems that can readily be implemented at a lower cost. First, we reduce the multiplexing loss due the half-duplex operation in non-orthogonal amplify-and-forward (NAF) MIMO relay broadband transmissions with automatic repeat request (ARQ). Different from existing research works, the proposed relaying protocol requires only one packet duration to operate over frequency-selective block-fading relay channels. Further, we propose a low-complexity iterative receiver design for this class of protocols which results in significant enhancement of the end-to-end transmission performance. Second, we focus on cognitive underlay single-input multiple-output (SIMO) relay systems and evaluate the impact of instantaneous and statistical interference constraints on their outage performance. Our results reveal that imposing a statistical interference constraint on the secondary system transmit power is most favored than its spectrum-consuming counterpart. Third, we capitalize on our second contribution to investigate cost-effective transmission schemes for cognitive MIMO decode-and-forward (DF) relaying systems employing transmit-antenna selection (TAS) along with maximum-ratio combining (MRC) at the transmitter and receiver sides, respectively. Driven by maximizing either the received signal-to-noise ratio (SNR) or signal-to-interference-plus-noise ratio (SINR), our newly derived outage performance results pertaining to both proposed TAS strategies are shown to entail an involved derivation roadmap yet demonstrate the optimality of the SINR-driven TAS against the detrimental effect of mutual interference in cognitive MIMO DF relay systems.

Keywords: Cognitive radio, MIMO, relaying, AF, broadband transmission, TAS, MRC, CSI, SNR, SINR, diversity gain, coding gain.

Résumé

Le relayage cognitif multiple-input multiple-output (MIMO) hérite l'efficacité spectrale de la radio cognitive et les systèmes de relayage MIMO, apportant ainsi des gains prometteurs en termes de débit de données et de fiabilité pour les futures communications sans fil et mobiles. Dans cette thèse, nous concevons et évaluons des schémas pratiques d'émetteurs et de récepteurs pour des systèmes de relayage MIMO cognitifs qui peuvent être mis en œuvre à moindre coût. Tout d'abord, nous réduisons l'affaiblissement du débit du mode half-duplex du relayage MIMO amplify-and-forward non-orthogonale (NAF) large bande avec demande de répétition automatique (ARQ). Différemment des travaux de recherche existants, le protocole de relayage proposé ne nécessite que la durée de transmission d'un seul paquet sur des canaux sélectifs en fréquence. De plus, nous proposons une conception de réception itérative à complexité réduite pour cette classe de protocoles, entraînant ainsi une amélioration significative des performances de transmission de bout-en-bout. Deuxièmement, nous nous concentrons sur les systèmes de relayage cognitive de partage du spectre single-input multiple-output (SIMO) et évaluons l'impact des contraintes d'interférence instantanée et statistique sur la qualité de leur probabilité de coupure. Nos résultats révèlent que l'imposition d'une contrainte statistique sur la puissance d'émission du système secondaire est plus favorable que son adversaire consommatrice de spectre. Troisièmement, nous capitalisons sur notre deuxième contribution pour étudier les systèmes de relayage MIMO decode-and-forward (DF) cognitifs utilisant la sélection d'antenne à l'émission (TAS) ainsi que le maximum-ratio combining (MRC) à la réception. Basés sur la maximisation du rapport signal-sur-bruit (SNR) ou du rapport signal-sur-interférence-plus-bruit (SINR), nos résultats de probabilité de coupure nouvellement dérivés pour les deux stratégies proposées de TAS démontre l'optimalité du système de sélection d'antenne basé sur le SINR par rapport aux effets néfastes d'interférence mutuelle dans les systèmes MIMO cognitifs.

Mots-clefs: Radio cognitive, MIMO, relayage, AF, DF, Turbo, MRC, SNR, SINR.

List of Publications

- Zakaria El-Moutaouakkil, Kamel Tourki, Halim Yanikomeroglu, and Samir Saoudi, "Optimal Interference-Aware TAS/MRC for Cognitive MIMO Systems," *to be submitted to IEEE Transactions.*

- Zakaria El-Moutaouakkil, Kamel Tourki, Halim Yanikomeroglu, and Samir Saoudi, "Energy-Efficient Non-Orthogonal MIMO AF Relaying for Broadband Spectrum Sharing," *to be submitted to IEEE Transactions.*

- Zakaria El-Moutaouakkil, Kamel Tourki, Halim Yanikomeroglu, and Samir Saoudi, "TAS Strategies for Incremental Cognitive MIMO Relaying: New Results and Accurate Comparison," *IEEE Access*, vol. 6, pp. 23480-23499, April 2018.

- Zakaria El-Moutaouakkil, Kamel Tourki, Samir Saoudi, "Exact Outage Analysis of SIMO Relay-aided Underlay Communications with Limited Feedback," in *Proc.*, *76th Semi-Annual VTC Spring*, Nanjing, China, May 2016.

- Zakaria El-Moutaouakkil, Kamel Tourki, Samir Saoudi, "Spectrally-efficient SIMO relay-aided underlay communications: An exact outage analysis," in *Proc.*, *IEEE ICC*, Sydney, Australia, June 2014.

- Zakaria El-Moutaouakkil, Kamel Tourki, Khalid Qaraqe, Samir Saoudi, "Exact Outage Analysis for Relayaided Underlay Cognitive Radio Communications," in *Proc.*, *76th Semi-Annual VTC Fall*, Québec City, Canada, September 2012.

- Zakaria El-Moutaouakkil, Tarik Ait-Idir, Samir Saoudi, Halim Yanikomeroglu, and Mounir Ghogho, "Turbo Receiver Design for MIMO Relay ARQ Transmissions," in *Proc.*, *55th Annual IEEE GLOBECOM*, California, USA, December 2012.

Contents

List of Tables

List of Figures

Chapter 1

Motivation and Basic Notions

The mobile business shift from voice to multimedia to data-centric applications and services have led to a growing stress on the wireless spectrum medium. Seemingly, the scarcity of this natural resource will pose a big challenge onto rethinking the traditional way it is used, still far from being optimal. Meanwhile, more research efforts should also be paid to optimally leveraging all forms of diversity in the wireless medium to guarantee a high quality-of-service (QoS) in return of the occupied spectrum. In this line of reasoning, cognitive radio has been introduced as an intelligent radio interface that aims to accommodate as many mobile users and smart devices as possible with a fair QoS delivery. In parallel to that, sophisticated diversity and signal processing techniques have been evolving to protect those users and/or devices against errors while transmitting over the wireless fading channel. Among these, cooperative multiple-input multiple-output (MIMO) relaying figures prominently as a practical cost-effective approach to achieve low-latency high-reliability wireless communications for 5G and beyond wireless networks. Therefore, the optimally distributed spectrum is optimally benefited from. Designing practical transmitter and receiver schemes that can both reap the available MIMO relay system diversities and operate in a cognitive manner has received much attention recently, and is the stimulating topic of this dissertation. In this chapter, we recall some basic notions we deem essential for the ease of presenting the contributions of our research work.

1.1 From MIMO to Virtual MIMO

1.1.1 MIMO Advantages

The use of multiple collocated antennas at both ends of a point-to-point wireless link, known as MIMO, is viewed as a revolutionary solution to wireless communication challenges caused by fading, multi-path fading and limited spectrum and energy resources. Arguably [1], it significantly improves the spectrum and energy efficiencies as well as the reliability of the wireless link through spatial multiplexing and diversity gains. In the following, we briefly describe these gains.

Spatial Multiplexing Gain: Interestingly, MIMO systems offer a linear (in the minimum number of the transmit and receive antennas) increase in capacity for no additional power or bandwidth expenditure. The corresponding gain is realized by simultaneously transmitting independent data streams within the same frequency band. Under certain conditions, such as rich scattering in the propagation environment and sufficient spacing between the antennas at both ends in order to achieve independent MIMO *routes*, the receiver can separate the data streams. Therefore, higher data rates can be attained via large-scale MIMO systems.

Spatial Diversity Gain: Contrary to spatial multiplexing which requires multiple antennas at both MIMO channel ends, spatial diversity can be realized even if the transmitter or receiver is equipped with a single antenna. Diversity techniques are used primarily to mitigate the fading and multi path fading phenomena. In a MIMO system, we distinguish between three forms of spatial diversity that can be collected: receive diversity, transmit diversity and the combination of the two.

- Receive diversity can be obtained through SIMO channels by means of coherent combining of the received replicas of the same transmitted signal so as the resultant signal exhibits a considerably reduced amplitude variation compared to the received signal at each receive antenna. Receive diversity is quantified by the number of independent fading branches in a wireless channel, known as the diversity order.

- Transmit diversity on the other hand can be reaped in a multiple-input single-output (MISO) channel given that a suitable coding (i.e. pre-processing at the transmitter side) design is required for its extraction at the receiver. Similar to receive diversity, the achievable transmit diversity order may reach the number of the transmit antennas

under the necessary but not sufficient condition of independent MISO channel links. In general MIMO systems, the spatial diversity we obtain is a combination of the receive and transmit diversities described above. As a result, the achievable diversity order may reach the product of the transmit and receive antenna numbers given that the channel between each pair of input and output antennas fades independently from the others.

Besides the above cited advantages, MIMO technology is efficient in co-channel interference reduction and avoidance. By means of beamforming, the antennas at either the transmitter or receiver can constructively direct their beams (i.e. signal energy) towards some targeted users without interfering on the others. Consequently, farther users from the base station would benefit from a larger network coverage by cleverly using the available amount of total energy to the base station.

1.1.2 Cooperative Diversity in Virtual MIMO Systems

If MIMO technology provides such significant performance gains, due to cost, complexity or other constraints the deployment of multiple antennas at user terminals in a network can be prohibitive. As an alternative, cooperative relaying has been suggested as enabler of spatial diversity in the face of the aforementioned limitations. The basic idea behind this concept stems from the broadcast nature of the wireless environment where the transmitted signal by a source can be overheard by as many receiving nodes as there might exist. Some of these nodes can play the role of relays that cooperate with the source in order to form a virtual MIMO leading to either transmit or receive diversity generation. Importantly, the cooperative diversity gain resulting from relaying can be leveraged into a multiplexing gain as we address a more balanced tradeoff between the two.

1.1.3 Coupling MIMO with Temporal and Frequency Diversities

Despite the resulting diversities a MIMO system has to offer, there also exists other types of diversity that can be coupled with traditional or virtual MIMO systems. For instance, the use of temporal and frequency diversities with MIMO have led to the invention of space-time and space-frequency codes (see [2] and references therein). Also, the joint design of ARQ re-transmission protocols with MIMO results in a substantial increase in the transmission

reliability [3] by exploring the ARQ delay, i.e. the number of ARQ rounds, into a diversity gain. Cooperative MIMO relaying with ARQ could bring interesting enhancements to eventually both diversity and multiplexing gains. In some situations, relays may act as packet re-transmitters giving rise to a generalization of the classical ARQ mechanisms. This provides a substantial increase in the diversity gain compared to conventional ARQ especially over a long-term quasi-static ARQ channel. In general, it is quite difficult to exploit all forms of diversity simultaneously due to conflicting system demands and constraints. Nevertheless, a combination of some of these forms may be sufficient to attain our design objectives in terms of latency, reliability and coverage.

1.2 Towards a Balanced Latency-Reliability Tradeoff

1.2.1 Relaying Protocols

In [4], a unified performance evaluation framework where different relaying protocols were introduced for relay-aided wireless networks. These protocols can straightforwardly be extended to the MIMO multi-relay cooperation case. They can be classified into three half-duplex protocols named as protocol I, protocol II and protocol III yielding homologous system models as in the traditional MIMO, SIMO and MISO schemes, respectively. In protocol I, the first relaying slot is dedicated to the source node to broadcast its single while the relay and the destination are listening. During the second relaying slot, both the relay and source nodes transmit to the destination node. Protocols I and II are alike in the first time slot, but only the relay which engages in the second relaying-hop transmission to the destination node. Protocol III is essentially similar to protocol I except that the destination node does not receive from the source during the first time-slot. Note that protocol I realizes maximum degrees of broadcasting and receive collision because of the non-orthogonal multiple access it results in during the second relaying slot. Herein, we distinguish between two famous types of signal processing at the relay: DF where the relay attempts to decode the received signal replica then forwards it to the destination and amplify-and-forward (AF) where the relay only transmits a normalized-to-the-symbol-energy version of the received signal to the destination node. Irrespective of the signal processing used in both cooperation phases at each node, any half-duplex relaying protocol must fall within one of the three categories we have just described. Full-duplex relaying is beyond the scope in our study.

1.2.2 Low-Latency Cooperative MIMO Relaying with ARQ

In cooperative MIMO relaying, the reliability is gained at the expense of an increased latency due to the half-duplex constraint at the relay nodes. Different methods have been proposed to recover this loss. For instance, successive relaying using repetition coding has been introduced in [5] for frequency-flat fading relay channels. In [6], relay selection methods have also been proposed for cooperative communication with decode-and-forward relaying. A prominent alternative to reducing the throughput loss in half-duplex cooperative relaying is the combination of both ARQ and relaying. This approach would significantly reduce the half-duplex multiplexing loss by activating ARQ for rare erroneously decoded data packets, when they occur. Approaches targeting the joint design of ARQ and relaying in one common protocol have received more interest (see for instance [7]–[9]). Motivated by the above suggestion, we investigate spectrum-efficient cooperative transmission techniques where both ARQ and relaying are jointly designed.

- *In chapter 2, we focus on single-carrier MIMO broadband cooperative transmissions with AF relaying. Most of the research work that has been carried out in this area has focused on frequency-flat fading channels. Relaying techniques for frequency-selective fading channels have recently been investigated by some authors (see for instance* [10, 11, 12]*). Among our contributions in this thesis manuscript, we propose spectrum-efficient relaying protocols where the multiplexing loss due to the half-duplex transmission constraint is reduced while providing interesting outage performance. We introduce two new relay ARQ protocols where the total time required for transmitting one data packet is significantly reduced compared with conventional relaying methods. We also evaluate both the outage error probability and average throughput performance of the proposed schemes, and show that they outperform classical cooperative MIMO relaying schemes.*

1.2.3 Receiver Design of the MIMO-ARQ Relay Channel

It is crucial in MIMO wireless communication systems to design receiver schemes that recover the information sent by the transmitter with the lowest probability of error. The optimal receiver implements either the maximum a-posteriori (MAP) or maximum-likelihood (ML) criteria. In which case, its computational complexity gets involved as our MIMO system gets large. Therefore, we mostly resort to sub-optimal receivers that guarantee

close-to-optimal performance results but with lower complexity. Pertaining to our proposed spectrum-efficient MIMO relay ARQ with slot-mapping reversal (SMR) transmission strategy in chapter 2, our next contribution in the same chapter is described as follows.

- *In chapter 2, we also investigate practical turbo receiver design that addresses the aforementioned considerations while alleviating the computational load that may arise when the number of ARQ rounds increases. Inspired by the concept of turbo packet combining, initially introduced by Ait-Idir et al. [13] and then extended in [14] for broadband MIMO ARQ systems in the presence of co-channel interference, we propose to perform signal-level sub-packet combining at the destination node jointly over both time slots and multiple ARQ rounds. Then, we introduce a recursive over-the-ARQ-rounds implementation of this combining strategy, that considerably reduces its computational complexity. Compared with conventional ARQ-based cooperative relaying protocols, the proposed turbo receiver scheme is assessed in terms of the average throughput and its superiority is quite remarkable over the entire SNR region.*

1.3 Cognitive Radio: Towards an Optimal Spectrum-Efficiency

In response to the ever-growing stress put on the wireless spectrum medium as a result of the huge demand on high big data rates, cognitive radio (CR) has been evolving as a set of rules to cope with the wireless spectrum under-utilization phenomenon [15]. Many concepts have been derived from the original idea of cognitive radio [16], drawing three active research lines under the names of spectrum *interweave*, spectrum *overlay*, and spectrum *underlay* [17, 18].

- The interweave principle relies on the idea of opportunistic communication within the vacant spectrum *holes* in the licensed spectrum band at a given time and location. They can be exploited by cognitive users for their communication by means of opportunistic frequency reuse. To be realized, the interweave technique relies also on monitoring the overall spectrum band to detect the spectrum frequencies being unused eventhough licensed and then reusing them as long as they are free.

- In the overlay concept, to tackle the issue of spectrum under-utilization, the cognitive users may share the spectrum band with the legitimate licensed users but from a win-win perspective. Assuming that the non cognitive user's message and/or codebook is known to the cognitive transmitter, the latter can be allowed to interfere with the non cognitive transmitter by making an appropriate choice of the power split. Therefore, any increase in the non cognitive user's SNR due to the assistance from cognitive relaying can be exactly offset by the decrease in the non cognitive user's SNR due to the interference caused by the remainder of the cognitive user's transmit power used for its own communication. This guarantees that the non cognitive user's rate remains unchanged while the cognitive user allocates part of its power for its own transmissions [17].

In this dissertation, we focus on the underlay spectrum-sharing concept as a means to allow secondary (unlicensed) users to share the same spectrum band with the primary (licensed) users. This concept has the potential of enabling the secondary users to blindly access the primary system spectrum band without any prior monitoring of its occupancy. However, as far as the interference issue is concerned, the secondary user's transmit power must be kept under a certain threshold that is predetermined by the primary system, so as to legitimately maintain its QoS.

1.3.1 Approaches for Improved Spectrum Sharing Performance

To strike a balance in the dilemma of minimizing the engendered interference on the primary system and ensuring additional degrees of freedom in targeting its own QoS, the secondary system can adopt several proactive approaches. In general, these approaches rely on a better combination of the available forms of diversity in time, frequency and space domains. For instance, the authors in [19, 20] have suggested repetition time diversity schemes using a type-II hybrid-ARQ protocol to improve the secondary link reliability. Alternatively, the authors in [21] exploited the frequency diversity among the primary and secondary users to maximize the secondary system capacity subject to the interference constraint imposed by the primary system. Also, MIMO transmissions using transmit/receive beamforming techniques have been adopted in [22, 23] to achieve high secondary system transmission rates, while minimizing the interference at the primary receiver. From a different angle, the authors in [24] conducted an asymptotic outage analysis, and demonstrated that a cooperative diversity order of $K + 1$ (where K refers to the number of the assisting relays)

can be achieved if the secondary source node adapts its transmit power to a proportional interference constraint, i.e. scaling with the primary system transmit power. Otherwise, if the interference constraint is independently fixed, the outage probability will saturate in the high SNR regime, implying that the achievable diversity order will be equal to zero [24]. This is the case whether the secondary source node is acquiring complete or partial interference CSI (I-CSI) knowledge.

1.3.2 Cognitive Cooperative Relaying

Recently, it was shown that introducing relays in cognitive networks can boost the secondary outage performance especially when the deployment of multiple antennas at the source node is costly or infeasible [25, 26, 27, 28, 29]. Therein, attention has been paid to express the outage probability of an underlay secondary system where the direct link is assisted by a set of K regenerative DF relaying nodes, yet the problem is still open when it comes to the proposed setup (in which the primary and secondary receivers are equipped with multiple antennas) and communication model (that is enabling spectrally-efficient communications). In particular, a closed-form expression of the outage probability had been derived under complete [30] or partial [31] I-CSI knowledge at the secondary transmitter while the secondary direct link undergoes a slow-fading quasi-static variations. Alternatively, [28] investigated selective-and-incremental regenerative DF relaying for the secondary system under a fixed interference constraint and for two I-CSI acquisition scenarios at the level of the secondary source node. However, in the first relaying hop worst case, i.e. when neither the destination node nor any of the relaying node have met their SNR thresholds during the first hop, the source node, instead of retransmitting the same information, it resets the cycle of re-transmissions and proceeds with a new attempt. This implies that a significant loss in terms of spectrum efficiency may occur for low secondary system SNR ratios. In another contribution, the authors in [29] considered a selective cooperation framework for a spectrum sensing cognitive radio network. Considering that all nodes are equipped with only one antenna, they derived the secondary system outage probability expression while a selective-and-incremental relaying scheme referred to as ACK-based selective cooperation has been adopted to assist the secondary direct link. However, the provided diversity and multiplexing tradeoff (DMT) is based on the assumption of a relaxed transmit power constraint, i.e. the cognitive radio interference channel variance is neglected compared to those of the secondary channels. In [32], the authors attained almost the same conclusions and,

considering unlimited transmit power at the secondary nodes, they derived the asymptotic outage probability as a function of some interference threshold. Under such assumptions, the obtained results reduce to those found in non-cognitive radio systems. Although relevant for preserving high spectrally-efficient communications, none of the previous research works has considered selective-and-incremental regenerative DF relaying [33, 34] for SIMO secondary systems, where both the primary and secondary destination nodes are equipped with multiple receive antennas.

1.3.3 Spectrum-Efficient Cognitive SIMO Relaying

Our motivating point in our next contribution is therefore to study the impact of the deployment of multiple relays and receive antennas at the primary and secondary destination nodes on the overall secondary system transmission reliability and spectrum efficiency. Specifically, we are keen on quantifying the secondary system performance by providing closed-form and asymptotic expressions of the end-to-end outage probability of the SIMO relay-aided secondary link.

- *Our contribution in Chapter 3 is organized as follows. Firstly, we present an outage-constrained transmit power model for the secondary system transmitting nodes. Then, two I-CSI acquisition scenarios are considered for the secondary system at the level of the source node and relays based on either complete or partial knowledge of the cognitive radio interference channel. According to each I-CSI scenario, we provide the CDF of the instantaneous received SNR at each secondary receiving node during both relaying hops. Interestingly, the recursive structure of the derived expressions makes them very compact and tractable when used to subsequently derive the end-to-end secondary system outage probability in its closed-form expression. Note that without these easy-to-manipulate expressions, it is too difficult to take further steps in our analytical derivations. Furthermore, we provide the asymptotic analysis of the secondary system outage probability. As a consequence, we derive the DMT under either a fixed or proportional, i.e. relaxes with the primary system QoS, outage interference constraint.*

It turns out on the one hand that equipping the primary receiver with multiple antennas leads to a relaxed secondary system transmit power. This gives rise to better opportunities for the secondary system to transmit alongside with the primary system using the latter spectrum band, as opposed to being obliged to keep silent in the single antenna case. On the

other hand, our analytical and simulation results show the positive impact of cooperative relaying and equipping the secondary destination node with multiple antennas on the overall secondary system outage performance. Interestingly, for a moderately loaded cognitive radio system with three receive antennas at the primary and secondary receivers, and four assisting relays, it is well argued that the secondary system outage performance is amply enhanced with only a partial (i.e., statistical) I-CSI acquisition of the underlying cognitive radio interference channel. As opposed to being severely degraded in the single receive antenna case, the secondary system QoS can now be maintained above a certain acceptable level.

1.4 Cognitive MIMO Relaying: Practical Challenges and Solutions

As pointed out earlier, MIMO relaying can serve the secondary system in different ways. One approach is the design of cooperative beamforming or space-time block coding (STBC) schemes that sort out the dilemma of coexistence on the same spectrum [35]-[37]. Inevitably, this approach requires large feedback overhead and additional complexity to compute the beamforming and precoding matrices. Besides, its performance is proportional to the number of radio-frequency (RF) chains that whenever increased it becomes costly to implement especially at the user equipment side. Another approach, simple and less expensive yet realizes a good tradeoff among performance, cost and complexity, is TAS. In its simplest form, only the RF chain causing less interference on the primary system and enabling greater secondary system performance is selected. TAS has been adopted in the LTE uplink (Rel. 8/9) and we adopt it herein as a promising technology candidate for beyond 5G massive-oriented MIMO systems [38]. If the MRC is applied at the receiver side, the technique is referred to as TAS/MRC. If selection combining is instead applied at the receiver side, the technique is referred to as TAS/SC. According to [39], TAS/MRC performs better than TAS/SC at the expanse of an increased complexity which does not pose a real burden if the MRC is implemented at the base station level.

1.4.1 Cross-interference Mitigation in Cognitive MIMO Relaying with TAS/MRC

In practical cognitive spectrum-sharing, the interference between the primary and secondary systems is mutual. Cross-interference mitigation using TAS/MRC has received much interest in cognitive MIMO systems whether with [39]-[42] or without the use of relaying [43]-[45]. In these works, the SNR-driven TAS/MRC strategy takes up the largest part. Besides its simplicity, it preserves, under certain ordinary conditions, the independence between the signal and interference components in the selected MRC-combined SINR ratio. This independence does not always hold as it relies on the TAS strategy being opted for. Indeed, it is not preserved in the SINR-driven TAS. Having a clear understanding on the impact of TAS on the post-processed received SINR is of great importance in the secondary system outage/capacity performance analysis. In this dissertation, we comprehensively address this challenge not only in cognitive point-to-point MIMO secondary systems, but more generally in MIMO DF relay-aided ones.

1.4.2 Point-to-Point Cognitive MIMO Systems with TAS/MRC

The outage/capacity performance of point-to-point cognitive MIMO systems using an SNR-driven TAS/MRC have been analyzed in [43] and [44] considering both instantaneous and mean-valued interference constraints. Pertaining to the latter, i.e. when the secondary transmitter acquires only partial CSI about its interference channel, the outage performance analysis bears resemblance with earlier works on non-cognitive MIMO systems with CCI where the SNR and SINR-driven TAS strategies have initially been introduced [47], [46]. Yet, to derive the outage probability for the SINR-driven TAS, the authors assumed that the per-antenna received SINRs are independent [47]. This assumption is controversial and does only lead to an approximate outage analysis. Note that in the single receive antenna case, the SINR-driven TAS reduces to its SNR-driven counterpart [45].

In this dissertation, we conduct a comprehensive and accurate outage performance analysis of cognitive MIMO incremental DF relaying for both, the SNR and SINR-driven TAS/MRC strategies. For practicality reasons, we assume that the secondary system can only acquire a partial state information about its engendered interference on the primary system.

- *In this context, chapter 4 enriches the aforementioned related works not using relays with the following novel contributions. Firstly, we derive an accurate outage analysis for the SINR-driven TAS besides putting the prior works on the SNR-driven TAS within the same framework. Herein, we shed more light on the assumption under which the results in [47]-[49] were obtained, and demonstrate that it only leads to an approximate outage analysis. As a preliminary step, we secondly derive new closed-form expressions of the CDF and PDF expressions of the MRC-combined SINR resulting from the SINR-driven TAS. Then, we validate our results by Monte-carlo simulations and interestingly show that the controversial assumption of independence among the per-transmit-antenna received SINRs gets more credibility as a large-scale received antenna array is deployed at the secondary receiver. The first-hop system outage performance is finally compared for both TAS/MRC strategies showing the optimality of the SINR-driven TAS/MRC under various secondary system settings and power adaptation scenarios.*

1.4.3 Cognitive MIMO Relaying with TAS/MRC

Very recently, cognitive MIMO relaying with TAS has received a substantial interest. In particular, Yeoh *and al.* [39] derived new expressions of the outage probability of cognitive MIMO dual-hop DF relaying using TAS/MRC and TAS/SC. Once again, the authors consider an SNR-driven TAS strategy and neglects the AWGN effect at the relay and destination nodes so as to facilitate the outage analysis. [42] investigates the outage and error-rate performance of dual-hop AF relaying in underlay MIMO systems using an SNR-driven TAS/SC. Herein, the authors neglects the primary system interference on the secondary system. In [48] and [49], AbdelNabi *and al.* partially elaborate on the SINR-driven TAS/MRC strategy in MIMO multi-hop relaying in a Poisson field of interferes but based on the same aforementioned assumption in related works not using relays. Former works have therefore not thoroughly examined the SINR-driven TAS/MRC strategy despite its optimality, and focused mainly on dual-hop relaying under the widely used SNR-driven TAS/MRC.

- *The end-to-end outage analysis of the proposed cognitive MIMO relay system is also addressed in chapter 4 and shown to entail a different derivation roadmap for each TAS/MRC strategy. Compared to the related works using relays, our findings are new and can be summarized as follows. Firstly, we evaluate the secondary system outage performance using an SNR-driven TAS. In this case, we show that the arisen*

four system variables are jointly correlated, and proceed with their quad-variate joint PDF derivation. We deduce new results on the type of correlating the MRC combining engenders among the variables of the newly established virtual cognitive MIMO system. Secondly, we extend the SINR-driven TAS to a relaying-adapted strategy where the combined SINR is jointly maximized over both relaying hops. Despite the complexity of deriving the end-to-end outage probability, we further express it in a more insightful mathematical expression. Thirdly, in the single receive antenna case, we manage to accurately evaluate our derived expressions for the newly introduced SINR-driven TAS/MRC by numerical integration and get more intuition into their general exact derivation. Finally, we compare our findings for both TAS strategies under an adaptive power allocation policy and different system settings, and confirm their accuracy by monte-carlo simulations revealing the outperformance of the SINR-driven TAS/MRC over its SNR-driven counterpart.

Chapter 2

Single-Carrier MIMO-ISI Relay ARQ Transmissions

2.1 Introduction

This chapter investigates throughput-efficient relay ARQ protocols for single-carrier MIMO systems with amplify-and-forward relaying. We focus on reducing the multiplexing loss due to the half-duplex operation at the relay. Compared to the conventional relaying techniques, the proposed mechanisms require only one time slot duration for transmitting the entire data packet at each ARQ round. Secondly, we design a practical turbo receiver at the destination side based on soft sub-packet combining. It allows the destination node to perform signal-level combining over both relaying time slots and multiple ARQ rounds jointly in the frequency domain (FD) using minimum mean square error MMSE filtering. Its computational load is then smoothly relaxed via a recursive implementation alleviating the memory requirements when the number of ARQ rounds increases. Simulation results show that the proposed transmission strategy along with turbo sub-packet combining at the destination side achieves significant average throughput performance gain compared with conventional ARQ-oriented cooperative relaying, especially in situations where the relay node is close to the source node.

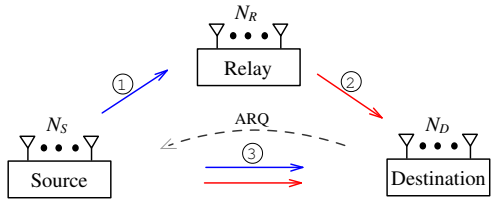

Figure 2.1: Multi-antenna Relay ARQ system.

2.2 Relay ARQ Sub-Packet Transmission Model

2.2.1 MIMO Relay ARQ System Model

We consider a cyclic-prefix (CP)-aided single-carrier (SC) block transmission between a source node S and a destination node D assisted by a relay node R. These nodes are equipped with N_S, N_D, N_R antennas, respectively, and thereby constitute the MIMO relay ARQ system model depicted in Fig. 2.1. The link connecting each pair of nodes $\{A, B\}$ where $A \in \{S, R\}$ and $B \in \{R, D\}$ is regarded, at the kth transmission, as a point-to-point quasi-static frequency selective fading MIMO channel having L_{AB} independent paths, and constant (time-invariant) over a duration of $\frac{T}{2} \in \mathbb{N}^*$ channel uses (cu)s. Each of these paths $l \in \{1, \cdots, L_{AB}\}$ is characterized by its flat fading MIMO channel matrix $\mathbf{H}_l^{AB^{(k)}} \in \mathbb{C}^{N_B \times N_A}$ with independent identically distributed (i.i.d) entries drawn from zero-mean and $1/L_{AB}$-variance circularly symmetric complex Gaussian distributions. Also, the link $\{A \to B\}$ is characterized by the channel energy E_{AB} capturing the effects of path loss and shadowing. To ensure high reliability and throughput-efficient transmission, we assume that node S uses a slots mapping reversal (SMR) re-transmission strategy in which R performs *amplify-and-forward* relaying in a *half-duplex* mode of operation.

2.2.2 Relay ARQ with SMR Strategy

In general, each packet transmission $k \in \{1, \cdots, K\}$, within a maximum of K ARQ rounds, is supposed to span two consecutive time slots (TS)s. Prior to the first transmission, the source node S proceeds by encoding the packet of information bits $\mathbf{b}$ with the aid of a space time bit interleaved coded modulation (STBICM) encoder [50]. Then, given that $\mathcal{X}$ is the constellation set, the resultant symbol packet[1]

[1]Due to the infinitely deep space-time interleaving, space and time independence between the elements of $\mathbf{x}$ is justified.

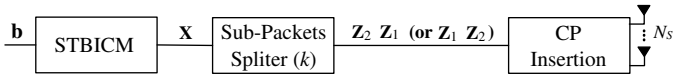

Figure 2.2: Source node transmitter scheme.

Node \ Transmission	k odd		k even	
	1st TS	2nd TS	1st TS	2nd TS
Source	$\mathbf{z}_1$	$\mathbf{z}_2$	$\mathbf{z}_2$	$\mathbf{z}_1$
Relay	$\mathbf{y}_R^{(k)}$	$\widetilde{\mathbf{y}}_R^{(k)}$	$\mathbf{y}_R^{(k)}$	$\widetilde{\mathbf{y}}_R^{(k)}$
Destination	$\mathbf{y}_D^{1,(k)}$	$\mathbf{y}_D^{2,(k)}$	$\mathbf{y}_D^{1,(k)}$	$\mathbf{y}_D^{2,(k)}$

Transmission Period Reception Period

Figure 2.3: SMR splitting rule at the kth transmission.

$$\mathbf{x} \triangleq [\mathbf{x}_0, \cdots, \mathbf{x}_{T-1}] \in \mathcal{X}^{N_S \times T} \tag{2.1}$$

is passed through a sub-packet splitter that successively generates two $N_S \times \frac{T}{2}$ equally sized small packets $\mathbf{z}_1 = \left[\mathbf{z}_{1,0}, \cdots, \mathbf{z}_{1,T/2-1}\right]$ and $\mathbf{z}_2 = \left[\mathbf{z}_{2,0}, \cdots, \mathbf{z}_{2,T/2-1}\right]$ based on $\mathbf{x}$. T is the total number of channel uses in the symbol packet $\mathbf{x}$. The splitting rule is basically given by

$$\begin{cases} \mathbf{z}_{1,t} = \mathbf{x}_{2t} & , \quad 0 \leq t \leq \frac{T}{2} - 1 \\ \mathbf{z}_{2,t} = \mathbf{x}_{2t+1} & , \quad 0 \leq t \leq \frac{T}{2} - 1 \end{cases}, \tag{2.2}$$

and is illustrated in general for the kth transmission in Fig. 2.2 and Fig. 2.3. As its name suggests, an SMR strategy is active when node S reverses the sub-packet splitting order as a function of the ARQ round index parity. Precisely, sub-packets z_1 and z_2 are mapped (i.e., transmitted) onto the first and the second time slots, respectively, for k odd, and the inverse for k even. This approach, in contrast to conventional ARQ-based cooperative relaying [51] where the symbol packet $\mathbf{x}$ is transmitted as such at each ARQ round, introduces a sort of correlation between the well know ARQ mechanism and the AF and/or DF relaying protocols. Consequently, a substantial gain in the transmission performance is attained. It is worth noting that the considered Relay ARQ strategy follows the Chase-type ARQ mechanism. That is, when a negative acknowledgment (NACK) is sent back to S at round k in the case of packet decoding failure at node D, the source node does not intervene in changing the STBICM function, providing instead the sub-packet splitter with the same

symbol packet $\mathbf{x}$ upon transmission at round $k+1$. Since no channel state information (CSI) about channel 1 (i.e., $S \to R$ link) and channel 3 (i.e., $S \to D$ link) is available at the level of node S, the symbol vectors $\{\mathbf{x}_m \in \mathcal{X}^{N_S \times 1} : m = 0, \cdots, T-1\}$ may be chosen to have equally powered entries, hence satisfying[2]

$$\mathrm{E}[\mathbf{x}_m \mathbf{x}_n^{\mathrm{H}}] = \mathrm{diag}\left\{\delta_{m,n} \mathbf{I}_{1,N_S}\right\}, \quad \forall\, m, n \in \{1, \cdots, T\}. \tag{2.3}$$

2.2.3 Sub-Packet ARQ Transmission Model

During the first TS of ARQ round k, node S appends to $\mathbf{z}_1$ (here we assume that k is odd, but later on we generalize our formulation despite k parity) a cyclic prefix (CP) symbol word of length $L_{cp} = \max\{L_{SD}, L_{SR}, L_{RD}\}$ to avoid inter block interference (IBI), then broadcasts the resulting symbol packet simultaneously to both R and D nodes. After removing the CP portion at the level of node R, the received sequence $\mathbf{y}_R^{(k)}$ (or block) of signal vectors

$$\mathbf{y}_{R,t}^{(k)} = \sqrt{\mathrm{E}_{SR}} \sum_{l=0}^{L_{SR}-1} \mathbf{H}_l^{SR^{(k)}} \mathbf{z}_{1,(t-l) \bmod \frac{T}{2}} + \mathbf{n}_{R,t}^{(k)} \tag{2.4}$$

for $t = 0, \cdots, T/2-1$, is amplified to have unit average energy per each entry . Therefore, the resulting sequence $\widetilde{\mathbf{y}}_R^{(k)}$ is made of signal vectors $\widetilde{\mathbf{y}}_{R,t}^{(k)} = \gamma \mathbf{y}_{R,t}^{(k)}$, where $\gamma = 1/\sqrt{N_S \mathrm{E}_{SR} + N_0}$. As for node R, the destination node D performs CP removal at first, then passes the received sequence $\mathbf{y}_D^{1,(k)}$ of signal vectors[3]

$$\mathbf{y}_{D,t}^{1,(k)} = \sqrt{\mathrm{E}_{SD}} \sum_{l=0}^{L_{SD}-1} \mathbf{H}_{1,l}^{SD^{(k)}} \mathbf{z}_{1,(t-l) \bmod \frac{T}{2}} + \mathbf{n}_{D,t}^{1,(k)}, \tag{2.5}$$

for $t = 0, \cdots, T/2-1$, to the receiver although it remains unprocessed until the end of the second slot. Note that the exponent $i \in \{1, 2\}$ in $\mathbf{y}_D^{i,(k)}$ denotes the TS index since the $\{S \to D\}$ link is involved in transmission over two consecutive time slots. For the second TS, node R forwards $\widetilde{\mathbf{y}}_R^{(k)}$ to the destination node D while node S is transmitting $\mathbf{z}_2$. Hence, the destination node will see during the second slot a superposition of two transmitted blocks $\widetilde{\mathbf{y}}_R^{(k)}$ and $\mathbf{z}_2$ after deleting the CP portion of length L_{cp} being added to both of them. The received sequence $\mathbf{y}_D^{2,(k)}$ made of signal vectors $\left\{\mathbf{y}_{D,t}^{2,(k)} : t = 0, \cdots, T/2-1\right\}$ at the level of

[2] $\delta_{m,n}$ is the Kronecker symbol that equals either to 1 if $m = n$ or 0 otherwise.

[3] For the sake of simplicity, we assume that the noise at the respective receiving node $B \in \{R, D\}$ follows a Gaussian distribution $\mathcal{N}(\mathbf{0}_{N_B \times 1}, N_0 \mathbf{I}_{N_B})$.

node D can therefore be expressed as

$$\mathbf{y}_{D,t}^{2,(k)} = \gamma\sqrt{\mathrm{E}_{SR}\mathrm{E}_{RD}}\sum_{l=0}^{L_{SRD}-1}\mathbf{H}_l^{SRD^{(k)}}\mathbf{z}_{1,(t-l)\bmod\frac{T}{2}} + \sqrt{\mathrm{E}_{SD}}\sum_{l=0}^{L_{SD}-1}\mathbf{H}_{2,l}^{SD^{(k)}}\mathbf{z}_{2,(t-l)\bmod\frac{T}{2}} + \mathbf{n}_{D,t}^{\mathrm{res},(k)}, \tag{2.6}$$

where the channel matrix $\mathbf{H}_l^{SRD^{(k)}}$ is computed, for $l = 0, \cdots, L_{SRD}-1$ with $L_{SRD} = L_{SR}+L_{RD}-1$, as the two-dimensional convolution of channel matrices $\mathbf{H}_l^{RD^{(k)}}$ and $\mathbf{H}_l^{SR^{(k)}}$.

$$\mathbf{n}_{D,t}^{\mathrm{res},(k)} = \gamma\sqrt{\mathrm{E}_{RD}}\sum_{l=0}^{L_{RD}-1}\mathbf{H}_l^{RD^{(k)}}\mathbf{n}_{R,(t-l)\bmod\frac{T}{2}}^{(k)} + \mathbf{n}_{D,t}^{2,(k)} \tag{2.7}$$

is the residual additive noise in $\mathbf{y}_{D,t}^{2,(k)}$ whose conditional covariance matrix, given that node D has perfect knowledge of channel 2 (i.e., $R \to D$ link), is expressed as

$$\Theta_{\mathbf{n}_{D,t}^{\mathrm{res},(k)}\left|\left\{\mathbf{H}_l^{RD^{(k)}}\right\}\right.} = N_0\left[\mathbf{I}_{N_D} + \frac{\mathrm{E}_{RD}}{N_S\mathrm{E}_{SR}+N_0}\sum_{l=0}^{L_{RD}-1}\mathbf{H}_l^{RD^{(k)}}\mathbf{H}_l^{RD^{(k)\mathrm{H}}}\right]. \tag{2.8}$$

To ensure spatial and temporal noise whitening at the destination node D during the second TS, we rather consider the outputs $\widetilde{\mathbf{y}}_{D,t}^{2,(k)} = \mathbf{F}\mathbf{y}_{D,t}^{2,(k)}$ of the whitening filter $\mathbf{F} = \mathbf{L}^{-1}$, where $\mathbf{L}$ results from the following Cholesky factorization

$$\Theta_{\widetilde{\mathbf{n}}_{D,t}^{2,(k)}\left|\left\{\mathbf{H}_l^{RD^{(k)}}\right\}\right.} = N_0\mathbf{L}\mathbf{L}^{\mathrm{H}}. \tag{2.9}$$

The resulting sequence $\widetilde{\mathbf{y}}_D^{2,(k)} = \left\{\widetilde{\mathbf{y}}_{D,t}^{2,(k)} : t = 0, \cdots, T/2-1\right\}$ is then passed to the receiver, which in turn builds up the augmented size signal vector

$$\mathbf{y}_{D,t}^{\mathrm{equ}^{(k)}} = \begin{bmatrix}\mathbf{y}_{D,t}^{1,(k)} \\ \widetilde{\mathbf{y}}_{D,t}^{2,(k)}\end{bmatrix} \in \mathbb{C}^{2N_D\times 1}, \tag{2.10}$$

for $t = 0, \cdots, T/2-1$, corresponding to reception over two consecutive time slots. Equation (2.10) can be re-written explicitly as

$$\mathbf{y}_{D,t}^{\mathrm{equ}^{(k)}} = \sum_{l=0}^{L_{equ}-1}\mathbf{H}_l^{\mathrm{equ}^{(k)}}\mathbf{z}_{(t-l)\bmod\frac{T}{2}} + \mathbf{n}_{D,t}^{\mathrm{equ}^{(k)}}, \tag{2.11}$$

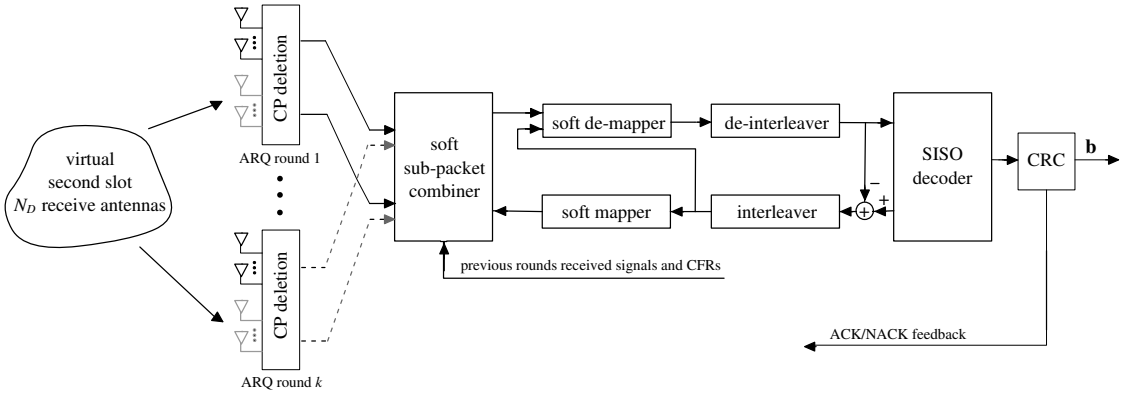

Figure 2.4: Building blocks of the proposed turbo receiver.

where the equivalent channel matrix $\mathbf{H}_l^{\mathrm{equ}^{(k)}} \in \mathbb{C}^{2N_D \times 2N_S}$ has been carefully introduced as a k-parity dependent matrix having the following form

$$\begin{cases} \mathbf{H}_l^{\mathrm{equ}^{(k)}} = \begin{bmatrix} \underline{\mathbf{A}}_l^{(k)} & \mathbf{0}_{N_S \times N_D} \\ \underline{\mathbf{B}}_l^{(k)} & \underline{\mathbf{C}}_l^{(k)} \end{bmatrix}, \ k \text{ odd} \\ \mathbf{H}_l^{\mathrm{equ}^{(k)}} = \begin{bmatrix} \mathbf{0}_{N_S \times N_D} & \underline{\mathbf{A}}_l^{(k)} \\ \underline{\mathbf{C}}_l^{(k)} & \underline{\mathbf{B}}_l^{(k)} \end{bmatrix}, \ k \text{ even} \end{cases} . \tag{2.12}$$

In fact, the splitting rule described earlier now becomes transparent to node D as no matter node S has to send firstly sub-packet $\mathbf{z}_1$ or $\mathbf{z}_2$, the issue is translated into perceiving differently the equivalent channel matrix $\mathbf{H}_l^{\mathrm{equ}^{(k)}}$ at each ARQ round k. The intermediate channel matrices $\underline{\mathbf{A}}_l^{(k)}$, $\underline{\mathbf{B}}_l^{(k)}$, and $\underline{\mathbf{C}}_l^{(k)}$ are defined as

$$\begin{cases} \underline{\mathbf{A}}_l^{(k)} = \sqrt{\mathrm{E}_{SD}}\mathbf{H}_{1,l}^{SD^{(k)}} & ; \ 0 \le l \le L_{SD} - 1 \\ \underline{\mathbf{A}}_l^{(k)} = \mathbf{0}_{N_D \times N_S} & ; \ l \le L_{SD} \\ \underline{\mathbf{B}}_l^{(k)} = \gamma\sqrt{\mathrm{E}_{SR}\mathrm{E}_{RD}}\mathbf{F}\mathbf{H}_l^{SRD^{(k)}} & ; \ 0 \le l \le L_{SRD} - 1 \\ \underline{\mathbf{B}}_l^{(k)} = \mathbf{0}_{N_D \times N_S} & ; \ l \le L_{SRD} \\ \underline{\mathbf{C}}_l^{(k)} = \sqrt{\mathrm{E}_{SD}}\mathbf{F}\mathbf{H}_{2,l}^{SD^{(k)}} & ; \ 0 \le l \le L_{SD} - 1 \\ \underline{\mathbf{C}}_l^{(k)} = \mathbf{0}_{N_D \times N_S} & ; \ l \le L_{SD} \end{cases} . \tag{2.13}$$

From (2.11), it is quit straightforward to infer that the two-slots transmission strategy used by node S allows us to come up with a virtual point-to-point $2N_D \times 2N_S$ MIMO system. Both ends of this system form a quasi-static frequency selective fading MIMO channel having $L_{equ} = \max\{L_{SRD}, L_{SD}\}$ independent paths, and time-invariant over a duration of $\frac{T}{2}$ channel uses. The virtual channel input symbol vector at channel use t is expressed as

$$\mathbf{z}_t \triangleq \begin{bmatrix} \mathbf{z}_{1,t} \\ \mathbf{z}_{2,t} \end{bmatrix} \triangleq \begin{bmatrix} \mathbf{z}_t^{(1)} \\ \vdots \\ \mathbf{z}_t^{(2N_S)} \end{bmatrix} \in \mathcal{X}^{2N_S \times 1}, \tag{2.14}$$

while the additive white Gaussian noise vector $\mathbf{n}_{D,t}^{\text{equ}^{(k)}}$ is explicitly given by

$$\mathbf{n}_{D,t}^{\text{equ}^{(k)})} \triangleq \begin{bmatrix} \mathbf{n}_{D,t}^{1,(k)} \\ \mathbf{F}\mathbf{n}_{D,t}^{\text{res},(k)} \end{bmatrix} \sim \mathcal{N}(\mathbf{0}_{2N_D \times 2N_D}, N_0 \mathbf{I}_{2N_D}). \tag{2.15}$$

In the sequel, we will refer to $\mathbf{z}_t^{(i)} \in \mathcal{X}$ as being virtually the transmitted symbol by node S at channel use $t = 0, \cdots, T/2-1$ from antenna $i = 1, \cdots, 2N_S$, and no longer look at (2.1). Once signal vector $\mathbf{y}_{D,t}^{\text{equ}^{(k)}}$ is constructed, it is then used jointly with all the previously received signals $\mathbf{y}_{D,t}^{\text{equ}^{(k-1)}}, \cdots, \mathbf{y}_{D,t}^{\text{equ}^{(1)}}$ kept in memory, to form the $2N_D k \times 1$ equivalent received signal vector[4]

$$\underbrace{\begin{bmatrix} \mathbf{y}_{D,t}^{\text{equ}^{(1)}} \\ \vdots \\ \mathbf{y}_{D,t}^{\text{equ}^{(k)}} \end{bmatrix}}_{\bar{\mathbf{y}}_{D,t}^{\text{equ},k}} = \sum_{l=0}^{L_{equ}-1} \underbrace{\begin{bmatrix} \mathbf{H}_l^{\text{equ}^{(1)}} \\ \vdots \\ \mathbf{H}_l^{\text{equ}^{(k)}} \end{bmatrix}}_{\bar{\mathbf{H}}_l^{\text{equ},k}} \mathbf{z}_{(t-l) \bmod \frac{T}{2}} + \underbrace{\begin{bmatrix} \mathbf{n}_{D,t}^{\text{equ}^{(1)}} \\ \vdots \\ \mathbf{n}_{D,t}^{\text{equ}^{(k)}} \end{bmatrix}}_{\bar{\mathbf{n}}_{D,t}^{\text{equ},k}}, \tag{2.16}$$

for $t = 0, \cdots, T/2-1$, which will serve to decode the transmitted packet of information bits $\mathbf{b}$. If the decoding outcome is erroneous and $k < K$, node D send a NACK feedback to S in order to start another ARQ round $k+1$. However, a positive acknowledgment (ACK) may be sent to S by node D if successful decoding is detected, in which case node S should

[4] An obvious practical issue related to constructing signal vector $\bar{\mathbf{y}}_{D,t}^{equ,k}$ and channel matrix $\bar{\mathbf{H}}_l^{equ,k}$ at round k, is that they are built upon those received and kept in memory at round $k-1$. Therefore, the demand in terms of storage memory size gradually increases with the ARQ delay, i.e., number of ARQ rounds. This issue is addressed in Section 2.4.3, and smoothly relaxed to keeping in memory only fixed and small size signal vectors and channel matrices at each ARQ round.

move on to the next symbol packet. We say that our system presents an error when the ARQ round K is reached, i.e. $k = K$, yet the decoding outcome is still erroneous.

2.3 Outage Probability and Average Throughput

In this section, we investigate both the outage probability and average throughput as two meaningful performance limits of the relay ARQ system under focus.

2.3.1 Outage Probability

Pertaining to (2.16) for $k = 1$, the outage probability at a given signal-to-noise ratio (SNR) ρ, denoted by P_{out}, refers to the probability half of the information rate $\mathcal{I}$ between the transmitted block $\underline{\mathbf{z}} = \underset{0\leq t\leq \frac{T}{2}-1}{\mathbf{clmn}} (\mathbf{z}_t)$ and the received block $\underline{\mathbf{y}}^{equ,1} = \underset{0\leq t\leq \frac{T}{2}-1}{\mathbf{clmn}} (\bar{\mathbf{y}}_{D,t}^{equ,1})$ is below a target rate $\mathcal{R}$,

$$P_{out}(\rho, \mathcal{R}) = \Pr\left\{ \frac{1}{2}\mathcal{I}\left(\underline{\mathbf{z}}; \underline{\mathbf{y}}^{equ,1} \left| \left\{ \bar{\mathbf{H}}_l^{equ,1} \right\}, \rho \right.\right) < \mathcal{R} \right\}. \tag{2.17}$$

The factor $\frac{1}{2}$ comes from the fact that one channel use of the equivalent received signal model (2.11) corresponds to two temporal channel uses. It is a contrived hypothesis, as most papers consider, to assume Gaussian channel inputs, i.e. the elements of $\underline{\mathbf{z}}$ follow a Gaussian distribution, for calculating the mutual information rate $\mathcal{I}$. Rather, the more accurate and realistic one consists of constraining the inputs to be from a specific constellation alphabet. The only weakness of this method is the computational complexity required to evaluate the constrained information rate. It increases dramatically as $\mathcal{O}(4^{|\mathcal{X}|N_S(L_{equ}-1)})$ for high constellation orders and large MIMO systems with moderate-to-large channel memories, where $|\mathcal{X}|$ is the constellation order. Therefore, we resort to the first assumption as an alternative that in any way still gives a valid approximation of the real outage probability especially for high loaded transmission scenarios [52, 53]. Information rates for quasi-static frequency selective fading MIMO channels have been addressed in [2, 54]. To extend these results towards expressing the outage probability for our ARQ relay system, we use the renewal theory [55, 57] as well as the observation that allows us to view the presented Chase-type ARQ mechanism, with a maximum number of rounds K, as a repetition coding scheme over K parallel sub-virtual channels [56, p. 194]. Accordingly, given the equivalent

MIMO-ARQ channel model (2.16), (2.17) can be re-written as

$$P_{out}\left(K,\rho,\mathcal{R}\right)=\Pr\left\{\frac{1}{2K}\mathcal{I}\left(\underline{\mathbf{z}};\underline{\mathbf{y}}^{equ,K}\left|\left\{\bar{\mathbf{H}}_l^{equ,K}\right\},\rho\right)<\mathcal{R},\overline{\mathcal{A}}_1,...,\overline{\mathcal{A}}_{K-1}\right\},\tag{2.18}$$

where $\mathcal{A}_k$ represents the event that an ACK feedback is sent to the source node S at round k. By definition, (2.18) represents the probability of the pessimistic event (worst case) for which all ARQ rounds up to the Kth one of our virtual K-round MIMO-ARQ system falls in outage. Therefore, it should give a lower bound on (2.18) for k inferior to K. Though it is quiet complicated to obtain the analytical expression of the outage probability, in subsection 2.3.3 we carry out extensive Monte-Carlo simulations to estimate (2.18).

2.3.2 Average System Throughput

It follows from [57] that the average throughput formula corresponding to the transmission over the equivalent MIMO-ARQ channel (2.16) is given by

$$\eta=\frac{\mathrm{E}\left[R\right]}{\mathrm{E}\left[\mathcal{K}\right]},\tag{2.19}$$

where R is a random reward associated either with $\mathcal{R}$bits/s/Hz when successful packet decoding is detected within the K ARQ rounds or with 0 otherwise, while $\mathcal{K}$ stands for the random inter-renewal time or simply the random number of ARQ rounds consumed to transmit one packet. In an outage probabilistic sense, R takes the values $\mathcal{R}$ and 0 with probabilities $1-P_{\overline{out}}(K,\rho,\mathcal{R})$ and $P_{\overline{out}}(K,\rho,\mathcal{R})$, respectively. Thus, $\mathrm{E}\left[R\right]=\mathcal{R}(1-P_{\overline{out}}(K,\rho,\mathcal{R}))$. We underline that the outage probability $P_{\overline{out}}(K,\rho,\mathcal{R})$, unlike (2.18), does not capture the effect of rate deficiency caused by multiple re-transmissions since we do not divide the mutual information rate $\mathcal{I}$ by K similarly to (2.18). Obviously, the entire throughput η is influenced by this effect through $\mathrm{E}\left[\mathcal{K}\right]$. Therefore, we have

$$P_{\overline{out}}\left(K,\rho,\mathcal{R}\right)=\Pr\left\{\frac{1}{2}\mathcal{I}\left(\underline{\mathbf{z}};\underline{\mathbf{y}}^{equ,K}\left|\left\{\bar{\mathbf{H}}_l^{equ,K}\right\},\rho\right)<\mathcal{R},\overline{\mathcal{B}}_1,...,\overline{\mathcal{B}}_{K-1}\right\},\tag{2.20}$$

where the events $\{\mathcal{B}_k\}$ are similarly defined as $\{\mathcal{A}_k\}$ in (2.18). It is then apparent that (2.20) can be used as a lower bound on the packet error rate (PER) of the relay ARQ system under consideration. Following the same procedure in [3], the explicit formula of

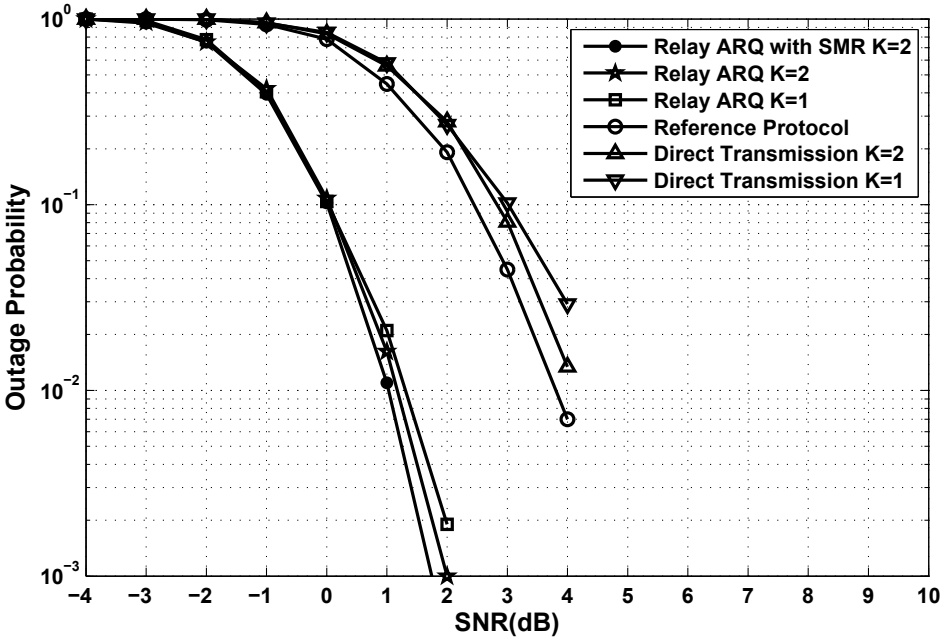

Figure 2.5: Outage probability versus SNR for $l_{SR} = 0.3$, $N_S = N_R = N_D = 2$, $L_{SR} = L_{RD} = L_{SD} = 3$, and $\kappa = 3$.

$\mathrm{E}[\mathcal{K}]$ can be expressed as

$$\mathrm{E}[\mathcal{K}] = \sum_{k=1}^{K} P_{\overline{out}}(k-1, \rho, \mathcal{R}), \tag{2.21}$$

with $P_{\overline{out}}(0, \rho, \mathcal{R}) = 1$, which leads to the following compact form of the average system throughput,

$$\eta = \frac{\mathcal{R}\left(1 - P_{\overline{out}}(K, \rho, \mathcal{R})\right)}{\sum_{k=1}^{K} P_{\overline{out}}(k-1, \rho, \mathcal{R})}. \tag{2.22}$$

2.3.3 Simulation Results

Monte-Carlo simulations are conducted to evaluate the outage probability (2.18) and average throughput (2.19) performances. Our main purpose in this section is to show that the proposed protocol offers high outage probability and throughput performance compared with the so-called AF Protocol II [4] (also refereed to as the orthogonal AF) where the source

broadcasts the symbol packet $\mathbf{x}$ as is (not divided) to both the relay and the destination during the first slot while only the relay node AF the received replicas to the destination during the second slot. Therefore, for the sake of fair comparison, we assume a maximum number of ARQ rounds $K = 2$ (since Protocol II requires two rounds per each symbol packet transmission). We also provide performance of conventional MIMO-ARQ transmission where relaying is not used. In all figures, Protocol II is referred to as "reference protocol".

All nodes have the same number of antennas, $N_S = N_R = N_D = 2$. Channel (1), channel (2), and channel (3) have the same length i.e., $L_{SD} = L_{SR} = L_{RD} = 3$, with equal power profiles, but unbalanced in terms of shadowing and path loss effect. Without loss of generality, we consider a normalized configuration in which the relay node R is located between node S and node D such that $l_{SR} + l_{RD} = l_{SD} = 1$, where l_{AB} denotes the distance between node $A \in \{S, R\}$ and node $B \in \{R, D\}$. Channel energy E_{AB} is also considered to be $E_{AB} = l_{AB}^{-\kappa}$ where κ is the parameter characterizing the path loss exponent. The SNR in all figures corresponds to that of the direct link and is defined as

$$\text{SNR} = \frac{E_{SD} E_b}{N_0}, \tag{2.23}$$

where E_b presents, in the absence of the relay node R, the received energy at node D per useful bit per receive antenna. In the following, we focus on two particular scenarios where the relay node is either close to the source S or the destination D.

2.3.3.1 Scenario 1: Relay close to Source ($l_{SR} = 0.3$)

Figure 2.5 shows that both relay ARQ communication schemes (i.e., with and without SMR) provide superior outage probability performance in comparison to Protocol II. The SNR gap is about 2.5 dB at 10^{-1}outage probability. More interestingly, both mapping techniques achieve high SNR gains starting from the first round due to relay diversity captured by the proposed sub-packet transmission strategy. Also, note that the proposed technique outperforms Protocol II in terms of average throughput as it can be seen from Fig. 2.6. While the latter suffers from the half-duplex constraint leading to throughput saturation at 1bit/s/Hz for SNR values greater than -1.5 dB, relay ARQ achieves this throughput value at only -3.5 dB SNR.

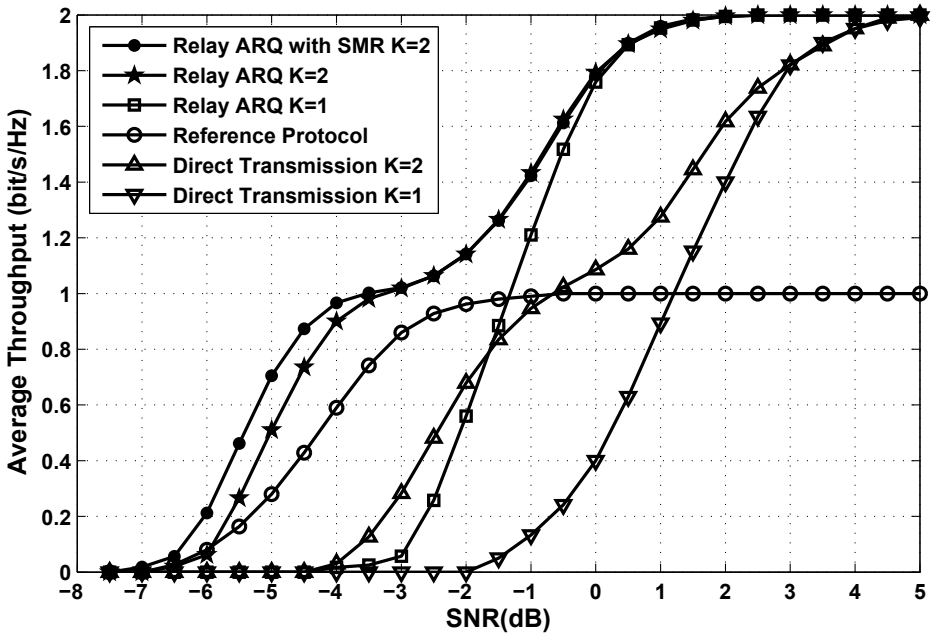

Figure 2.6: Average throughput versus SNR for $l_{SR} = 0.3$, $N_S = N_R = N_D = 2$, $L_{SR} = L_{RD} = L_{SD} = 3$, and $\kappa = 3$.

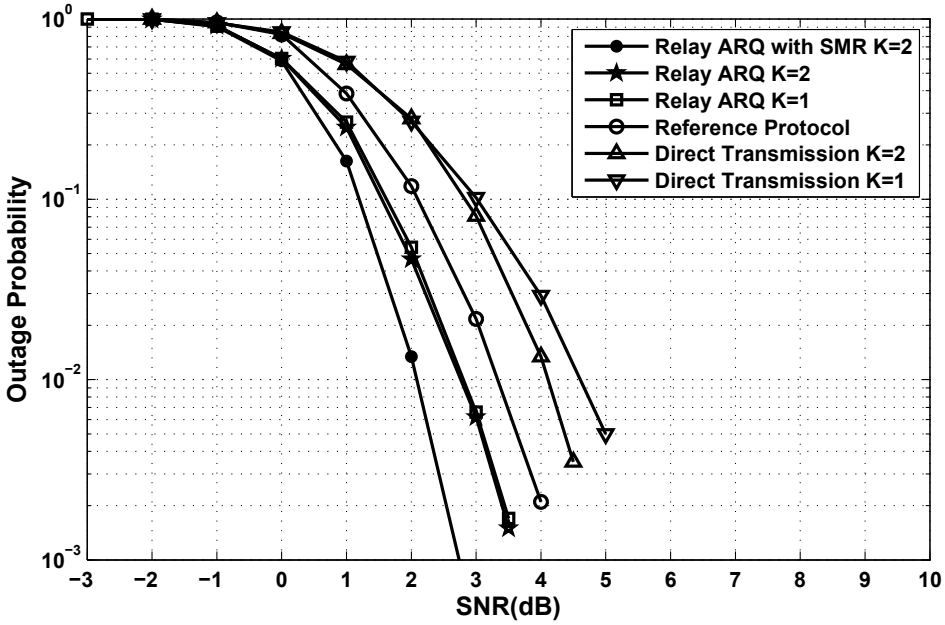

Figure 2.7: Outage probability versus SNR for $l_{SR} = 0.7$, $N_S = N_R = N_D = 2$, $L_{SR} = L_{RD} = L_{SD} = 3$, and $\kappa = 3$.

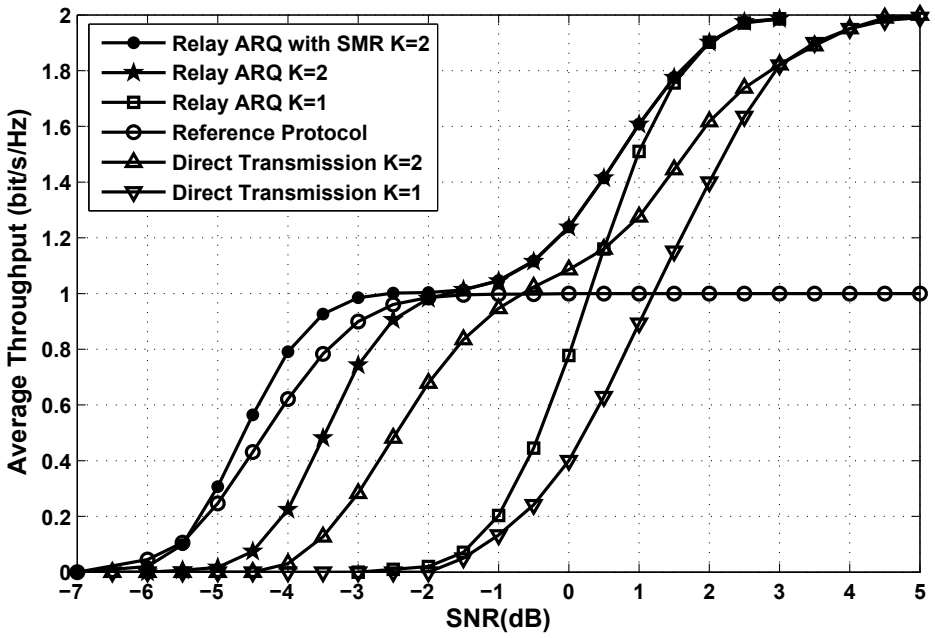

Figure 2.8: Average throughput versus SNR for $l_{SR} = 0.7$, $N_S = N_R = N_D = 2$, $L_{SR} = L_{RD} = L_{SD} = 3$, and $\kappa = 3$.

2.3.3.2 Scenario 2: Relay close to Destination ($l_{SR} = 0.7$)

From Fig. 2.7, we see that relay ARQ with SMR provides a relay diversity gain about 2 dB along with an ARQ gain of about 0.7 dB that appear at the first and the second rounds, respectively. Thus, a sum of 2.7 dB at 10^{-2}outage probability is attained. The relay node location is therefore a determinant factor that greatly influences these gains.

Average throughput curves are reported in Fig. 2.8. We observe that the proposed relay ARQ protocol without SMR suffers from throughput loss due to the long distance between the source and the relay. Conventional relaying provides better throughput performance for the region of low SNR values (typically for SNR < -2 dB). Interestingly, relay ARQ with SMR achieves better throughput performance compared with conventional relaying for the entire SNR region. This improvement is due to the fact that the destination node D leverages the ARQ gain at the second round $K = 2$ in enhancing the average throughput.

2.4 Turbo Packet Combining Receiver Design

In this section, we derive a low complexity recursive over the ARQ rounds turbo receiver. Our main scope is on the design of a soft sub-packet combiner allowing for a joint-over-antenna equalization of the virtual $2N_D k \times 2N_S$ MIMO ARQ channel (2.16), and signal-level sub-packet combining (referring to the combining strategy illustrated in (2.10) and (2.16)). Both tasks are jointly realized in the frequency domain using the MMSE filtering criterion. The building blocks that constitute the proposed receiver scheme are shown in Fig. 2.4.

2.4.1 Brief Description of the Concept

The processing of each received sequence $\bar{\mathbf{y}}_D^{equ,k}$ of signal vectors $\left\{\bar{\mathbf{y}}_{D,t}^{equ,k} : t = 0, \cdots, T/2-1\right\}$, resulting from the joint sub-packet combination over both time slots and multiple ARQ rounds, relies on exchanging (in an iterative fashion) extrinsic information about coded and interleaved bits between the soft sub-packet combiner and the SISO decoder. First of all, assuming that node D has perfect knowledge of round $1, \cdots, k-1$ equivalent CSIs, the soft sub-packet combiner produces a soft estimate $\widetilde{\underline{\mathbf{z}}}^{(k)}$ about $\underline{\mathbf{z}}$ based upon $\bar{\mathbf{y}}_D^{equ,k}$, the

$N_S T \times 1$ conditional mean signal vector $\overline{\underline{\mathbf{z}}} = \underset{0 \le t \le \frac{T}{2}-1}{\mathbf{clmn}} \left(\overline{\mathbf{z}}_t\right)$ where

$$\overline{\mathbf{z}}_t \triangleq \begin{bmatrix} \overline{\mathbf{z}}_t^{(1)} \\ \vdots \\ \overline{\mathbf{z}}_t^{(2N_S)} \end{bmatrix} \in \mathbb{C}^{2N_S \times 1},$$

and the diagonal $N_S T \times N_S T$ conditional covariance matrix $\mathbf{\Theta}_{\overline{\underline{\mathbf{z}}}}^{(k)}$ delivered by the soft mapper. In the following subsections we will elaborate more on how $\widetilde{\underline{\mathbf{z}}}^{(k)}$ is produced based upon $\bar{\mathbf{y}}_D^{equ,k}$, $\overline{\underline{\mathbf{z}}}$ and $\mathbf{\Theta}_{\overline{\underline{\mathbf{z}}}}^{(k)}$. The $(2N_S t + i)$th element in $\overline{\underline{\mathbf{z}}}$ and the $(2N_S t + i, 2N_S t + i)$th element in $\mathbf{\Theta}_{\overline{\underline{\mathbf{z}}}}^{(k)}$ are respectively evaluated by the soft-mapper for $i = 1, \cdots, 2N_S$, and $t = 0, \cdots, T/2 - 1$ as

$$\begin{cases} \overline{\mathbf{z}}_t^{(i)} = \sum_{\mathbf{z} \in \mathcal{X}} \mathbf{z} \mathbf{P}_t^{(i)} \left(\mathbf{z} | \mathcal{A}_t^{(i)}\right) \\ \theta_{i,t}^{(k)} = \sum_{\mathbf{z} \in \mathcal{X}} |\mathbf{z}|^2 \mathbf{P}_t^{(i)} \left(\mathbf{z} | \mathcal{A}_t^{(i)}\right) - \left|\overline{\mathbf{z}}_t^{(i)}\right|^2 \end{cases}, \tag{2.24}$$

where the conditional probability function $\mathbf{P}_t^{(i)} \left(\mathbf{z} | \mathcal{A}_t^{(i)}\right)$ is measured as the probability that symbol $\mathbf{z} \in \mathcal{X}$ had been virtually transmitted by node S at channel use t from antenna i, given the vector $\mathcal{A}_t^{(i)} \in \mathbb{R}^{\log_2(|\mathcal{X}|) \times 1}$ of a-priori LLRs about coded bits corresponding to the transmission of $\mathbf{z}_t^{(i)}$. We return back to the soft sub-packet combiner output, and assume that $\widetilde{\underline{\mathbf{z}}}^{(k)}$ has been produced. Then, the soft de-mapper, also benefiting from the a-priori LLRs in $\mathcal{A}_t^{(i)}$, resorts to the $(2N_S t + i)$th component in $\widetilde{\underline{\mathbf{z}}}^{(k)}$ to extract the corresponding vector of extrinsic LLRs $\mathcal{E}_t^{(i)} \in \mathbb{R}^{\log_2(|\mathcal{X}|) \times 1}$ before being re-grouped as

$$\left[\mathcal{E}_0^{(1)^{\mathrm{T}}}, \cdots, \mathcal{E}_0^{(2N_S)^{\mathrm{T}}}, \cdots, \mathcal{E}_{\frac{T}{2}-1}^{(1)^{\mathrm{T}}}, \cdots, \mathcal{E}_{\frac{T}{2}-1}^{(2N_S)^{\mathrm{T}}}\right] \in \mathbb{R}^{1 \times \log_2(|\mathcal{X}|) N_S T}, \tag{2.25}$$

de-interleaved, and given to the SISO decoder. The updated extrinsic LLRs to be provided to the interleaver are formed by subtracting the a-posteriori LLRs at the output of the SISO decoder from the a-priori LLRs at its input. Then, the soft-mapper, depending on the constellation set and a-priori information received from the interleaver, computes the conditional probabilities $\mathbf{P}_t^{(i)} \left(\mathbf{z} | \mathcal{A}_t^{(i)}\right)$ and fed the soft sub-packet combiner with $\overline{\underline{\mathbf{z}}}$ and $\mathbf{\Theta}_{\overline{\underline{\mathbf{z}}}}^{(k)}$. This completes one iteration, and the same processing is repeated for a preset number of iterations before hard-decision being taken by the SISO decoder. The result is a reliable estimate $\widetilde{\mathbf{b}}$ of the transmitted packet of information bits. The estimated packet is checked using a cyclic redundancy check (CRC) error-detecting code, then an ACK/NACK feedback

is sent back to node S. If it incidentally moves up to round $k+1$, the soft sub-packet combiner and soft-demapper in their initial iteration will benefit from the output of the soft-mapper and interleaver in the last iteration of round k, respectively, as input in the current iteration.

2.4.2 Soft Sub-Packet Combiner Derivation

Pertaining to (2.16), the corresponding $N_D kT \times N_S T$ sub-packet ARQ transmission model is given by

$$\underline{\mathbf{y}}^{equ,k} = \underline{\mathbf{H}}^{equ,k}\underline{\mathbf{z}} + \underline{\mathbf{n}}^{equ,k}, \tag{2.26}$$

where

$$\begin{cases} \underline{\mathbf{z}} = \underset{0\le t\le \frac{T}{2}-1}{\mathbf{clmn}}\,(\mathbf{z}_t) \\ \underline{\mathbf{y}}^{equ,k} = \underset{0\le t\le \frac{T}{2}-1}{\mathbf{clmn}}\,(\bar{\mathbf{y}}_{D,t}^{equ,k}) \\ \underline{\mathbf{n}}^{equ,k} = \underset{0\le t\le \frac{T}{2}}{\mathbf{clmn}}(\bar{\mathbf{n}}_{D,t}^{equ,k}) \end{cases}, \tag{2.27}$$

and $\underline{\mathbf{H}}^{equ,k}$ is a block circulant matrix whose first $N_D kT \times 2N_S$ block column is equal to

$$\left[\bar{\mathbf{H}}_0^{equ,k^{\mathrm{T}}}, \cdots, \bar{\mathbf{H}}_{L_{equ}-1}^{equ,k^{\mathrm{T}}}, \mathbf{0}_{2N_S\times 2N_D k(T/2-L_{equ})}\right]^{\mathrm{T}}. \tag{2.28}$$

Therefore, it can be block-diagonalized in the Fourier basis as

$$\underline{\mathbf{H}}^{equ,k} = \mathbf{U}_{T/2,2N_D k}^{\mathrm{H}}\underline{\Delta}^{(k)}\mathbf{U}_{T/2,2N_S k}, \tag{2.29}$$

where $\underline{\Delta}^{(k)} \in \mathbb{C}^{N_D kT\times N_S T}$ is a block diagonal matrix holding on its diagonal the $2N_D k\times 2N_S$ matrices $\underline{\Delta}_0^{(k)}, \cdots, \underline{\Delta}_{T/2-1}^{(k)}$ that can be computed for $t = 0, \cdots, T/2-1$ as

$$\underline{\Delta}_t^{(k)} = \sum_{l=0}^{L_{equ}-1} \bar{\mathbf{H}}_l^{equ,k} \exp\left\{-j\frac{4\pi tl}{T}\right\}. \tag{2.30}$$

As we may also be interested in expressing the memoryless single round k sub-packet transmission model, we similarly to (2.26) get from (2.11) the following $N_D T \times N_S T$ model

$$\underline{\mathbf{y}}^{equ^{(k)}} = \underline{\mathbf{H}}^{equ^{(k)}}\underline{\mathbf{z}} + \underline{\mathbf{n}}^{equ^{(k)}}, \tag{2.31}$$

where

$$\begin{cases} \underline{\mathbf{y}}^{equ^{(k)}} = \underset{0\le t\le \frac{T}{2}-1}{\mathbf{clmn}} (\mathbf{y}_{D,t}^{equ^{(k)}}) \\ \underline{\mathbf{n}}^{equ^{(k)}} = \underset{0\le t\le \frac{T}{2}}{\mathbf{clmn}} (\mathbf{n}_{D,t}^{equ^{(k)}}) \end{cases}, \tag{2.32}$$

and $\underline{\mathbf{H}}^{equ^{(k)}}$ is a block circulant matrix whose first $N_D T \times 2N_S$ block column is equal to

$$\left[\mathbf{H}_0^{equ^{(k)^{\mathrm{T}}}}, \cdots, \mathbf{H}_{L_{equ}-1}^{equ^{(k)^{\mathrm{T}}}}, \mathbf{0}_{2N_S\times 2N_D(T/2-L_{equ})}\right]^{\mathrm{T}}. \tag{2.33}$$

It can be block diagonalized in the Fourier basis to $\underline{\Upsilon}^{(k)}$ as $\underline{\mathbf{H}}^{equ,k}$ in (2.29). By applying the DFT to both sides of (2.31) and (2.26), we respectively obtain the following single and multi-round frequency domain (FD) sub-packet ARQ transmission models

$$\underline{\mathbf{y}}_f^{equ^{(k)}} = \underline{\Upsilon}^{(k)}\underline{\mathbf{z}}_f + \underline{\mathbf{n}}_f^{equ^{(k)}}, \tag{2.34}$$

$$\underline{\mathbf{y}}_f^{equ,k} = \underline{\Delta}^{(k)}\underline{\mathbf{z}}_f + \underline{\mathbf{n}}_f^{equ,k}. \tag{2.35}$$

By solving the optimization problem in the MMSE filtering sense related to (2.35), we obtain a soft estimate $\widetilde{\underline{\mathbf{z}}}_f^{(k)}$ about $\underline{\mathbf{z}}_f$ according to the following joint forward-backward filtering and signal-level sub-packet combining structure

$$\widetilde{\underline{\mathbf{z}}}_f^{(k)} = \mathbf{\Phi}^{(k)}\underline{\mathbf{y}}_f^{equ,k} - \mathbf{\Psi}^{(k)}\overline{\underline{\mathbf{z}}}_f, \tag{2.36}$$

where the forward filter $\mathbf{\Phi}^{(k)} = \mathrm{diag}\left\{\mathbf{\Phi}_0^{(k)}, \cdots, \mathbf{\Phi}_{T/2-1}^{(k)}\right\}$, and backward filter $\mathbf{\Psi}^{(k)} = \mathrm{diag}\left\{\Psi_0^{(k)}, \cdots, \Psi_{T/2-1}^{(k)}\right\}$ are expressed, for $t = 0, \cdots, T/2-1$, as

$$\begin{cases} \mathbf{\Phi}_t^k = \frac{1}{N_0}\underline{\Delta}_t^{(k)^{\mathrm{H}}}\left\{\mathbf{I}_{2N_D k} + \underline{\Delta}_t^{(k)}\mathbf{C}_t^{-1}\underline{\Delta}_t^{(k)^{\mathrm{H}}}\right\} \\ \mathbf{C}_t^{-1} = N_0\widetilde{\mathbf{\Theta}}_{\underline{\mathbf{z}}}^{(k)^{-1}} + \underline{\Delta}_t^{(k)^{\mathrm{H}}}\underline{\Delta}_t^{(k)} \\ \Psi_t^k = \mathbf{\Phi}_t^{(k)}\underline{\Delta}_t^{(k)} - \frac{2}{T}\sum_{i=0}^{T/2-1}\mathbf{\Phi}_t^{(k)}\underline{\Delta}_t^{(k)} \end{cases}. \tag{2.37}$$

In (2.37), the diagonal matrix $\widetilde{\mathbf{\Theta}}_{\underline{\mathbf{z}}}^{(k)}$ has been introduced as the time average of $\mathbf{\Theta}_{\underline{\mathbf{z}}}^{(k)}$, whose $(2N_S t + i, 2N_S t + i)$th diagonal element is computed as

$$\widetilde{\theta}_i^{(k)} = \frac{2}{T}\sum_{t=0}^{T/2-1}\theta_{i,t}^{(k)}. \tag{2.38}$$

For the purpose of reducing the computational load of the proposed receiver, notice that inverting channel matrices $\left\{\mathbf{C}_t^{-1}\right\}$ in (2.37) incurs, thanks to the matrix inversion lemma [76], only a computational complexity order that is cubic against $2N_S$, instead of $2N_Dk$ [75]. This is a critical solved issue in our analysis since the complexity order would have been increasing with the ARQ delay. Once the soft sub-packet combiner constructs the soft symbol vector $\widetilde{\underline{\mathbf{z}}}_f^{(k)}$, it takes its DFT inverse to get the equalized time domain vector $\widetilde{\underline{\mathbf{z}}}^{(k)}$. The rest goes with what we have already described in the previous subsection.

2.4.3 Recursive Implementation

To get some intuition behind the recursion process, we re-express the matrix product $\underline{\Delta}_t^{(k)^{\mathrm{H}}}\underline{\Delta}_t^{(k)}$ in (2.37) as

$$\underline{\Delta}_t^{(k)^{\mathrm{H}}}\underline{\Delta}_t^{(k)} \;=\; \sum_{p=1}^{k}\underline{\Upsilon}^{(p)^{\mathrm{H}}}\underline{\Upsilon}^{(p)}. \tag{2.39}$$

After some manipulations, we introduce the following recursive variables $\underline{\Gamma}_t^{(k)} = \underline{\Gamma}_t^{(k-1)} + \underline{\Upsilon}_t^{(k)^{\mathrm{H}}}\underline{\Upsilon}_t^{(k)}$ (with $\underline{\Gamma}_t^{(0)} = \mathbf{0}_{2N_S\times 2N_S}$) and $\widetilde{\underline{\mathbf{y}}}_f^{equ^{(k)}} = \widetilde{\underline{\mathbf{y}}}_f^{equ^{(k-1)}} + \underline{\Upsilon}^{(k)^{\mathrm{H}}}\underline{\mathbf{y}}_f^{equ^{(k)}}$ (with $\widetilde{\underline{\mathbf{y}}}_f^{equ^{(0)}} = \mathbf{0}_{2N_S\times 1}$) within the equations of (2.37). Therefore, one may re-write (2.36) in a new structure as

$$\widetilde{\underline{\mathbf{z}}}_f^{(k)} = \widetilde{\mathbf{\Phi}}^{(k)}\widetilde{\underline{\mathbf{y}}}_f^{equ^{(k)}} - \widetilde{\mathbf{\Psi}}^{(k)}\overline{\underline{\mathbf{z}}}_f. \tag{2.40}$$

In particular, the previous backward-forward filters have now been adjusted to $\widetilde{\mathbf{\Phi}}^{(k)} = \mathrm{diag}\left\{\widetilde{\mathbf{\Phi}}_0^{(k)},\cdots,\widetilde{\mathbf{\Phi}}_{T/2-1}^{(k)}\right\}$ and $\widetilde{\mathbf{\Psi}}^{(k)} = \mathrm{diag}\left\{\widetilde{\mathbf{\Psi}}_0^{(k)},\cdots,\widetilde{\mathbf{\Psi}}_{T/2-1}^{(k)}\right\}$ with

$$\begin{cases}\widetilde{\mathbf{\Phi}}_t^{(k)} = \frac{1}{N_0}\left\{\mathbf{I}_{2N_S} - \underline{\Gamma}_t^{(k)}\mathbf{C}_t^{-1}\right\}\\ \mathbf{C}_i = N_0\widetilde{\mathbf{\Theta}}_{\overline{\underline{\mathbf{z}}}}^{(k)^{-1}} + \underline{\Gamma}_t^{(k)}\\ \widetilde{\mathbf{\Psi}}_t^{(k)} = \widetilde{\mathbf{\Phi}}_t^{(k)}\underline{\Gamma}_t^{(k)} - \frac{2}{T}\sum_{t=0}^{T/2-1}\widetilde{\mathbf{\Phi}}_t^{(k)}\underline{\Gamma}_t^{(k)}\end{cases}. \tag{2.41}$$

Importantly, implementing these recursions will enable us to avoid storing in memory equivalent received signals and channel frequency responses whose size gradually increase with the ARQ delay. Instead, the soft sub-packet combiner now requires to keep in memory at round k (in the case of packet decoding failure) only two variables $\widetilde{\underline{\mathbf{y}}}_f^{equ^{(k)}} \in \mathbb{C}^{2N_S}$ and $\underline{\Gamma}_t^{(k)} \in \mathbb{C}^{2N_S}$ of fixed size. Furthermore, the computational cost of the proposed recursive

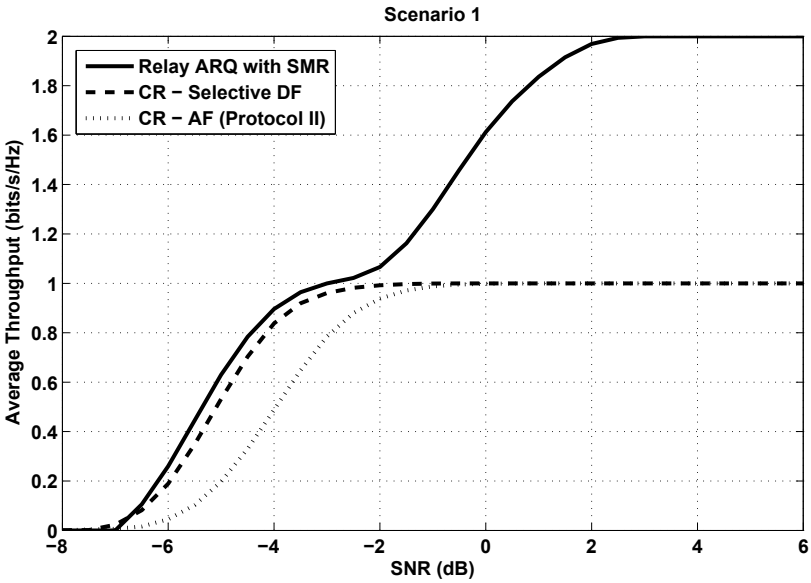

Figure 2.9: Average Throughput versus SNR for $l_{SR} = 0.3$.

implementation is much more reduced compared with the direct implementation of (2.36), since the operations in (2.41) involve only small and fixed channel matrix additions and multiplications.

2.5 Simulation Results and Remarks

Similar to its definition for uncoded transmissions, we focus herein as well on the average throughput as a meaningful performance measure influenced by the packet error rate (PER) and the system latency $\mathcal{L}$ as $\mathcal{T}_a = \mathcal{S}(1-\text{PER})/\mathcal{L}$ where $\mathcal{L}$ is computed as the average of the ARQ system delay over a sufficiently large number of packet transmissions, and $\mathcal{S}$ is the spectral efficiency. Specifically, we assess the proposed turbo receiver scheme in terms of the average throughput via Monte-Carlo simulations in comparison to turbo reception in the context of the AF protocol II named as "AF cooperative relaying" (CR - AF) and "Selective DF cooperative relaying" (CR - Selective DF) protocols [51]. These protocols suggest that node S broadcasts the whole packet $\mathbf{x}$ at once to both R and D nodes during the first TS, while only node R transmits during the second TS. We infer then that in this context each packet transmission will span four time slots (or two ARQ rounds). The system parameters

Table I
Simulation Settings

Parameter	**Description**
T	516
N_S, N_R	2
N_D	3
L_{SR}, L_{RD}, L_{SD}	3
Encoding	$\frac{1}{2}$-Rate Convolutional Encoder $(25, 23)_8$
Interleaver size	1040 (including tail bits)
Modulation	QPSK
Decoding Algorithm	Max-log-Map
De-mapping Approximation	Max-log-Map
Number of iterations	3
Filtering	FD unconditional MMSE
K	2
κ	3
d_{SR}	0.3, 0.6

are shown in Table I. In all figures, the SNR corresponds to that of the direct link and is defined as

$$\text{SNR} = \frac{E_{SD} E_b}{N_0}, \tag{2.42}$$

where in general $E_{AB} = l_{AB}^{-\kappa}$ with κ the path loss exponent and l_{AB} the distance between node A and node B. For the sake of simplicity, we consider a normalized configuration in which node S is located between node R and node D such that $l_{SD} = l_{SR} + l_{RD} = 1$. E_b denotes, in the absence of the relay node, the received energy at the destination node D per useful bit per receive antenna.

The simulations are conducted with distinction between two scenarios. In scenario 1, the relay is closer to the source, while in scenario 2, the relay is closer to the destination. From Fig. 2.9 and Fig. 2.10, we observe that the proposed transmission strategy along with turbo sub-packet combining at the destination node lead to a better average throughput over the entire SNR region compared with turbo reception in the context of conventional ARQ-based relaying protocols. Clearly, when the latters saturate at the value of 1bit/s/Hz for SNR ratios greater than 2 dB due to the half-duplex constraint, the Relay ARQ with SMR scheme continues to increase in average throughput until it achieves the full rate transmission of 2bit/s/Hz. Interestingly, the superiority of the proposed relaying and receiver schemes do

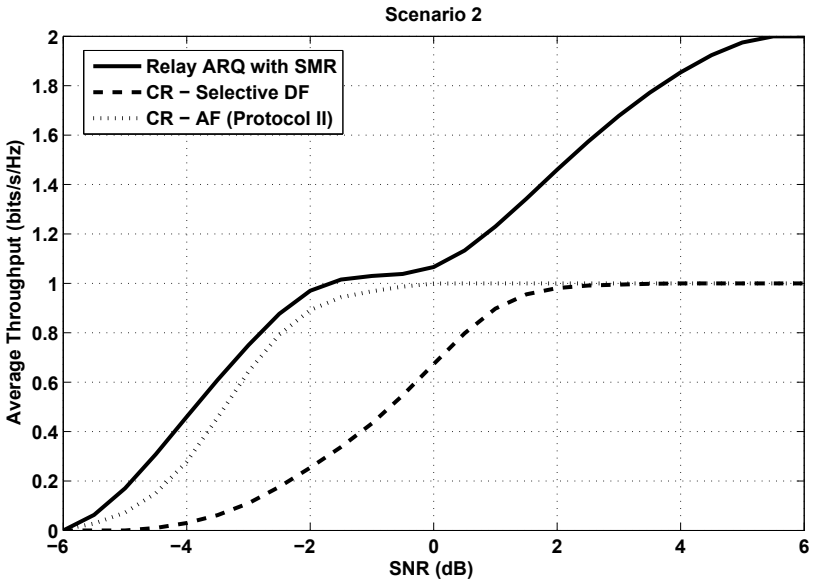

Figure 2.10: Average Throughput versus SNR for $l_{SR} = 0.6$.

not rely on the distance between the source and the relay node. Though CR - AF performs better than selective DF when the relay node R approaches node D (Fig. 2.10) and the opposite when node R approaches node S (Fig. 2.9), the relay ARQ with SMR attains the highest average throughput despite of the relay node position in between the two S and D nodes. This is justified by the fact that node D succeeds in leveraging the available relaying and ARQ diversities via the proposed turbo sub-packet combining strategy in enhancing the average throughput.

Chapter 3

Cognitive SIMO Relaying: An Exact Outage Analysis

3.1 Introduction

In a spectrum-sharing underlay environment, we carry out a comprehensive outage analysis for a secondary (unlicensed) system operating under strict primary (licensed) system outage constraints. We focus on single-user SIMO secondary communications where the direct link is being assisted by a set of single-antenna DF relay nodes acting in a half-duplex selective-and-incremental relaying mode. We propose two transmit power scenarios for the secondary system based on complete or partial knowledge of the cognitive interference channel. For both scenarios, the CDF of the received SNR at the secondary receiving nodes are devised in recursive and tractable closed-form expressions. These statistics are then used to derive the exact end-to-end secondary system outage probability. Also, we investigate the asymptotic outage analysis of the secondary network, and derive the achievable DMT under an interference constraint that is either fixed or proportional to the primary system QoS. Finally, the analytical and simulation results are compared and interestingly shown to perfectly match, while revealing that with a moderate number of primary and secondary receive antennas, the secondary system average spectral efficiency is amply enhanced as opposed to being severely degraded in the single receive antenna case.

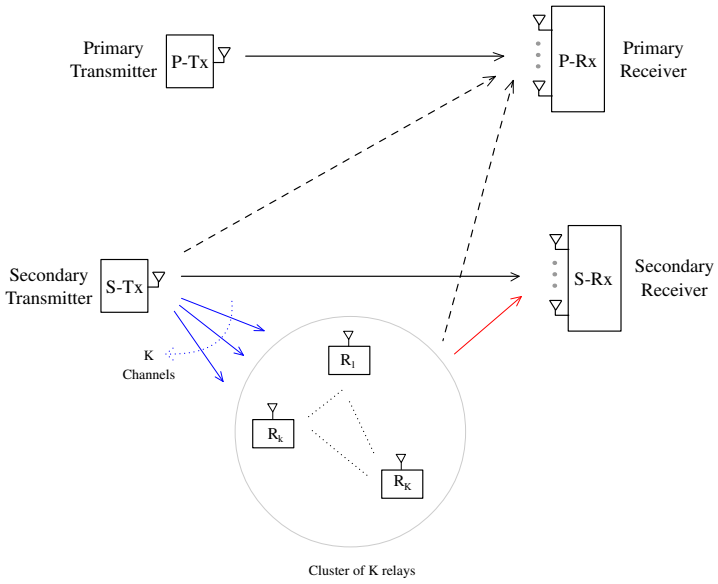

Figure 3.1: SIMO Relay-aided Underlay Cognitive Radio System Model.

3.2 Framework Description

3.2.1 Proposed System Model

Our cognitive radio setup consists of a secondary single-antenna transmitter S-Tx and an N_{s}-antenna receiver S-Rx, both nodes are sharing the same spectrum band with a primary single-antenna transmitter P-Tx and an N_{p}-antenna receiver P-Rx. For a spectrally-efficient secondary system transmission, a cluster $\mathcal{C} = \left\{\mathrm{R_k} : \mathrm{k} = 1, \ldots, \mathrm{K}\right\}$ of K single-antenna relay nodes operating in a half-duplex decode-and-forward selective relaying mode is supposed to assist S-Tx in its transmission towards S-Rx. In a cellular system, a typical communication scenario may arise in the uplink with the primary and secondary base-stations are equipped with multiple receive antennas. A schematic description of the proposed cognitive radio system model is depicted in Fig. 3.1. We denote by indices s, p and $\mathrm{k} \in \{1, \ldots, \mathrm{K}\}$ the secondary, the primary and the k^{th} relay nodes, respectively. Then, we refer to $\mathbf{h}_{\mathrm{pp}}$, $\mathbf{h}_{\mathrm{ss}}$, $\mathbf{h}_{\mathrm{sp}}$, $\mathbf{h}_{\mathrm{sk}}$, $\mathbf{h}_{\mathrm{ks}}$ and $\mathbf{h}_{\mathrm{kp}}$ as the frequency-flat fading mutually-independent SIMO quasi-static channel vectors connecting P-Tx with P-Rx, S-Tx with S-Rx, S-Tx with P-Rx, S-Tx with $\mathrm{R_k}$, $\mathrm{R_k}$ with S-Rx and $\mathrm{R_k}$ with P-Rx, respectively. The components of $\mathbf{h}_{\mathrm{ab}} \in \mathbb{C}^{N_{\mathrm{b}} \times 1}$ with $\mathrm{a} \in \{\mathrm{s}, \mathrm{p}, \mathrm{k}\}$ and $\mathrm{b} \in \{\mathrm{s}, \mathrm{p}, \mathrm{k}\}$ are assumed to be independent identically distributed (i.i.d) and drawn from a zero-mean and λ_{ab}-variance circularly symmetric complex (CSC) Gaussian

distribution. Note that when index b equals to k, we have $N_{\mathrm{k}} = 1$, and thus $\mathbf{h}_{\mathrm{sk}}$ reduces to a one component channel vector. Also, since the relays are forming a cluster of K co-located relays, we can in fact assume that $\lambda_{\mathrm{sk}} = \lambda_{\mathrm{sr}}$, $\lambda_{\mathrm{kp}} = \lambda_{\mathrm{rp}}$ and $\lambda_{\mathrm{ks}} = \lambda_{\mathrm{rs}}$ $\forall \mathrm{k} \in \{1, \ldots, \mathrm{K}\}$. For the ease of presentation, we consider the random variable change,

$$z_{\mathrm{ab}} = \mathbf{h}_{\mathrm{ab}}^{\mathrm{H}} \mathbf{h}_{\mathrm{ab}}, \tag{3.1}$$

leading to the definition of z_{ab} as a random variable that is drawn from a Gamma distribution with shape and scale parameters N_{b} and λ_{ab}, respectively. Herein, we consider a cognitive radio channel where the interference caused by the primary system on the secondary system receiving nodes is negligible, thereby referring to a "Z" topology of the proposed cognitive radio channel model. However, if an "X" topology of the proposed cognitive radio channel model is adopted, our results will still hold as insightful lower bounds on the secondary system outage performance.

3.2.2 Secondary System Transmit Power Model

Prior to each secondary system transmission, the transmitting nodes S-Tx and $\mathrm{R_k}$ for $\mathrm{k} \in \{1, \ldots, \mathrm{K}\}$ have to keep their transmit power under a maximum $\mathrm{P_{s\text{-}max}}$ and $\mathrm{P_{k\text{-}max}}$, respectively, while transmitting simultaneously with P-Tx. In other words, the interference caused by the secondary system at the level of the primary receiver must be limited so as not to violate the QoS of the primary system. From an outage probability perspective, $\mathrm{P_{s\text{-}max}}$ (and similarly $\mathrm{P_{k\text{-}max}}$) can be derived as the solution to the following optimization problem,

$$\begin{aligned} &\text{maximize } \mathrm{P_s} \\ &\begin{cases} \text{subject to } \mathrm{OP_p}(\mathrm{P_s}) \leq \varepsilon_{\mathrm{p}} \\ \text{and } \mathrm{P_s} \leq \bar{\mathrm{P}}_{\mathrm{s}} \end{cases} \end{aligned} \tag{3.2}$$

where $\mathrm{OP_p}$ denotes the outage probability of the primary system, ε_p is an outage threshold that is defined by the primary system to maintain its QoS, and $\bar{\mathrm{P}}_{\mathrm{s}}$ is a practical power limit that should not be exceeded by S-Tx. In resolving the above optimization problem, we distinguish between two transmit power scenarios: the first one when complete I-CSI about the link connecting S-Tx with P-Rx can perfectly be estimated by S-Tx prior to sending its symbol packet to S-Rx, and the second one when S-Tx can only acquire the second order

statistic of the underlying interference channel. The same reasoning applies to a relay $\mathrm{R_k}$ where $\mathrm{k} \in \{1, \ldots, \mathrm{K}\}$ if it is selected to transmit alongside with P-Tx.

Proposition 1: If complete I-CSI about the interference channel $\mathbf{h}_{\mathrm{sp}}$ is acquired at S-Tx, then $\mathrm{P_{s\text{-}max}}$ is given by,

$$\mathrm{P_{s\text{-}max}} = \min\left\{\frac{\bar{\mathrm{P}}_{\mathrm{p}}\lambda_{\mathrm{pp}}\overline{\gamma}^{-1}(N_{\mathrm{p}}, \varepsilon_{\mathrm{p}}) - N_0\Phi_{\mathrm{p}}}{\Phi_{\mathrm{p}} z_{\mathrm{sp}}}, \bar{\mathrm{P}}_{\mathrm{s}}\right\}, \tag{3.3}$$

where Φ_{p} is the received SNR threshold below which the primary system falls in outage. For a given real number $\mathrm{a} \in \mathbb{R}$, $\overline{\gamma}^{-1} : \mathrm{x} \in \mathbb{R} \rightarrow \overline{\gamma}^{-1}(\mathrm{a}, \mathrm{x}) \in \mathbb{R}$ is the inverse function of the regularized lower incomplete Gamma function $\overline{\gamma} : (\mathrm{a}, \mathrm{x}) \in \mathbb{R}^2 \rightarrow \overline{\gamma}(\mathrm{a}, \mathrm{x}) \in \mathbb{R}$ [71, Eq. 8.350.1] with respect to x. N_0 denotes the variance of the additive noise at the primary receiver P-Rx and at the secondary receiver S-Rx as well, that is modeled as a zero-mean CSC Gaussian variable.

Proof: The outage probability of the primary system, that is simply the CDF of the received signal to interference plus noise at the primary receiver, can be expressed as,

$$\mathrm{OP_p}(\mathrm{P_s}) = \overline{\gamma}\left(N_{\mathrm{p}}, \frac{\Phi_{\mathrm{p}}\left(\mathrm{P_s} z_{\mathrm{sp}} + N_0\right)}{\bar{\mathrm{P}}_{\mathrm{p}}\lambda_{\mathrm{pp}}}\right), \tag{3.4}$$

where the quantity $\mathrm{P_s} z_{\mathrm{sp}}$ reflects the residual interference caused by S-Tx. Given z_{sp}, $\mathrm{OP_p}$ is an increasing function of $\mathrm{P_s}$, therefore the maximum transmit power $\mathrm{P_s}$ is achieved when $\mathrm{OP_p}(\mathrm{P_s}) = \varepsilon_{\mathrm{p}}$. Solving this equation, S-Tx can finally adapt its transmit power according to (3.3). Note that in (3.4) we did not integrate $\mathrm{OP_p}$ over the PDF of z_{sp} because the quantity $\mathrm{P_s} z_{\mathrm{sp}}$ is regarded as a constant by P-Tx that is equaling to $\left(\bar{\mathrm{P}}_{\mathrm{p}}\lambda_{\mathrm{pp}}\overline{\gamma}^{-1}(N_{\mathrm{p}}, \varepsilon_{\mathrm{p}}) - N_0\Phi_{\mathrm{p}}\right)/\Phi_{\mathrm{p}}$. In the special case of $\mathrm{P_s}$ is clipped to $\bar{\mathrm{P}}_{\mathrm{s}}$, we know that $\bar{\mathrm{P}}_{\mathrm{s}}$ already satisfies the condition $\mathrm{OP_p}(\bar{\mathrm{P}}_{\mathrm{s}}) \leq \varepsilon_{\mathrm{p}}$.

Even though sometimes advantageous to achieve good outage performance results, acquiring complete I-CSI prior to each secondary system transmission is recognized as a spectrum-consuming strategy, especially if the cognitive interference channel undergoes fast fading variations. A more practical scenario indeed would consist of assuming that S-Tx can only acquire the second order statistic of the interference channel components. In section 3.5, we analyze the impact of both I-CSI estimation scenarios on the overall secondary system outage performance.

Proposition 2: If S-Tx has only a partial I-CSI knowledge about $\mathbf{h}_{\mathrm{sp}}$ measured by the second order statistic, λ_{sp}, of its components, $\mathrm{P}_{\text{s-max}}$ can consequently be derived as,

$$\mathrm{P}_{\text{s-max}} = \min\left\{\frac{\bar{\mathrm{P}}_{\mathrm{p}}\lambda_{\mathrm{pp}}(\mathrm{O}_{\max}-1)}{\Phi_{\mathrm{p}}\lambda_{\mathrm{sp}}}, \bar{\mathrm{P}}_{\mathrm{s}}\right\}, \tag{3.5}$$

where $\mathrm{O}_{\max}$ denotes the greatest root of the following $2N_{\mathrm{p}}$-degree polynomial,

$$\mathrm{P}(\alpha) = (\varepsilon_{\mathrm{p}}-1)\alpha^{2N_{\mathrm{p}}} + \frac{\boldsymbol{e}^{-\frac{\Phi_{\mathrm{p}}N_0}{\bar{\mathrm{P}}_{\mathrm{p}}\lambda_{\mathrm{pp}}}}}{\Gamma(N_{\mathrm{p}})}\sum_{\mathrm{i}_1=0}^{N_{\mathrm{p}}-1}\sum_{\mathrm{i}_2=0}^{\mathrm{i}_1}\frac{\Gamma(\mathrm{i}_2+N_{\mathrm{p}})}{\mathrm{i}_2!(\mathrm{i}_1-\mathrm{i}_2)!}\left(\frac{\Phi_{\mathrm{p}}N_0}{\bar{\mathrm{P}}_{\mathrm{p}}\lambda_{\mathrm{pp}}}\right)^{\mathrm{i}_1-\mathrm{i}_2}(\alpha-1)^{\mathrm{i}_2}\,\alpha^{N_{\mathrm{p}}-\mathrm{i}_2}. \tag{3.6}$$

Kindly refer to Appendix A.

For a small $N_{\mathrm{p}} \in \{1,2,3\}$, $\mathrm{O}_{\max}$ can be expressed in closed-form. Yet, for high values of N_{p}, it can accurately be evaluated using numerical efficient algorithms such as the Jenkins–Traub algorithm.

It is worth noting here that $\mathrm{P}_{\text{s-max}}$ should obviously be positive, i.e. the conditions $\bar{\mathrm{P}}_{\mathrm{p}}\lambda_{\mathrm{pp}}\gamma^{-1}(N_{\mathrm{p}},\varepsilon_{\mathrm{p}}) - \Phi_{\mathrm{p}}N_0 > 0$ and $\mathrm{O}_{\max} - 1 > 0$ must be satisfied in Proposition 1 and Proposition 2, respectively. Interestingly, the satisfaction of both conditions depends only on the primary system settings. That is, the secondary system should keep silent with no transmission opportunity if the primary system settings are not favorable.

3.3 Relaying Protocol and Received SNR Statistics

3.3.1 Scenario 1 - Complete I-CSI Acquisition

We consider the first scenario for which the secondary system transmitting nodes S-Tx and R_{k} for $\mathrm{k} \in \{1,\ldots,\mathrm{K}\}$ are being capable of acquiring perfect CSI about their interference channels, and therefore, transmitting with an adaptive maximum transmit power $\mathrm{P}_{\text{s-max}}$ (3.3) for S-Tx and similarly derived $\mathrm{P}_{\text{k-max}}$ for R_{k}. During the first-hop of the proposed communication protocol, S-Tx broadcasts its symbol packet while all receiving nodes S-Rx, P-Rx, and R_{k} for $\mathrm{k} \in \{1,\ldots,\mathrm{K}\}$ listen to the transmitted symbol packet. In the case the instantaneous received SNR at S-Rx is greater than a certain threshold Φ_{s}, the transmitter S-Tx will move on to another symbol packet. Otherwise, one relay among the relays that have succeeded to meet their SNR thresholds will be selected to forward the

received symbol packet. The ruling on the best relay selection criterion is based on the best second-hop received SNR, and is therefore given by,

$$\mathbf{r} = \underset{\mathrm{k}|\mathrm{R_k}\in\mathcal{S}}{\arg\max} \left\{\mathrm{P_{k\text{-}max}} z_{\mathrm{ks}}\right\}, \tag{3.7}$$

where $\mathrm{P_{k\text{-}max}}$ is the adaptive maximum transmit power of the relay $\mathrm{R_k}$ within $\mathcal{S}$, the subset including all relays that have met their SNR thresholds during the first-hop, thus its cardinal $|\mathcal{S}| \in \{0, \ldots, \mathrm{K}\}$. $\mathrm{P_{k\text{-}max}}$ can be derived similarly to (3.3) as,

$$\mathrm{P_{k\text{-}max}} = \min\left\{\frac{\bar{\mathrm{P}}_{\mathrm{p}}\lambda_{\mathrm{pp}}\overline{\gamma}^{-1}(N_{\mathrm{p}}, \varepsilon_{\mathrm{p}}) - N_0\Phi_{\mathrm{p}}}{\Phi_{\mathrm{p}} z_{\mathrm{kp}}}, \bar{\mathrm{P}}_{\mathrm{s}}\right\}. \tag{3.8}$$

Occasionally, the communication scheme between S-Tx and S-Rx may span two hops. During the first-hop, S-Rx receives the transmitted symbol packet from S-Tx, while during the second-hop, S-Rx receives from $\mathrm{R_r}$ (index $\mathbf{r}$ refers to the selected relay) what it successfully decoded during the first-hop. In the particular case of $|\mathcal{S}| = 0$, the secondary transmitter S-Tx will retransmit during the second-hop the same symbol packet that has been transmitted during the first-hop. Therefore, at the end of the second-hop, the receiver S-Rx will sum up the two instantaneous received SNRs during both hops,

$$\gamma_{\mathrm{ss}}^{(1)} = \min\left\{\frac{\mathrm{I}}{z_{\mathrm{sp}}^{(1)}}, \frac{\bar{\mathrm{P}}_{\mathrm{s}}}{N_0}\right\} z_{\mathrm{ss}}^{(1)} \tag{3.9}$$

and either

$$\gamma_{\mathbf{rs}} = \min\left\{\frac{\mathrm{I}}{z_{\mathbf{rp}}}, \frac{\bar{\mathrm{P}}_{\mathrm{s}}}{N_0}\right\} z_{\mathbf{rs}} \ , \ \text{if } |\mathcal{S}| \neq 0 \tag{3.10}$$

or

$$\gamma_{\mathrm{ss}}^{(2)} = \min\left\{\frac{\mathrm{I}}{z_{\mathrm{sp}}^{(2)}}, \frac{\bar{\mathrm{P}}_{\mathrm{s}}}{N_0}\right\} z_{\mathrm{ss}}^{(2)} \ , \ \text{otherwise}, \tag{3.11}$$

where $\mathrm{I} = \left(\bar{\mathrm{P}}_{\mathrm{p}}\lambda_{\mathrm{pp}}\overline{\gamma}^{-1}\left(N_{\mathrm{p}}, \varepsilon_{\mathrm{p}}\right) / \left(\Phi_{\mathrm{p}} N_0\right)\right) - 1$, before it decides whether the secondary system falls in outage or not. Note that the exponent $\mathrm{i} \in \{1, 2\}$ in $z_{\mathrm{ss}}^{(\mathrm{i})}$ and $z_{\mathrm{sp}}^{(\mathrm{i})}$ has been added to z_{ss} and z_{sp} to differentiate between the first and the second hops since all the cognitive radio channel links experience a quasi-static change from one hop to another. The CDF of the instantaneous received SNRs $\gamma_{\mathrm{ss}}^{(1)}$, $\gamma_{\mathrm{ss}}^{(2)}$, and γ_{sk} for $\mathrm{k} \in \{1, \ldots, \mathrm{K}\}$ can generally be

given by,

$$F_{\mathrm{sb}}(z) = P_{\mathrm{rob}}\left[\min\left\{\frac{\mathrm{I}}{z_{\mathrm{sp}}}, \frac{\bar{\mathrm{P}}_{\mathrm{s}}}{N_0}\right\} z_{\mathrm{sb}} \leq z\right] \tag{3.12}$$

$$= \int_0^{\mathrm{I}N_0/\bar{\mathrm{P}}_{\mathrm{s}}} P_{\mathrm{rob}}\left[\frac{\bar{\mathrm{P}}_{\mathrm{s}}}{N_0} z_{\mathrm{sb}} \leq z\right] \frac{\mathrm{x}^{(N_{\mathrm{p}}-1)}\boldsymbol{e}^{-\mathrm{x}/\lambda_{\mathrm{sp}}}}{\lambda_{\mathrm{sp}}^{N_{\mathrm{p}}}\Gamma(N_{\mathrm{p}})}\mathrm{d}\mathrm{x} + \int_{\mathrm{I}N_0/\bar{\mathrm{P}}_{\mathrm{s}}}^{+\infty} P_{\mathrm{rob}}\left[\frac{\mathrm{I}}{\mathrm{x}} z_{\mathrm{sb}} \leq z\right] \frac{\mathrm{x}^{(N_{\mathrm{p}}-1)}\boldsymbol{e}^{-\mathrm{x}/\lambda_{\mathrm{sp}}}}{\lambda_{\mathrm{sp}}^{N_{\mathrm{p}}}\Gamma(N_{\mathrm{p}})}\mathrm{d}\mathrm{x}$$

$$= 1 - \overline{\gamma}\left(N_{\mathrm{p}}, \frac{\mathrm{I}N_0}{\bar{\mathrm{P}}_{\mathrm{s}}\lambda_{\mathrm{sp}}}\right)\overline{\Gamma}\left(N_{\mathrm{b}}, \frac{zN_0}{\bar{\mathrm{P}}_{\mathrm{s}}\lambda_{\mathrm{sb}}}\right) - \sum_{\mathrm{m}=0}^{N_{\mathrm{s}}-1} \frac{\left(\frac{z}{\mathrm{I}\lambda_{\mathrm{sb}}}\right)^{\mathrm{m}}}{\lambda_{\mathrm{sp}}^{N_{\mathrm{p}}}\Gamma\left(N_{\mathrm{p}}\right)\mathrm{m}!} \frac{\Gamma\left(N_{\mathrm{p}}+\mathrm{m}, \frac{\mathrm{I}N_0}{\bar{\mathrm{P}}_{\mathrm{s}}}\left(\frac{z}{\mathrm{I}\lambda_{\mathrm{sb}}}+\frac{1}{\lambda_{\mathrm{sp}}}\right)\right)}{\left(\frac{z}{\mathrm{I}\lambda_{\mathrm{sb}}}+\frac{1}{\lambda_{\mathrm{sp}}}\right)^{N_{\mathrm{p}}+\mathrm{m}}}$$

where index b should be set to s or k depending at which node S-Rx or $\mathrm{R_k}$ the received SNR is computed, $\Gamma(\mathrm{n},\mathrm{x})$ is the upper incomplete Gamma function [71, Eq. 8.352.2], while $\overline{\gamma}(\mathrm{n},\mathrm{x}) = \gamma(\mathrm{n},\mathrm{x})/\gamma(\mathrm{n})$ and $\overline{\Gamma}(\mathrm{n},\mathrm{x}) = \Gamma(\mathrm{n},\mathrm{x})/\Gamma(\mathrm{n})$ stand for the regularized lower and upper incomplete Gamma functions, respectively. Let us now consider that $|\mathcal{S}| \in \{1,\ldots,\mathrm{K}\}$, i.e. $|\mathcal{S}|$ relays are now eligible candidates to forward the decoded symbol packet within the second-hop.

Lemma 1: According to the proposed best relay selection method (3.7), the conditional CDF of the instantaneous received SNR $\gamma_{\mathbf{rs}}$ at S-Rx during the second-hop can be expressed as,

$$F_{\mathbf{rs}||\mathcal{S}|}(z) = \sum_{\mathrm{u}=0}^{|\mathcal{S}|} \boldsymbol{e}^{-\frac{zN_0\mathrm{u}}{\bar{\mathrm{P}}_{\mathrm{s}}\lambda_{\mathrm{rs}}}} \sum_{\mathrm{v}=0}^{\mathrm{u}(2N_{\mathrm{s}}+N_{\mathrm{p}}-2)} \mathcal{E}_{\mathrm{u,v}} \left(\frac{z}{\mathrm{I}\lambda_{\mathrm{rs}}} + \frac{1}{\lambda_{\mathrm{rp}}}\right)^{\mathrm{v}-\mathrm{u}(N_{\mathrm{s}}+N_{\mathrm{p}}-1)}, \tag{3.13}$$

where $\mathcal{E}_{\mathrm{u,v}}$ for $\mathrm{u} \in \{0,\ldots,|\mathcal{S}|\}$ and $\mathrm{v} \in \{0,\ldots,\mathrm{u}(2N_{\mathrm{s}}+N_{\mathrm{p}}-2)\}$ is a multiplicative constant that is explicitly derived in the proof of this lemma. Kindly refer to Appendix B.

3.3.2 Scenario 2 - Partial I-CSI Acquisition

Herein, we consider that S-Tx and $\mathrm{R_k}$ for $\mathrm{k} \in \{1,\ldots,\mathrm{K}\}$ can only acquire the second order statistics λ_{sp} and λ_{rp}, respectively, of their interference channels components. Consequently, the CDF of the received SNR at S-Rx and $\mathrm{R_k}$ during the first-hop can simply be expressed as,

$$F_{\mathrm{sb}}(z) = \overline{\gamma}\left(N_{\mathrm{b}}, \frac{zN_0}{\lambda_{\mathrm{sp}}\mathrm{P}_{\text{s-max}}}\right), \tag{3.14}$$

where index b should either be replaced by s or k indices depending on the receiving node S-Rx or $\mathrm{R_k}$, and $\mathrm{P_{s\text{-}max}}$ is given by (3.5). The ruling on the best relay selection now relaxes to the best squared modules sum of the second hop channel gains. Hence, it can be formulated as,

$$\mathbf{r} = \underset{\mathrm{k}|\mathrm{R_k}\in\mathcal{S}}{\arg\max}\left\{z_{\mathrm{ks}}\right\}. \tag{3.15}$$

Lemma 2: Under partial I-CSI acquisition, and given that (3.15) is applied in the case of $|\mathcal{S}| \neq 0$, the conditional CDF of the received SNR at S-Rx during the second-hop is given by,

$$F_{\mathbf{rs}||\mathcal{S}|}\left(z\right) = \sum_{\mathrm{u}=0}^{|\mathcal{S}|} \boldsymbol{e}^{-\frac{z\mathrm{u}N_0}{\lambda_{\mathrm{rs}}\mathrm{P}_{\mathbf{r}\text{-}\max}}} \sum_{\mathrm{v}=0}^{\mathrm{u}(N_{\mathrm{s}}-1)} \mathcal{E}_{\mathrm{u,v}} z^{\mathrm{v}}, \tag{3.16}$$

where $\mathcal{E}_{\mathrm{u,v}}$ for $\mathrm{u} \in \{0,\ldots,|\mathcal{S}|\}$ and $\mathrm{v} \in \{0,\ldots,\mathrm{u}(N_{\mathrm{s}}-1)\}$ are recursively computed as,

$$\begin{cases} \mathcal{E}_{\mathrm{u},0} = \binom{|\mathcal{S}|}{\mathrm{u}}(-1)^{\mathrm{u}} & , \mathrm{v}=0 \\ \mathcal{E}_{\mathrm{u,v}} = \dfrac{1}{\mathrm{v}} \displaystyle\sum_{\mathrm{n}=1}^{\min\{\mathrm{v},N_{\mathrm{s}}-1\}} \dfrac{(\mathrm{nu}-\mathrm{v}+\mathrm{n})\,\mathcal{E}_{\mathrm{u,v-n}}}{\mathrm{n}!\left(\lambda_{\mathrm{rs}}\mathrm{P}_{\mathbf{r}\text{-}\max}/N_0\right)^{\mathrm{n}}} & , 1 \leq \mathrm{v} \leq \mathrm{u}(N_{\mathrm{s}}-1). \end{cases} \tag{3.17}$$

Kindly refer to Appendix C.

3.4 Exact and Asymptotic Outage Analysis

3.4.1 Outage Probability

Using the total probability law, the end-to-end outage probability of the proposed SIMO relay-aided cognitive radio system at a given $\rho = \bar{\mathrm{P}}_{\mathrm{s}}/N_0$ and transmission rate $\mathcal{R}_{\mathrm{s}}$ is be given by,

$$\mathrm{OP_s}\left(\rho,\mathcal{R}_{\mathrm{s}}\right) = \mathrm{OP}_{\mathrm{s}}^{(1)}\left(\rho,\mathcal{R}_{\mathrm{s}}\right) + \sum_{\mathrm{k}=1}^{\mathrm{K}} \binom{\mathrm{k}}{\mathrm{K}} \mathrm{OP}_{\mathrm{s,k}}^{(2)}\left(\rho,\mathcal{R}_{\mathrm{s}}\right), \tag{3.18}$$

where the first term $\mathrm{OP}_{\mathrm{s}}^{(1)}\left(\rho,\mathcal{R}_{\mathrm{s}}\right)$ measures the probability of the event occurring when the secondary receiver S-Rx fails to meet its SNR threshold $\Phi_{\mathrm{s}} = 2^{\mathcal{R}_{\mathrm{s}}} - 1$ and $\dot{\Phi}_{\mathrm{s}} = 2^{2\mathcal{R}_{\mathrm{s}}} - 1$ during the first and second hops, respectively, given that no relay within the cluster $\mathcal{C}$ has succeeded to meet its instantaneous SNR threshold $\dot{\Phi}_{\mathrm{s}}$ during the first-hop. Also,

each term $\mathrm{OP}_{\mathrm{s,k}}^{(2)}(\rho, \mathcal{R}_{\mathrm{s}})$ of the summation in (3.18) corresponds to the probability of the complementary event occurring when $|\mathcal{S}| = \mathrm{k} \geq 1$, yet the sum $\gamma_{\mathrm{ss}}^{(1)} + \gamma_{\mathbf{r}_{\mathrm{s}|\mathrm{k}}}$ of the received SNRs at S-Rx during the first and second hops is still inferior to $\dot{\Phi}_{\mathrm{s}}$. Therefore, they can respectively be expressed as,

$$\mathrm{OP}_{\mathrm{s}}^{(1)}(\rho, \mathcal{R}_{\mathrm{s}}) = P_{\mathrm{rob}}\left(\gamma_{\mathrm{ss}}^{(1)} < \Phi_{\mathrm{s}}, \gamma_{\mathrm{ss}}^{(1)} + \gamma_{\mathrm{ss}}^{(2)} < \dot{\Phi}_{\mathrm{s}}, \gamma_{\mathrm{s1}} < \dot{\Phi}_{\mathrm{s}}, \ldots, \gamma_{\mathrm{sK}} < \dot{\Phi}_{\mathrm{s}}\right), \tag{3.19}$$

$$\mathrm{OP}_{\mathrm{s,k}}^{(2)}(\rho, \mathcal{R}_{\mathrm{s}}) = P_{\mathrm{rob}}\left(\gamma_{\mathrm{ss}}^{(1)} < \Phi_{\mathrm{s}}, \gamma_{\mathrm{ss}}^{(1)} + \gamma_{\mathbf{r}_{\mathrm{s}|\mathrm{k}}} < \dot{\Phi}_{\mathrm{s}}, \gamma_{\mathrm{s1}} \geq \dot{\Phi}_{\mathrm{s}}, \ldots, \gamma_{\mathrm{sk}} \geq \dot{\Phi}_{\mathrm{s}}, \gamma_{\mathrm{sk+1}} < \dot{\Phi}_{\mathrm{s}}, \ldots, \gamma_{\mathrm{sK}} < \dot{\Phi}_{\mathrm{s}}\right). \tag{3.20}$$

It is noteworthy that due to the clustered structure of the relay nodes within $\mathcal{C}$, what it matters in the derivation of $\mathrm{OP}_{\mathrm{s,k}}^{(2)}(\rho, \mathcal{R}_{\mathrm{s}})$ is the cardinal $|\mathcal{S}| = \mathrm{k}$, and not the indices of the relays belonging to the subset $\mathcal{S}$.

Scenario 1

To derive $\mathrm{OP}_{\mathrm{s}}^{(1)}(\rho, \mathcal{R}_{\mathrm{s}})$ with respect to scenario 1, we proceed by conditioning the probability (3.19) on $\gamma_{\mathrm{ss}}^{(2)}$ and averaging over its probability distribution function, then we invoke the result via the integration by parts. As a result, (3.20) can be rewritten as,

$$\mathrm{OP}_{\mathrm{s}}^{(1)}(\rho, \mathcal{R}_{\mathrm{s}}) = \int_{0}^{\dot{\Phi}_{\mathrm{s}}} P_{\mathrm{rob}}\left(\gamma_{\mathrm{ss}}^{(1)} < \min\left\{\Phi_{\mathrm{s}}, \dot{\Phi}_{\mathrm{s}} - z\right\}, \gamma_{\mathrm{s1}} < \dot{\Phi}_{\mathrm{s}}, \ldots, \gamma_{\mathrm{sK}} < \dot{\Phi}_{\mathrm{s}}\right) f_{\mathrm{ss}}(z)\mathrm{d}z, \tag{3.21}$$

$$= -\int_{\dot{\Phi}_{\mathrm{s}} - \Phi_{\mathrm{s}}}^{\dot{\Phi}_{\mathrm{s}}} \frac{\mathrm{d}}{\mathrm{d}z}\left(\underbrace{P_{\mathrm{rob}}\left(\gamma_{\mathrm{ss}}^{(1)} < \dot{\Phi}_{\mathrm{s}} - z, \gamma_{\mathrm{s1}} < \dot{\Phi}_{\mathrm{s}}, \ldots, \gamma_{\mathrm{sK}} < \dot{\Phi}_{\mathrm{s}}\right)}_{\mathcal{P}_1(z)}\right) F_{\mathrm{ss}}(z)\mathrm{d}z, \tag{3.22}$$

where $F_{\mathrm{ss}}(.)$ (resp $f_{\mathrm{ss}}(.)$) refers to the CDF (resp. PDF) of $\gamma_{\mathrm{ss}}^{(2)}$ whose expression is given by (3.12) before index b being replaced by s. Once again, by conditioning $\gamma_{\mathrm{ss}}^{(1)}$ and γ_{sk} for $\mathrm{k} \in \{1, \ldots, \mathrm{K}\}$ on $z_{\mathrm{sp}}^{(1)}$, the resulting variables become mutually independent, therefore integrating over the PDF of $z_{\mathrm{sp}}^{(1)}$ becomes more tractable. This leads to writing the probability

$\mathcal{P}_1(z)$ in a compact formula as,

$$\mathcal{P}_1(z) = \overline{\gamma}\left(N_{\rm s}, \frac{1}{\rho\lambda_{\rm ss}}\left(\dot{\Phi}_{\rm s} - z\right)\right)\overline{\gamma}\left(N_{\rm p}, \frac{\rm I}{\rho\lambda_{\rm sp}}\right)\left(1 - \boldsymbol{e}^{-\frac{\dot{\Phi}_{\rm s}}{\rho\lambda_{\rm sr}}}\right)^{\rm K} + \sum_{\rm e=0}^{\rm K}\frac{1}{\lambda_{\rm sp}^{N_{\rm p}}\Gamma\left(N_{\rm p}\right)}(-1)^{\rm e}\binom{\rm K}{\rm e}$$
$$\left[\frac{\Gamma\left(N_{\rm p}, \frac{\rm I}{\rho}\left(\frac{\dot{\Phi}_{\rm s}{\rm e}}{{\rm I}\lambda_{\rm sr}} + \frac{1}{\lambda_{\rm sp}}\right)\right)}{\left(\frac{\dot{\Phi}_{\rm s}{\rm e}}{{\rm I}\lambda_{\rm sr}} + \frac{1}{\lambda_{\rm sp}}\right)^{N_{\rm p}}} - \sum_{\rm p=0}^{N_{\rm s}-1}\frac{\left(\dot{\Phi}_{\rm s} - z\right)^{\rm p}}{{\rm p}!\left({\rm I}\lambda_{\rm ss}\right)^{\rm p}}\frac{\Gamma\left(N_{\rm p}+{\rm p}, \frac{\rm I}{\rho}\left(\frac{(\dot{\Phi}_{\rm s}-z)}{{\rm I}\lambda_{\rm ss}} + \frac{\dot{\Phi}_{\rm s}{\rm e}}{{\rm I}\lambda_{\rm sr}} + \frac{1}{\lambda_{\rm sp}}\right)\right)}{\left(\frac{(\dot{\Phi}_{\rm s}-z)}{{\rm I}\lambda_{\rm ss}} + \frac{\dot{\Phi}_{\rm s}{\rm p}}{{\rm I}\lambda_{\rm sr}} + \frac{1}{\lambda_{\rm sp}}\right)^{N_{\rm p}+{\rm p}}}\right], \quad (3.23)$$

before its derivative being replaced into (3.22). After some manipulations, one can rewrite the first probability as

$$\begin{aligned}\mathrm{OP}_{\rm s}^{(1)}\left(\rho, \mathcal{R}_{\rm s}\right) &= \mathcal{P}_1(\dot{\Phi}_{\rm s} - \Phi_{\rm s}) + \sum_{\rm u=0}^{N_{\rm s}-1}\left[\overline{\gamma}\left(N_{\rm p}, \frac{\rm I}{\rho\lambda_{\rm sp}}\right)\frac{\left(\frac{1}{\rho\lambda_{\rm ss}}\right)^{\rm u}{\rm F}_1({\rm u})}{{\rm u}!} + \right., \quad (3.24)\\ &\left.\sum_{\rm v=0}^{N_{\rm p}+{\rm u}-1}\frac{\Gamma\left(N_{\rm p}+{\rm u}\right)}{\Gamma\left(N_{\rm p}\right)\lambda_{\rm sp}^{N_{\rm p}}}\frac{\left(\frac{\rm I}{\rho}\right)^{\rm v}{\rm F}_2({\rm u},{\rm v})}{{\rm u}!{\rm v}!}\right]\end{aligned}$$

where the intermediate functions ${\rm F}_1({\rm u})$ and ${\rm F}_2({\rm u},{\rm v})$ with ${\rm u} \in \{0,\ldots,N_{\rm s}-1\}$ and ${\rm v} \in \{0,\ldots,N_{\rm p}+{\rm u}-1\}$ have carefully been introduced and subsequently shown to be given by,

$${\rm F}_1({\rm u}) = -\frac{\boldsymbol{e}^{-\frac{\dot{\Phi}_{\rm s}}{\rho\lambda_{\rm ss}}}}{\left(\rho\lambda_{\rm ss}\right)^{N_{\rm s}}}\overline{\gamma}\left(N_{\rm p}, \frac{\rm I}{\rho\lambda_{\rm sp}}\right)\left(1 - \boldsymbol{e}^{-\frac{\dot{\Phi}_{\rm s}}{\rho\lambda_{\rm sr}}}\right)^{\rm K}\mathcal{I}_{0,0}^{0}({\rm u}, N_{\rm s}-1, 0, 0) - \frac{1}{\Gamma\left(N_{\rm p}\right)\lambda_{\rm sp}^{N_{\rm p}}}$$
$$\times\sum_{\rm e=0}^{\rm K}(-1)^{\rm e}\binom{\rm K}{\rm e}\boldsymbol{e}^{-\frac{\rm I}{\rho}\left(\frac{\dot{\Phi}_{\rm s}}{{\rm I}\lambda_{\rm ss}} + \frac{\dot{\Phi}_{\rm s}{\rm e}}{{\rm I}\lambda_{\rm sr}} + \frac{1}{\lambda_{\rm sp}}\right)}\sum_{\rm p=0}^{N_{\rm s}-1}\frac{1}{{\rm p}!\left({\rm I}\lambda_{\rm ss}\right)^{{\rm p}+1}}\left\{\left(\frac{\rm I}{\rho}\right)^{N_{\rm p}+{\rm p}}\mathcal{I}_{0,{\rm e}}^{0}({\rm u},{\rm p},0,1) + \right.$$
$$\Gamma\left(N_{\rm p}+{\rm p}\right)\sum_{\rm q=0}^{N_{\rm p}+{\rm p}-1}\frac{\left(\frac{\rm I}{\rho}\right)^{\rm q}}{{\rm q}!}\left[-{\rm p}{\rm I}\lambda_{\rm ss}\left(\frac{\dot{\Phi}_{\rm s}{\rm e}}{{\rm I}\lambda_{\rm sr}} + \frac{1}{\lambda_{\rm sp}}\right)\mathcal{I}_{0,{\rm e}}^{0}({\rm u},{\rm p}-1,0,N_{\rm p}+{\rm p}-{\rm q}+1) + \right. \quad (3.25)$$
$$\left.\left.N_{\rm p}\mathcal{I}_{0,{\rm e}}^{0}({\rm u},{\rm p},0,N_{\rm p}+{\rm p}-{\rm q}+1)\right]\right\},$$

$$\mathrm{F}_2(\mathrm{u},\mathrm{v}) = -\frac{\boldsymbol{e}^{-\frac{1}{\rho}\left(\frac{\dot{\Phi}_\mathrm{s}}{\lambda_\mathrm{ss}}+\frac{\mathrm{I}}{\lambda_\mathrm{sp}}\right)}}{(\mathrm{I}\lambda_\mathrm{ss})^{\mathrm{v}-N_\mathrm{p}}\,\lambda_\mathrm{ss}^{N_\mathrm{s}}}\overline{\gamma}\left(N_\mathrm{p},\frac{N_0}{\rho\lambda_\mathrm{sp}}\right)\left(1-\boldsymbol{e}^{-\frac{\dot{\Phi}_\mathrm{s}}{\rho\lambda_\mathrm{sr}}}\right)^{\mathrm{K}}\mathcal{I}^{0}_{\frac{\mathrm{I}\lambda_\mathrm{ss}}{\lambda_\mathrm{sp}},0}(\mathrm{u},N_\mathrm{s}-1,N_\mathrm{p}+\mathrm{u}-\mathrm{v},0)-$$
$$\frac{1}{\Gamma(N_\mathrm{p})\,\lambda_\mathrm{sp}^{N_\mathrm{p}}}\sum_{\mathrm{e}=0}^{\mathrm{K}}\sum_{\mathrm{p}=0}^{N_\mathrm{s}-1}\frac{(-1)^{\mathrm{e}}\binom{\mathrm{K}}{\mathrm{e}}\boldsymbol{e}^{-\frac{\mathrm{I}}{\rho}\left(\frac{\dot{\Phi}_\mathrm{s}}{\mathrm{I}\lambda_\mathrm{ss}}+\frac{\dot{\Phi}_\mathrm{s}\mathrm{e}}{\mathrm{I}\lambda_\mathrm{sr}}+\frac{2}{\lambda_\mathrm{sp}}\right)}}{\mathrm{p}!\,(\mathrm{I}\lambda_\mathrm{ss})^{\mathrm{p}+\mathrm{v}-N_\mathrm{p}+1}}\left\{\left(\frac{\mathrm{I}}{\rho}\right)^{N_\mathrm{p}+\mathrm{p}}\mathcal{I}^{0}_{\frac{\mathrm{I}\lambda_\mathrm{ss}}{\lambda_\mathrm{sp}},\mathrm{e}}(\mathrm{u},\mathrm{p},N_\mathrm{p}+\mathrm{u}-\mathrm{v},1)\right.$$
$$+\sum_{\mathrm{q}=0}^{N_\mathrm{p}+\mathrm{p}-1}\frac{\Gamma(N_\mathrm{p}+\mathrm{p})}{\mathrm{q}!\left(\frac{\mathrm{I}}{\rho}\right)^{\mathrm{q}}}\left[-\mathrm{p}\mathrm{I}\lambda_\mathrm{ss}\left(\frac{\dot{\Phi}_\mathrm{s}\mathrm{e}}{\mathrm{I}\lambda_\mathrm{sr}}+\frac{1}{\lambda_\mathrm{sp}}\right)\mathcal{I}^{0}_{\frac{\mathrm{I}\lambda_\mathrm{ss}}{\lambda_\mathrm{sp}},\mathrm{e}}(\mathrm{u},\mathrm{p}-1,N_\mathrm{p}+\mathrm{u}-\mathrm{v},N_\mathrm{p}+\mathrm{p}-\mathrm{q}+1)\right.$$
$$\left.\left.+N_\mathrm{p}\mathcal{I}^{0}_{\frac{\mathrm{I}\lambda_\mathrm{ss}}{\lambda_\mathrm{sp}},\mathrm{e}}(\mathrm{u},\mathrm{p},N_\mathrm{p}+\mathrm{u}-\mathrm{v},N_\mathrm{p}+\mathrm{p}-\mathrm{q}+1)\right]\right\}. \tag{3.26}$$

In both functions, the integral $\mathcal{I}^{\delta}_{\mathrm{d},\mathrm{e}}(\mathrm{n}_0,\mathrm{n}_1,\mathrm{n}_2,\mathrm{n}_3)$, where $\delta\in\{0,1\}$, $\mathrm{d}\in\mathbb{R}^{+*}$, $\mathrm{n}_1\in\mathbb{N}\cup\{-1\}$ and $\mathrm{n}_0,\mathrm{n}_2,\mathrm{n}_3,\mathrm{e}\in\mathbb{N}$, can be expressed in its general form as,

$$\mathcal{I}^{\delta}_{\mathrm{d},\mathrm{e}}(\mathrm{n}_0,\mathrm{n}_1,\mathrm{n}_2,\mathrm{n}_3)=\frac{\dot{\Phi}_\mathrm{s}^{\mathrm{n}_1}\boldsymbol{e}^{\frac{\delta\dot{\Phi}_\mathrm{s}}{\rho\lambda_\mathrm{ss}}}}{(-\mathrm{I}\lambda_\mathrm{ss})^{\mathrm{n}_3}}\underbrace{\int_{\dot{\Phi}_\mathrm{s}-\Phi_\mathrm{s}}^{\dot{\Phi}_\mathrm{s}}\frac{z^{\mathrm{n}_0}\left(\dot{\Phi}_\mathrm{s}-z\right)^{\mathrm{n}_1}\boldsymbol{e}^{-\delta z\left(\frac{\mathrm{e}}{\rho\lambda_\mathrm{rs}}-\frac{1}{\rho\lambda_\mathrm{ss}}\right)}}{\left(z+\underbrace{\mathrm{d}}_{\mathrm{e}_2}\right)^{\mathrm{n}_2}\left(z-\underbrace{\left(\dot{\Phi}_\mathrm{s}+\frac{\dot{\Phi}_\mathrm{s}\lambda_\mathrm{ss}\mathrm{e}}{\lambda_\mathrm{sr}}+\frac{\mathrm{I}\lambda_\mathrm{ss}}{\lambda_\mathrm{sp}}\right)}_{\mathrm{e}_3}\right)^{\mathrm{n}_3}}\mathrm{d}z}_{\mathcal{J}^{a}_{\mathrm{e}_2,\mathrm{e}_3}(\mathrm{n}_0,\mathrm{n}_1,\mathrm{n}_2,\mathrm{n}_3)} \tag{3.27}$$

After writing $(\dot{\Phi}_\mathrm{s}-z)^{\mathrm{n}_1}$ for $\mathrm{n}_1\in\mathbb{N}$ in the form of a binomial expansion (in the particular case of $\mathrm{n}_1=-1$, the same integral resolution methodology applies), we then carry out for $\mathrm{v}\in\{0,\ldots,\mathrm{n}_1\}$ the partial fraction expansion of the following euclidean polynomial division,

$$\frac{z^{\mathrm{n}_0+\mathrm{v}}}{(z+\mathrm{e}_2)^{\mathrm{n}_2}(z+\mathrm{e}_3)^{\mathrm{n}_3}}=\boldsymbol{Q}_\nu(z)+\frac{\boldsymbol{R}(z)}{(z+\mathrm{e}_2)^{\mathrm{n}_2}(z+\mathrm{e}_3)^{\mathrm{n}_3}}=\boldsymbol{Q}_\nu(z)+\sum_{\mathrm{i}=2}^{3}\sum_{\mathrm{s}=1}^{\mathrm{n}_\mathrm{i}}\frac{\mathcal{G}_\mathrm{is}}{(z+\mathrm{e}_\mathrm{i})^{\mathrm{s}}}, \tag{3.28}$$

where $\boldsymbol{Q}_\nu(z)$ and $\boldsymbol{R}(z)$ refers to its ν-degree polynomial quotient and remainder, respectively, while the coefficients $\mathcal{G}_\mathrm{is}$ for $\mathrm{i}\in\{2,3\}$ and $\mathrm{s}\in\{1,\mathrm{n}_\mathrm{i}\}$ are derived by differentiation as,

$$\mathcal{G}_\mathrm{is}=\frac{1}{(\mathrm{n}_\mathrm{i}-\mathrm{s})!}\frac{\mathrm{d}^{(\mathrm{n}_\mathrm{i}-\mathrm{s})}}{\mathrm{d}z}\left\{\frac{(z+\mathrm{e}_\mathrm{i})^{\mathrm{n}_\mathrm{i}}\boldsymbol{R}(z)}{(z+\mathrm{e}_2)^{\mathrm{n}_2}(z+\mathrm{e}_3)^{\mathrm{n}_3}}\right\}\Bigg|_{z=-\mathrm{e}_\mathrm{i}}. \tag{3.29}$$

Next, expression (3.28) is replaced into (3.27). Therefore, given that $a = \delta\left(\frac{1}{\rho\lambda_{\rm ss}} - \frac{\rm e}{\rho\lambda_{\rm rs}}\right)$, $\mathrm{e}_2 = \mathrm{d}$, and $\mathrm{e}_3 = -\left(\dot{\Phi}_{\rm s} + \frac{\dot{\Phi}_{\rm s}\lambda_{\rm ss}\mathrm{e}}{\lambda_{\rm sr}} + \frac{\mathrm{I}\lambda_{\rm ss}}{\lambda_{\rm sp}}\right)$, the integral $\mathcal{J}^{a}_{\mathrm{e}_2,\mathrm{e}_3}(\mathrm{n}_0,\mathrm{n}_1,\mathrm{n}_2,\mathrm{n}_3)$ can now be rewritten as,

$$\mathcal{J}^{a}_{\mathrm{e}_2,\mathrm{e}_3}(\mathrm{n}_0,\mathrm{n}_1,\mathrm{n}_2,\mathrm{n}_3) = \sum_{\mathrm{v}=0}^{\mathrm{n}_1}\binom{\mathrm{n}_1}{\mathrm{v}}(-1)^{\mathrm{v}}\,\dot{\Phi}_{\rm s}^{-\mathrm{v}}\int\limits_{\dot{\Phi}_{\rm s}-\Phi_{\rm s}}^{\dot{\Phi}_{\rm s}}\left[\boldsymbol{Q}_{\nu}(z) + \sum_{\mathrm{i}=2}^{3}\sum_{\mathrm{s}=1}^{\mathrm{n}_{\mathrm{i}}}\frac{\mathcal{G}_{\mathrm{is}}}{(z+\mathrm{e}_{\mathrm{i}})^{\mathrm{s}}}\right]\boldsymbol{e}^{az}\mathrm{d}z, \tag{3.30}$$

which, after being invoked with the help of [71, Eq. 2.323] and [72, Eq. 1.3.2.23], leads to the following closed-form expression

$$\mathcal{J}^{a}_{\mathrm{e}_2,\mathrm{e}_3}(\mathrm{u},\mathrm{n}_1,\mathrm{n}_2,\mathrm{n}_3) = \begin{cases} \mathcal{Q}_{\nu+1}(\dot{\Phi}_{\rm s}) - \mathcal{Q}_{\nu+1}(\dot{\Phi}_{\rm s}-\Phi_{\rm s}) + \\ \sum_{\mathrm{i}=2}^{3}\left[\log\left(z+\mathrm{e}_{\mathrm{i}}\right) + \frac{-1}{(z+\mathrm{e}_{\mathrm{i}})} + \cdots + \frac{1}{(1-\mathrm{n}_{\mathrm{i}})\,(z+\mathrm{e}_{\mathrm{i}})^{\mathrm{n}_{\mathrm{i}}-1}}\right]_{\dot{\Phi}_{\rm s}-\Phi_{\rm s}}^{\dot{\Phi}_{\rm s}} & ,\ \text{if } a=0 \\ \sum_{\mathrm{v}=0}^{\mathrm{n}_1}\binom{\mathrm{n}_1}{\mathrm{v}}\left(-\dot{\Phi}_{\rm s}\right)^{-\mathrm{v}}\left[\boldsymbol{e}^{az}\sum_{\mathrm{k}=0}^{\nu}\frac{(-1)^{\mathrm{k}}\boldsymbol{Q}_{\nu}^{(\mathrm{k})}(z)}{a^{\mathrm{k}+1}}\right]_{\dot{\Phi}_{\rm s}-\Phi_{\rm s}}^{\dot{\Phi}_{\rm s}} & \\ \left[\sum_{\mathrm{i}=2}^{3}\sum_{\mathrm{s}=1}^{\mathrm{n}_{\mathrm{i}}}\frac{(-a)^{\mathrm{s}}}{a}\mathcal{G}_{\mathrm{is}}\boldsymbol{e}^{-a\mathrm{e}_{\mathrm{i}}}\Gamma\left(1-\mathrm{s},-a\left(z+\mathrm{e}_{\mathrm{i}}\right)\right)\right]_{\dot{\Phi}_{\rm s}-\Phi_{\rm s}}^{\dot{\Phi}_{\rm s}} & ,\ \text{if } a\neq 0 \end{cases} \tag{3.31}$$

where $\mathcal{Q}_{\nu+1}(z)$ refers to the $\nu+1$-degree polynomial resulting from the indefinite integral of $\boldsymbol{Q}_{\nu}(z)$, and $\boldsymbol{Q}_{\nu}^{(\mathrm{k})}(z)$ its k^{th} derivative. At this stage, we conclude with the derivation of the first term of the end-to-end outage probability, $\mathrm{OP}_{\rm s}^{(1)}\left(\rho,\mathcal{R}_{\rm s}\right)$. As for the second probability terms, $\mathrm{OP}_{\rm s,k}^{(2)}\left(\rho,\mathcal{R}_{\rm s}\right)$, they can similarly to (3.22) be expressed as,

$$\mathrm{OP}_{\rm s,k}^{(2)}\left(\rho,\mathcal{R}_{\rm s}\right) = -\int\limits_{\dot{\Phi}_{\rm s}-\Phi_{\rm s}}^{\dot{\Phi}_{\rm s}} F_{\mathbf{rs}}(z)\frac{\mathrm{d}}{\mathrm{d}z}\underbrace{P_{\rm rob}\left(\gamma_{\rm ss}^{(1)} < \dot{\Phi}_{\rm s}-z, \gamma_{\rm s1}\geq\dot{\Phi}_{\rm s},\ldots,\gamma_{\rm sk}\geq\dot{\Phi}_{\rm s},\gamma_{\rm sk+1}<\dot{\Phi}_{\rm s},\ldots,\gamma_{\rm sK}<\dot{\Phi}_{\rm s}\right)}_{\mathcal{P}_2(z)}\mathrm{d}z, \tag{3.32}$$

where $F_{\mathbf{rs}|\mathrm{k}}(z)$ refers to the CDF of $\gamma_{\mathbf{rs}}$ conditioned on $|\mathcal{S}| = \mathrm{k} \in \{1,\ldots,\mathrm{K}\}$. Its expression is given by (3.13). After deriving $\mathcal{P}_2(z)$ in its closed-form expression similarly to $\mathcal{P}_1(z)$ in

(3.22), and taking its derivative, the result is substituted into (3.32) before ending up with the following closed-form expression of the second outage probability terms,

$$\begin{aligned}
\mathrm{OP}_{\mathrm{s,k}}^{(2)}\left(\rho,\mathcal{R}_{\mathrm{s}}\right)=\sum_{\mathrm{u}=0}^{\mathrm{k}}\sum_{\mathrm{v}=0}^{\mathrm{u}(2N_{\mathrm{s}}+N_{\mathrm{p}}-2)}\mathcal{E}_{\mathrm{u,v}}\left(\mathrm{I}\lambda_{\mathrm{rs}}\right)^{\mathrm{u}(N_{\mathrm{p}}+N_{\mathrm{s}}-1)-\mathrm{v}}\left\{\boldsymbol{e}^{-\frac{\dot{\Phi}_{\mathrm{s}}\mathrm{k}}{\rho\lambda_{\mathrm{sr}}}}\overline{\gamma}\left(N_{\mathrm{p}},\frac{\mathrm{I}}{\rho\lambda_{\mathrm{sp}}}\right)\right.\\
\left(1-\boldsymbol{e}^{-\frac{\dot{\Phi}_{\mathrm{s}}}{\rho\lambda_{\mathrm{sr}}}}\right)^{\mathrm{K-k}}\left(\frac{1}{\rho\lambda_{\mathrm{ss}}}\right)^{N_{\mathrm{s}}}\mathcal{I}^{1}_{\frac{\mathrm{I}\lambda_{\mathrm{rs}}}{\lambda_{\mathrm{rp}}},0}(\mathrm{v},N_{\mathrm{s}}-1,\mathrm{u}(N_{\mathrm{p}}+N_{\mathrm{s}}-1)-\mathrm{v},0)+\frac{1}{\lambda_{\mathrm{sp}}^{N_{\mathrm{p}}}\Gamma\left(N_{\mathrm{p}}\right)}\times\\
\sum_{\mathrm{e}=0}^{\mathrm{K}}(-1)^{\mathrm{e}}\binom{\mathrm{K-k}}{\mathrm{e}}\boldsymbol{e}^{-\frac{\mathrm{I}}{\rho}\left(\frac{\dot{\Phi}_{\mathrm{s}}}{\mathrm{I}\lambda_{\mathrm{ss}}}+\frac{\dot{\Phi}_{\mathrm{s}}(\mathrm{e+k})}{\mathrm{I}\lambda_{\mathrm{sr}}}+\frac{1}{\lambda_{\mathrm{sp}}}\right)}\sum_{\mathrm{p}=0}^{N_{\mathrm{s}}-1}\frac{1}{\mathrm{p!}\left(\mathrm{I}\lambda_{\mathrm{ss}}\right)^{\mathrm{p}+1}}\times\\
\left[\left(\frac{\mathrm{I}}{\rho}\right)^{N_{\mathrm{p}}+\mathrm{p}}\mathcal{I}^{1}_{\frac{\mathrm{I}\lambda_{\mathrm{rs}}}{\lambda_{\mathrm{rp}}},\mathrm{e+k}}(\mathrm{v},\mathrm{p},\mathrm{u}(N_{\mathrm{p}}+N_{\mathrm{s}}-1)-\mathrm{v},1)+\Gamma\left(N_{\mathrm{p}}+\mathrm{p}\right)\times\right.\\
\sum_{\mathrm{q}=0}^{N_{\mathrm{p}}+\mathrm{p}-1}\frac{1}{\mathrm{q!}}\left(\frac{\mathrm{I}}{\rho}\right)^{\mathrm{q}}\left(-\mathrm{pI}\lambda_{\mathrm{ss}}\left(\frac{\dot{\Phi}_{\mathrm{s}}(\mathrm{e+k})}{\mathrm{I}\lambda_{\mathrm{sr}}}+\frac{1}{\lambda_{\mathrm{sp}}}\right)\mathcal{I}^{1}_{\frac{\mathrm{I}\lambda_{\mathrm{rs}}}{\lambda_{\mathrm{rp}}},\mathrm{e+k}}(\mathrm{v},\mathrm{p}-1,\mathrm{u}(N_{\mathrm{p}}+N_{\mathrm{s}}-1)-\mathrm{v},\right.\\
\left.\left.\left.N_{\mathrm{p}}+\mathrm{p}-\mathrm{q}+1)+N_{\mathrm{p}}\mathcal{I}^{1}_{\frac{\mathrm{I}\lambda_{\mathrm{rs}}}{\lambda_{\mathrm{rp}}},\mathrm{e+k}}(\mathrm{v},\mathrm{p}-1,\mathrm{u}(N_{\mathrm{p}}+N_{\mathrm{s}}-1)-\mathrm{v},N_{\mathrm{p}}+\mathrm{p}-\mathrm{q}+1)\right)\right]\right\}.
\end{aligned}\tag{3.33}$$

As evidence of both expressions (3.24) and (3.33), the derived closed-form of expression of the end-to-end outage probability (3.18) is valid for any value K, $\bar{\mathrm{P}}_{\mathrm{s}}$, N_{s}, and channel statistics λ_{ab} with $\mathrm{a}\in\{\mathrm{s,p,k}\}$ and $\mathrm{b}\in\{\mathrm{s,p,k}\}$. Consequently, it can be used to evaluate the outage performance of a wide range of SIMO relay-aided underlay cognitive radio system models.

Scenario 2

Contrary to scenario 1, the received SNRs $\gamma_{\mathrm{ss}}^{(1)}$ and γ_{sk} at node S-Rx and $\mathrm{R_k}$, respectively, are always independent because now S-Tx transmits with a constant power, which is no longer depending on the interference channel instantaneous variations. Therefore, applying the same derivation strategy used in scenario 1 (with minor complexity), the secondary system end-to-end outage probability can be expressed as,

$$\begin{aligned}
\mathrm{OP_s}\left(\rho,\mathcal{R}_{\mathrm{s}}\right)=-\left[F_{\mathrm{s1}}\left(\dot{\Phi}_{\mathrm{s}}\right)\right]^{\mathrm{K}}\int_{\dot{\Phi}_{\mathrm{s}}-\Phi_{\mathrm{s}}}^{\dot{\Phi}_{\mathrm{s}}}\frac{\mathrm{d}}{\mathrm{dz}}\left[F_{\mathrm{ss}}\left(\dot{\Phi}_{\mathrm{s}}-z\right)\right]F_{\mathrm{ss}}\left(z\right)\mathrm{d}z-\\
\sum_{\mathrm{k}=1}^{\mathrm{K}}\binom{\mathrm{k}}{\mathrm{K}}\left[1-F_{\mathrm{s1}}\left(\dot{\Phi}_{\mathrm{s}}\right)\right]^{\mathrm{k}}\left[F_{\mathrm{s1}}\left(\dot{\Phi}_{\mathrm{s}}\right)\right]^{\mathrm{K-k}}\int_{\dot{\Phi}_{\mathrm{s}}-\Phi_{\mathrm{s}}}^{\dot{\Phi}_{\mathrm{s}}}\frac{\mathrm{d}}{\mathrm{dz}}\left[F_{\mathrm{ss}}\left(\dot{\Phi}_{\mathrm{s}}-z\right)\right]F_{\mathbf{rs}|\mathrm{k}}\left(z\right)\mathrm{d}z,
\end{aligned}\tag{3.34}$$

where the CDFs $F_{\mathrm{sb}}(.)$ and $F_{\mathbf{rs}|\mathrm{k}}(.)$ for index $\mathrm{b} \in \{\mathrm{s}, 1\}$ and $\mathrm{k} \in \{1, \ldots, \mathrm{K}\}$ are given by (3.14) and (3.16), respectively. Both integrals in (3.34) can further be developed using usual integral manipulations. Finally, they can respectively be expressed as

$$\int_{\dot{\Phi}_{\mathrm{s}}-\Phi_{\mathrm{s}}}^{\dot{\Phi}_{\mathrm{s}}} \frac{\mathrm{d}}{\mathrm{dz}}\left[F_{\mathrm{ss}}\left(\dot{\Phi}_{\mathrm{s}}-z\right)\right] F_{\mathrm{ss}}(z)\,\mathrm{d}z = -\overline{\gamma}\left(N_{\mathrm{s}}, \frac{\Phi_{\mathrm{s}} N_0}{\lambda_{\mathrm{ss}} \mathrm{P}_{\text{s-max}}}\right) + \frac{\left[N_0/\mathrm{P}_{\text{s-max}}\right]^{N_{\mathrm{s}}}}{\Gamma(N_{\mathrm{s}})\,\lambda_{\mathrm{ss}}^{N_{\mathrm{s}}}} e^{-\frac{\dot{\Phi}_{\mathrm{s}} N_0}{\lambda_{\mathrm{ss}} \mathrm{P}_{\text{s-max}}}} \sum_{\mathrm{n}=0}^{N_{\mathrm{s}}-1} \frac{\left[N_0/\mathrm{P}_{\text{s-max}}\right]^{\mathrm{n}}}{\mathrm{n}!\lambda_{\mathrm{ss}}^{\mathrm{n}}} \sum_{\mathrm{i}=0}^{N_{\mathrm{s}}-1} \binom{N_{\mathrm{s}}-1}{\mathrm{i}} \frac{(-1)^{\mathrm{i}}\,\dot{\Phi}_{\mathrm{s}}^{N_{\mathrm{s}}-1-\mathrm{i}}}{\mathrm{n}+\mathrm{i}+1}\left[\dot{\Phi}_{\mathrm{s}}^{\mathrm{n}+\mathrm{i}+1} - \left(\dot{\Phi}_{\mathrm{s}}-\Phi_{\mathrm{s}}\right)^{\mathrm{n}+\mathrm{i}+1}\right] \tag{3.35}$$

and

$$\int_{\dot{\Phi}_{\mathrm{s}}-\Phi_{\mathrm{s}}}^{\dot{\Phi}_{\mathrm{s}}} \frac{\mathrm{d}}{\mathrm{dz}}\left[F_{\mathrm{ss}}\left(\dot{\Phi}_{\mathrm{s}}-z\right)\right] F_{\mathbf{rs}|\mathrm{k}}(z)\,\mathrm{d}z = \frac{\left[N_0/\mathrm{P}_{\text{s-max}}\right]^{N_{\mathrm{s}}}}{\Gamma(N_{\mathrm{s}})\,\lambda_{\mathrm{ss}}^{N_{\mathrm{s}}}} e^{-\frac{\dot{\Phi}_{\mathrm{s}} N_0}{\lambda_{\mathrm{ss}} \mathrm{P}_{\text{s-max}}}} \sum_{\mathrm{i}=0}^{N_{\mathrm{s}}-1} \binom{N_{\mathrm{s}}-1}{\mathrm{i}} \dot{\Phi}_{\mathrm{s}}^{N_{\mathrm{s}}-1-\mathrm{i}} \sum_{\mathrm{u}=0}^{\mathrm{k}} (-1)^{\mathrm{i}+\mathrm{u}} \sum_{\mathrm{v}=0}^{\mathrm{u}(N_{\mathrm{s}}-1)} \binom{\mathrm{k}}{\mathrm{v}} \frac{\mathcal{E}_{\mathrm{u,v}}}{\left(\frac{\mathrm{u}N_0}{\lambda_{\mathrm{rs}} \mathrm{P}_{\text{r-max}}} - \frac{N_0}{\lambda_{\mathrm{ss}} \mathrm{P}_{\text{s-max}}}\right)^{\mathrm{i}+\mathrm{v}+1}} \left[\Gamma\left(\mathrm{i}+\mathrm{v}+1, z\left(\frac{\mathrm{u}N_0}{\lambda_{\mathrm{rs}} \mathrm{P}_{\text{r-max}}} - \frac{N_0}{\lambda_{\mathrm{ss}} \mathrm{P}_{\text{s-max}}}\right)\right)\right]_{\dot{\Phi}_{\mathrm{s}}-\Phi_{\mathrm{s}}}^{\dot{\Phi}_{\mathrm{s}}}. \tag{3.36}$$

3.4.2 Diversity-and-Multiplexing Tradeoff

We study the outage behavior of our SIMO relay-aided cognitive radio system in the high SNR regime assuming a general case where $\bar{\mathrm{P}}_{\mathrm{s}}$ scales with $\bar{\mathrm{P}}_{\mathrm{p}}$ as $\bar{\mathrm{P}}_{\mathrm{p}} = \sigma \bar{\mathrm{P}}_{\mathrm{s}}^{\upsilon}$ with $\sigma \in \mathbb{R}^{*+}$ and $\upsilon \in \mathbb{R}^{+}$. Interestingly, two particular cases appear to be of great impact on the diversity-multiplexing tradeoff characterizing the secondary system communications in the high SNR regime: 1) when $\bar{\mathrm{P}}_{\mathrm{p}}$ and $\bar{\mathrm{P}}_{\mathrm{s}}$ are independently fixed (i.e., $\upsilon = 0$), and 2) when $\bar{\mathrm{P}}_{\mathrm{p}}$ grows proportionally with $\bar{\mathrm{P}}_{\mathrm{s}}$ implying that $\upsilon > 0$. Intuitively, the latter case will relax the outage constraints imposed by the primary system on the secondary system transmit power, because for high values of $\bar{\mathrm{P}}_{\mathrm{s}}$, $\bar{\mathrm{P}}_{\mathrm{p}}$ becomes high and so do the terms $\mathrm{I} = (\bar{\mathrm{P}}_{\mathrm{p}} \lambda_{\mathrm{pp}} \overline{\gamma}^{-1}(N_{\mathrm{p}}, \varepsilon_{\mathrm{p}})/(N_0 \Phi_{\mathrm{p}})) - 1$ and $\mathrm{II} = \bar{\mathrm{P}}_{\mathrm{p}} \lambda_{\mathrm{pp}} (\mathrm{O}_{\max} - 1)/(N_0 \Phi_{\mathrm{p}})$ in (3.3) and (3.5), respectively.

3.4.3 Fixed Outage Constraint

To derive the outage probability floor for high $\bar{\mathrm{P}}_{\mathrm{s}}$ values, we rewrite (3.3) and (3.5) as $\mathrm{P}_{\text{s-max}} = \mathrm{I}N_0/z_{\mathrm{sp}}$ and $\mathrm{P}_{\text{s-max}} = \mathrm{II}N_0/\lambda_{\mathrm{sp}}$, respectively. Then, we just follow the same steps

(with minor complexity) used in the previous section to derive $\mathrm{OP_s}\left(\rho, \mathcal{R}_\mathrm{s}\right)$ with respect to both transmit power scenarios. As a result, when scenario 1 is adopted, the end-to-end outage probability floor occurring when $\bar{\mathrm{P}}_\mathrm{s} \to +\infty$ can be given by,

$$\begin{aligned}\mathrm{OP_s}\left(\infty, \mathcal{R}_\mathrm{s}\right) = \mathcal{P}_1(\dot{\Phi}_\mathrm{s} - \Phi_\mathrm{s}) - \sum_{\mathrm{u}=0}^{N_\mathrm{s}-1} \frac{\Gamma\left(N_\mathrm{p}+\mathrm{u}\right)}{\left[\Gamma\left(N_\mathrm{p}\right)\lambda_\mathrm{sp}^{N_\mathrm{p}}\right]^2 \mathrm{u}!} \\ \times \sum_{\mathrm{e}=0}^{\mathrm{K}} \sum_{\mathrm{v}=0}^{N_\mathrm{s}-1} \frac{(-1)^\mathrm{e}\binom{\mathrm{K}}{\mathrm{e}}\Gamma\left(N_\mathrm{p}+\mathrm{v}\right)}{\mathrm{v}!\left(\mathrm{I}\lambda_\mathrm{ss}\right)^{\mathrm{v}+1-N_\mathrm{p}}} + \sum_{\mathrm{k}=0}^{\mathrm{K}} \sum_{\mathrm{l}=0}^{\mathrm{k}} \frac{(-1)^\mathrm{l}\binom{\mathrm{k}}{\mathrm{l}}\binom{\mathrm{K}}{\mathrm{k}}}{\left[\Gamma\left(N_\mathrm{p}\right)\lambda_\mathrm{rp}^{N_\mathrm{p}}\right]^\mathrm{l}} \\ \sum_{\mathrm{i}=0}^{\mathrm{l}(N_\mathrm{s}-1)} \sum_{\mathrm{j}=0}^{\mathrm{K}-\mathrm{k}} \sum_{\mathrm{p}=0}^{N_\mathrm{s}-1} \frac{\mathcal{V}_{\mathrm{l,i}}\,(-1)^\mathrm{j}\binom{\mathrm{K}-\mathrm{k}}{\mathrm{j}}\Gamma\left(N_\mathrm{p}+\mathrm{p}\right)}{\mathrm{p}!\left(\mathrm{I}\lambda_\mathrm{ss}\right)^{\mathrm{p}+1+\mathrm{i}-\mathrm{l}(N_\mathrm{p}+N_\mathrm{s}-1)}} \Big[-\mathrm{pI}\lambda_\mathrm{ss}\left(\tfrac{\dot{\Phi}_\mathrm{s}(\mathrm{j}+\mathrm{k})}{\mathrm{I}\lambda_\mathrm{sr}} + \tfrac{1}{\lambda_\mathrm{sp}}\right) \\ \times \mathcal{I}^0_{\frac{\mathrm{I}\lambda_\mathrm{rs}}{\lambda_\mathrm{rp}},\mathrm{j}+\mathrm{k}}(0, \mathrm{p}-1, \mathrm{l}(N_\mathrm{p}+N_\mathrm{s}-1)-\mathrm{i}, N_\mathrm{p}+\mathrm{p}+1) \\ + N_\mathrm{p}\mathcal{I}^0_{\frac{\mathrm{I}\lambda_\mathrm{rs}}{\lambda_\mathrm{rp}},\mathrm{j}+\mathrm{k}}(0, \mathrm{p}, \mathrm{l}(N_\mathrm{p}+N_\mathrm{s}-1)-\mathrm{i}, N_\mathrm{p}+\mathrm{p}+1)\Big].\end{aligned} \tag{3.37}$$

where the coefficients $\mathcal{V}_{\mathrm{l,i}}$ for $\mathrm{l} \in \{0, \ldots, \mathrm{k}\}$ and $\mathrm{i} \in \{0, \ldots, \mathrm{l}(N_\mathrm{s}-1)\}$ are recursively expressed as,

$$\begin{cases} \mathcal{V}_{\mathrm{l},0} = 1 & , \mathrm{i} = 0 \\ \mathcal{V}_{\mathrm{l,i}} = \dfrac{1}{\mathrm{i}} \displaystyle\sum_{\mathrm{n}=1}^{\min\{\mathrm{i}, N_\mathrm{s}-1\}} \left(\frac{-1}{\lambda_\mathrm{rp}}\right)^{N_\mathrm{s}-1-\mathrm{n}} (\mathrm{nl}-\mathrm{i}+\mathrm{n})\,\mathcal{V}_{\mathrm{l,i}-\mathrm{n}} \times & \\ \qquad \displaystyle\sum_{\mathrm{m}=0}^{\mathrm{n}} \binom{N_\mathrm{s}-1-\mathrm{m}}{\mathrm{n}-\mathrm{m}} \frac{\Gamma\left(N_\mathrm{p}+N_\mathrm{s}-1-\mathrm{m}\right)}{\mathrm{m}!} & , 1 \le \mathrm{i} \le \mathrm{l}(N_\mathrm{s}-1) \end{cases}.$$

In the case of the secondary system transmitting nodes act under scenario 2, the end-to-end outage probability floor can simply be deduced from (3.34) by replacing $\mathrm{P_{b\text{-}max}}$ by $\mathrm{II}N_0/\lambda_\mathrm{bp}$.

3.4.4 Proportional Outage Constraint

In general, if $\upsilon > 0$, the secondary system outage probability will decay as $\bar{\mathrm{P}}_\mathrm{s} \to +\infty$, because the outage constraint $\mathrm{OP_p} \le \varepsilon_\mathrm{p}$ will relax for both transmit power scenarios as $\bar{\mathrm{P}}_\mathrm{p}$ increases. Recently, several contributions (see for instance [31] and [28]) have adopted a new definition of the diversity gain in a secondary system that consists of measuring the slope of the outage probability floor as a decaying function of $1/\lambda_\mathrm{sp}$ or $1/\lambda_\mathrm{rp}$. While this definition leads to the same results obtained in a non-cognitive relay-aided system, because when

$\lambda_{\rm sp} \to 0$ and $\lambda_{\rm rp} \to 0$ we are no longer operating under an underlay cognitive paradigm, these results still do not reflect to which extent the secondary system is affected by the primary system outage constraint in the high SNR regime. Hence, we keep the traditional definition of the diversity gain as it is, but with the relationship $\bar{\rm P}_{\rm p} = \sigma \bar{\rm P}_{\rm s}^{\upsilon}$ with $\sigma > 0$ and $\upsilon > 0$ in mind. In fact, we can express the achievable diversity gain by the secondary system at a given rate $\mathcal{R}_{\rm s}$ as,

$$d = -\lim_{\rho \to +\infty} \frac{\log {\rm OP}_{\rm s}\left(\rho, \mathcal{R}_{\rm s}\right)}{\log_2 \rho}. \tag{3.38}$$

If the outage probability reflects the percentage of the fading channel realizations our system can not support at a certain rate, the outage capacity indeed, brings to our attention the system rate that our system can support at a certain outage percentage. Therefore, looking at the two performance metrics may lead to a better understanding of the tradeoff by which are governed. The achievable multiplexing gain can be expressed at a given outage percentage p as [1],

$$r = \lim_{\rho \to +\infty} \frac{{\rm OC}_p(\rho)}{\log_2 \rho}, \tag{3.39}$$

where ${\rm OC}_p(\rho)$ denotes the $p\%$ outage capacity at a given SNR value $\rho = \bar{\rm P}_{\rm s}/N_0$, and is associated with the outage probability via this formula, ${\rm OP}_{\rm s}\left(\rho, {\rm OC}_p(\rho)\right) = p/100$. We also look at the average spectral efficiency defined as $\eta_{\rm s} = \mathcal{R}_{\rm s}\left(1 - {\rm OP}_{\rm s}\left(\rho, \mathcal{R}_{\rm s}\right)\right)$ as a meaningful performance metric to measure the impact of cooperative relaying and the deployment of multiple antennas at the primary and secondary receivers on the secondary system outage performance.

Theorem 1

In an underlay cognitive radio system where, (i) the secondary network is assisted by a number of K single-antenna co-located relays acting in a half-duplex decode-and-forward incremental relaying mode, (ii) the secondary transmitting nodes adapts their transmit power to a proportional primary system outage constraint where the primary transmit power $\bar{\rm P}_{\rm p}$ scales with the secondary transmit power limit $\bar{\rm P}_{\rm s}$ as $\bar{\rm P}_{\rm p} = \sigma \bar{\rm P}_{\rm s}^{\upsilon}$ with $\sigma, \upsilon \in \mathbb{R}^{*+}$, (iii) the secondary receiver is equipped with $N_{\rm s}$ antennas, and (iv) all the cognitive radio channel links undergo a frequency-flat Rayleigh fading variations, the diversity-multiplexing

tradeoff by which the secondary communications are governed is given by,

$$d(r) = (2N_{\mathrm{s}} + \mathrm{K} - 1)\,(\min(\upsilon, 1) - r)^{+}\,. \tag{3.40}$$

Kindly refer to Appendix D. For some practical reasons, we underline the important conclusion from (3.40) that an increase in K under a limited N_{s} is translated into a linear increase in the achievable diversity gain of our system as if we are increasing N_{s} yet virtually.

3.5 Simulation Results and Remarks

In this section, we provide our results of the end-to-end outage probability derivation with respect to both I-CSI acquisition scenarios. Depending on each scenario, much emphasis will be put on analyzing the impact of the number of the assisting relay nodes K and receive antennas N_{p} and N_{s}. We carry out this analysis for a quiet strict primary system outage constraint $\varepsilon_{\mathrm{p}} = 0.001$.

3.5.1 Network Geometry

If we take into account large-scale variations of the cognitive radio channel, the second-order statistics of the link connecting each pair of nodes in our system can be expressed as $\lambda_{\mathrm{ab}} = d_{\mathrm{ab}}^{-\kappa}$ where d_{ab} refers to the local distance between the transmitting and receiving nodes whose indices are $\mathrm{a} \in \{\mathrm{s}, \mathrm{p}, \mathrm{k}\}$ and $\mathrm{b} \in \{\mathrm{s}, \mathrm{p}, \mathrm{k}\}$, respectively. The environment parameter κ denotes the path-loss exponent, and is set to 4 as a practical value. For the sake of simplicity, we consider, without loss of generality, a normalized linear configuration in which the cluster $\mathcal{C}$ is located between the secondary transmitter S-Tx and the secondary receiver S-Rx such that $d_{\mathrm{sr}} + d_{\mathrm{rs}} = d_{\mathrm{ss}} = d_{\mathrm{sp}} = d_{\mathrm{pp}} = 1$. Despite of the relay location in between S-Tx and S-Rx, to obtain a good outage performance results one may suggest to choose the farthest possible position of the cluster $\mathcal{C}$ from P-Rx so as not to severely interfere with its own reception. In fact, if $0 < d_{\mathrm{rp}} < 1$, we can choose $d_{\mathrm{rp}} = 0.9$ as a comprehensive value. The relays cluster location is centered around the conventional position $d_{\mathrm{sr}} = 0.5$. In the sequel, we keep these cognitive radio system settings unchanged, and confirm the exactitude of our analytical derivations in this chapter by Monte-Carlo simulations.

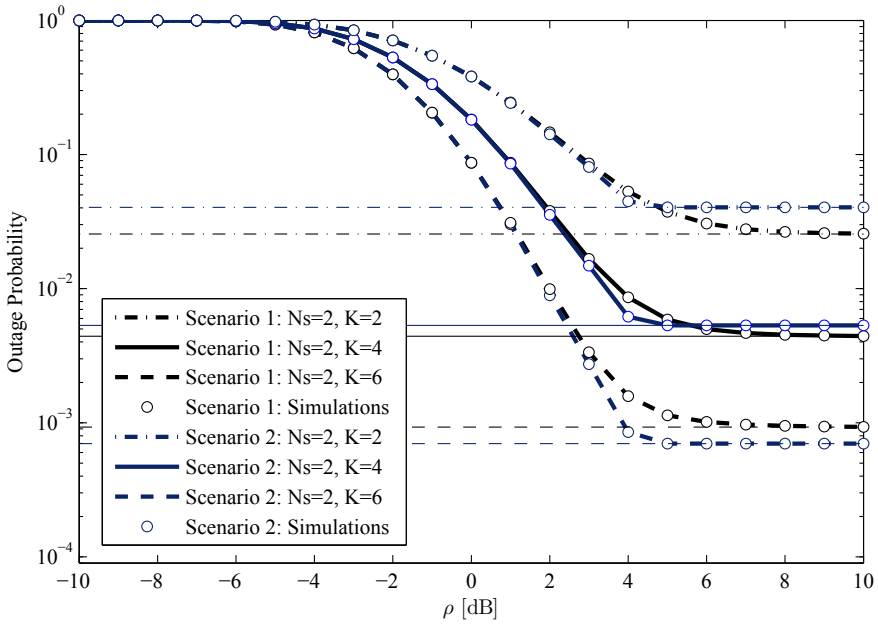

Figure 3.2: End-to-end outage probability of the secondary system for both transmit power scenarios and under several system settings. The analytical expressions of the derived outage probability (3.18) are compared to those found by Monte Carlo simulations, for $\kappa = 4$, $\bar{\mathrm{P}}_{\mathrm{p}} = 20\,\mathrm{dB}$, $d_{\mathrm{ss}} = d_{\mathrm{sp}} = d_{\mathrm{pp}} = 2d_{\mathrm{sr}} = 1$, $d_{\mathrm{rp}} = 0.9$, $N_{\mathrm{p}} = 4$, and $\mathcal{R}_{\mathrm{s}} = \mathcal{R}_{\mathrm{p}} = 2\mathrm{bits/s/Hz}$.

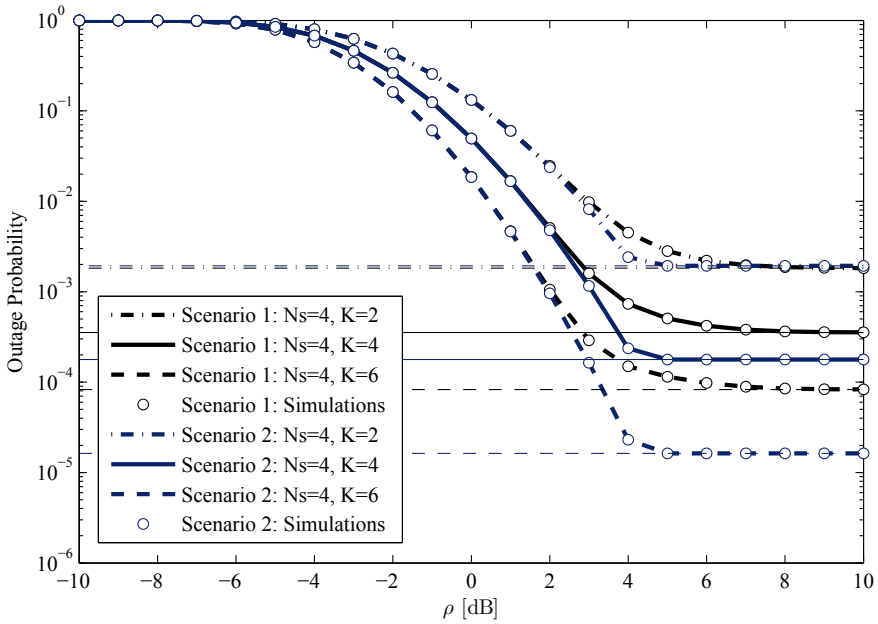

Figure 3.3: End-to-end outage probability of the secondary system for both transmit power scenarios and under several system settings. The analytical expressions of the derived outage probability (3.18) are compared to those found by Monte Carlo simulations, for $\kappa = 4$, $\bar{\mathrm{P}}_{\mathrm{p}} = 20\,\mathrm{dB}$, $d_{\mathrm{ss}} = d_{\mathrm{sp}} = d_{\mathrm{pp}} = 2d_{\mathrm{sr}} = 1$, $d_{\mathrm{rp}} = 0.9$, $N_{\mathrm{p}} = 4$, and $\mathcal{R}_{\mathrm{s}} = \mathcal{R}_{\mathrm{p}} = 2\mathrm{bits/s/Hz}$.

3.5.2 Simulation Results and Remarks

In Fig. (3.2) and (3.3), the end-to-end outage probability expressions (3.18) of the proposed SIMO relay-aided cognitive radio system are depicted for both I-CSI acquisition scenarios and for several secondary system settings. In both figures, we have considered that $\bar{\mathrm{P}}_{\mathrm{p}}$ is fixed at the value of 20 dB (i.e., $\upsilon = 0$), and consequently independent of $\bar{\mathrm{P}}_{\mathrm{s}}$ which is growing up in the x-axis. Therefore, the end-to-end outage probability saturates at its floor values. Clearly, the outage probability floor derived in (3.37) decrease with an increasing number of N_{s} and K. For instance, from a system configuration where $N_{\mathrm{s}} = 2$ and $\mathrm{K} = 2$ to another one where $N_{\mathrm{s}} = 4$ and $\mathrm{K} = 4$, the end-to-end outage probability decreases from the value of 3.10^{-2} to 3.10^{-4}. This suggests that in an underlay cognitive radio system, the secondary transmitter may greatly gain from the assistance of relays and the deployment of multiple antennas at the secondary and primary receivers. Furthermore, it is quiet remarkable for a moderate number of K and N_{s} (for instance, $N_{\mathrm{s}} = 3$ and $\mathrm{K} = 4$) that, instead of acquiring complete I-CSI by the secondary transmitting nodes, partial I-CSI knowledge is quiet sufficient to achieve similar (for low values of ρ) if not better (for high values of ρ) outage performances. Therefore, S-Tx could simply resort to the distance and path-loss of the cognitive interference channel to calculate its second order statistic instead of consuming more spectrum to acquire perfect I-CSI. This is shown clearly in Fig. (3.4) where the outage probability floor significantly improves with an increasing number of N_{s}, N_{p}, and K. The same remarks hold true even when $\bar{\mathrm{P}}_{\mathrm{p}} < 20\,\mathrm{dB}$ and $N_{\mathrm{p}} < 4$, but with the curves will be translating up.

As is evident, our study confirms that when multiple receive antennas N_{p} are deployed at the level of the primary receiver, the interference constraint imposed on the secondary system transmit power will considerably be relaxed giving more degrees of freedom to the secondary system in acquiring a better outage performance. From Fig. (3.4), poor outage performance results are obtained in the case of $N_{\mathrm{p}} = 1$, but tend to quickly improve when N_{p} increases. Therefore, deploying more than one antenna at the primary system receiver is viewed as an obligation to attain spectrally-efficient secondary transmissions. Further results demonstrating the substantial gains that can be reaped, in terms of the average spectral efficiency, via cooperative relaying and the deployment of multiple antennas at the primary and secondary receivers are shown in Fig. (3.6).

In the general case, when $\bar{\mathrm{P}}_{\mathrm{p}}$ and $\bar{\mathrm{P}}_{\mathrm{s}}$ are associated with the relationship $\bar{\mathrm{P}}_{\mathrm{p}} = \sigma \bar{\mathrm{P}}_{\mathrm{s}}^{\upsilon}$ where $\sigma, \upsilon \in \mathbb{R}^{*+}$, the end-to-end outage probability will decay as ρ increases. The same

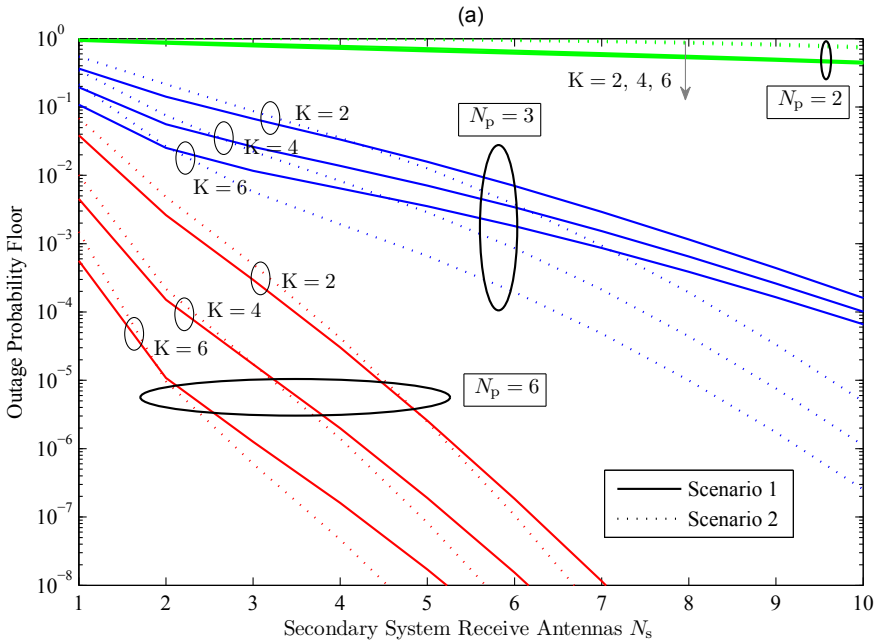

Figure 3.4: End-to-end outage probability floor of the secondary system for both transmit power scenarios and under several system settings, for $\kappa = 4$, $\bar{\mathrm{P}}_{\mathrm{p}} = 20\,\mathrm{dB}$, $d_{\mathrm{ss}} = d_{\mathrm{sp}} = d_{\mathrm{pp}} = 2d_{\mathrm{sr}} = 1$, $d_{\mathrm{rp}} = 0.9$, and $\mathcal{R}_{\mathrm{s}} = \mathcal{R}_{\mathrm{p}} = 2\mathrm{bits/s/Hz}$. The analytical expressions corresponding to the presented results are given by (3.37) and (3.34) where in the latter equation $\mathrm{P}_{\text{b-max}}$ should be replaced by $\mathrm{II}N_0/\lambda_{\mathrm{bp}}$.

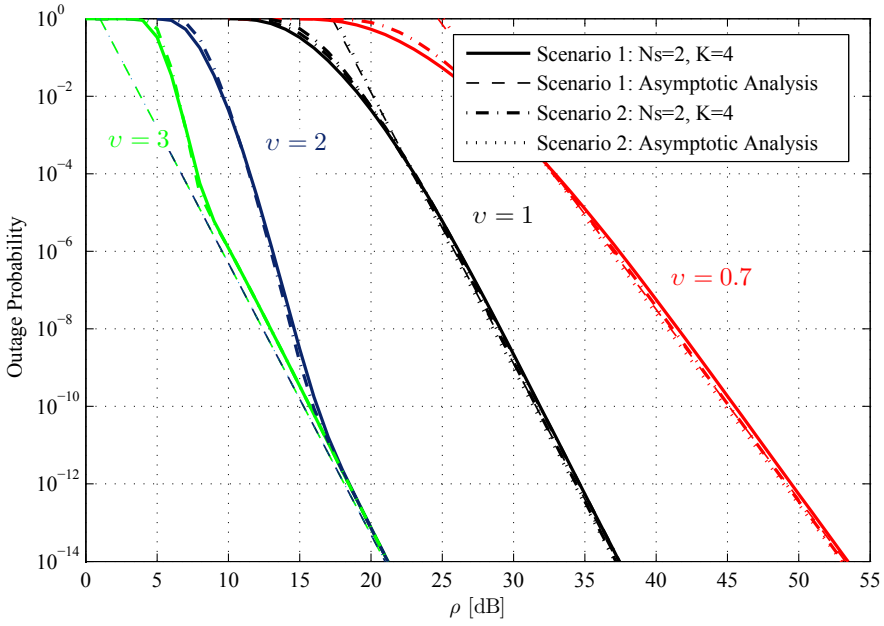

Figure 3.5: End-to-end outage probability of the secondary system for both transmit power scenarios and under several system settings. The analytical expressions of the derived outage probability (3.18) are compared to those found asymptotically for $N_{\mathrm{s}} = 4$, $N_{\mathrm{p}} = \mathrm{K} = 4$, and $\mathcal{R}_{\mathrm{s}} = \mathcal{R}_{\mathrm{p}} = 2$bits/s/Hz.

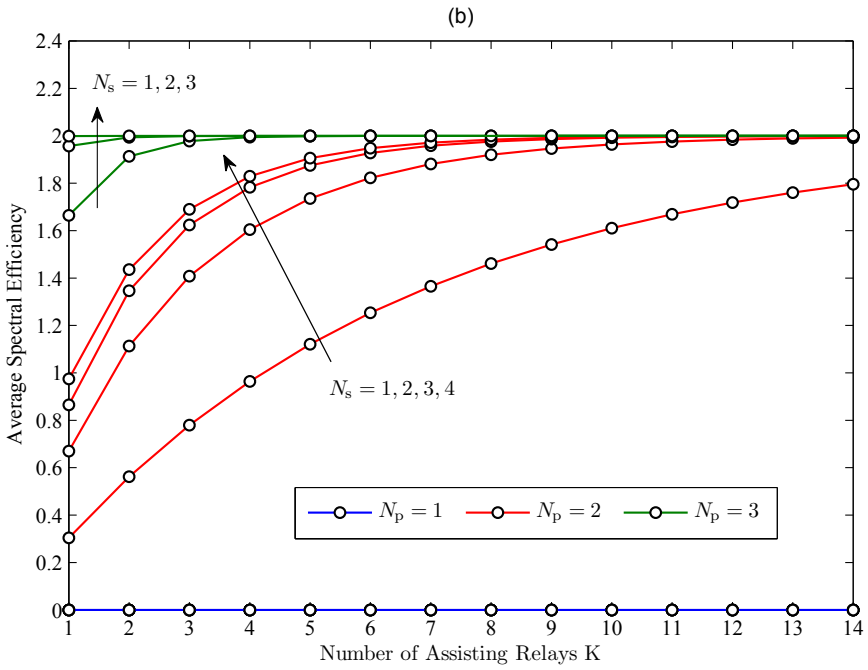

Figure 3.6: Secondary system average spectral efficiency in bits/s/Hz vs the number of the assisting relays K, for for $\kappa = 4$, $\bar{\mathrm{P}}_{\mathrm{p}} = 20\,\mathrm{dB}$, $d_{\mathrm{ss}} = d_{\mathrm{sp}} = d_{\mathrm{pp}} = 2d_{\mathrm{sr}} = 1$, $d_{\mathrm{rp}} = 0.9$, and $\mathcal{R}_{\mathrm{s}} = \mathcal{R}_{\mathrm{p}} = 2\mathrm{bits/s/Hz}$.

reasoning applies to the $p\%$ outage capacity of the proposed SIMO relay-aided cognitive radio system, that is supposed to proportionally increase with ρ. As depicted in Fig (3.5), we observe that the slope of the outage probability reflects well the achievable diversity gain of $d(0) = (2N_s + K - 1)\min(\upsilon, 1)$ derived in theorem 1, a result that is valid for both transmit power scenarios. Another important performance metric to look at the achievable multiplexing gain by our cognitive radio system is the outage capacity. In Fig. (3.7), the 10% outage capacity is depicted versus ρ. Again, our results show that the multiplexing gain of $r = \min(\upsilon, 1)$ is achieved by the secondary system under the primary system outage constraint.

The achievable DMT of the secondary system is presented in Fig. (3.8) for $\upsilon = 0.5$, $\upsilon = 1$, $K = 3$ and various values of $N_{\mathrm{s}} \in \{1, 2, 3, 4\}$. It turns out that the interference constraint imposed on the secondary system transmit power has been translated into a DMT bottleneck (typically for $\upsilon < 1$). In the particular case of $\bar{\mathrm{P}}_{\mathrm{p}} = \bar{\mathrm{P}}_{\mathrm{s}}$, i.e. $\sigma = \upsilon = 1$,

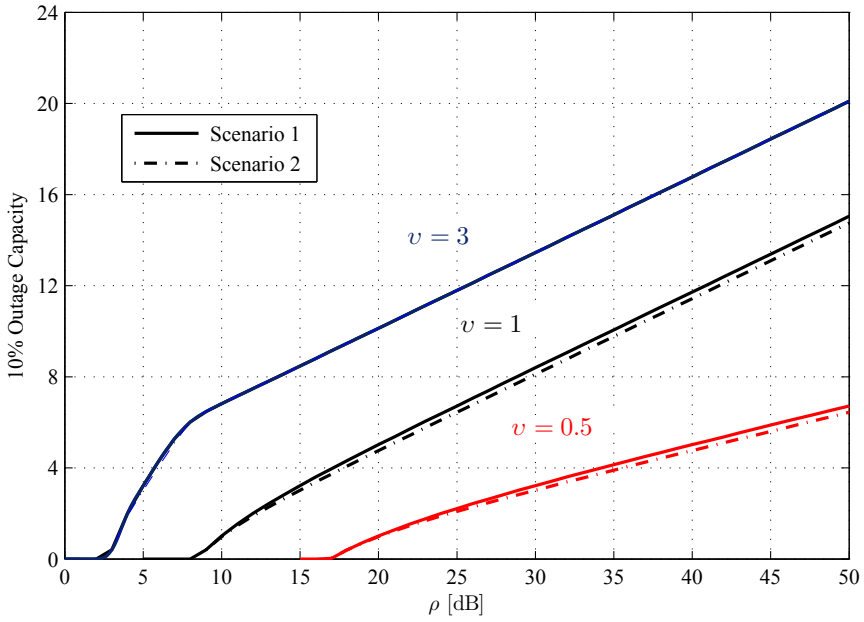

Figure 3.7: 10% outage capacity of the secondary system versus $\rho = \bar{\mathrm{P}}_{\mathrm{s}}/N_0$. It is assumed that $\kappa = 4$, $\bar{\mathrm{P}}_{\mathrm{p}} = \bar{\mathrm{P}}_{\mathrm{s}}^{\upsilon}$, $d_{\mathrm{ss}} = d_{\mathrm{sp}} = d_{\mathrm{pp}} = 2d_{\mathrm{sr}} = 1$, $d_{\mathrm{rp}} = 0.9$, $N_{\mathrm{s}} = N_{\mathrm{p}} = 4$, and $\mathrm{K} = 4$. The curves are depicted for different values of υ leading to different achievable multiplexing gains.

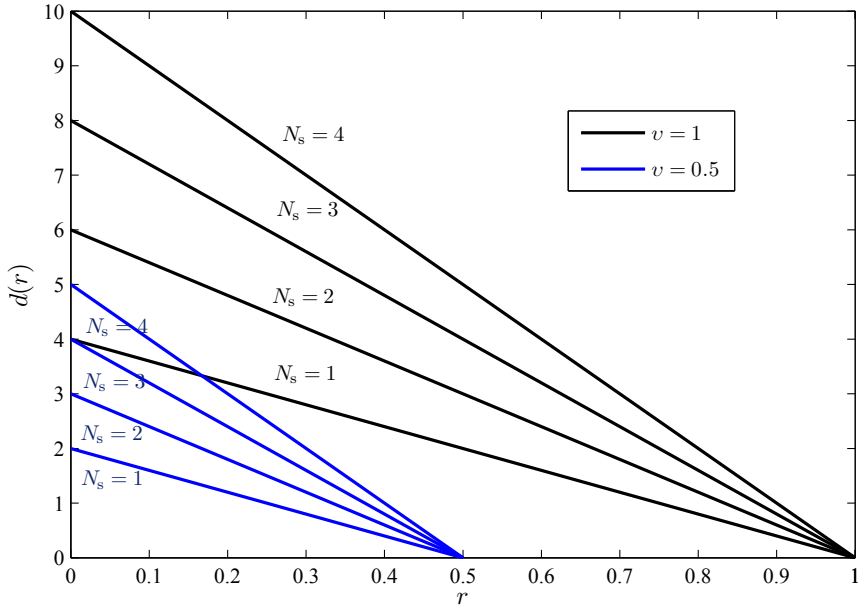

Figure 3.8: The DMT tradeoff (3.40).

the DMT of a non-cognitive radio transmission will be attained by the proposed cognitive radio system in the high SNR regime.

Chapter 4

TAS Strategies for Cognitive MIMO Relaying

4.1 Introduction

Different TAS criteria have different statistical impacts on the received SINR in cognitive MIMO relaying. If MRC is applied at the receiver, these impacts are not always trivial after the SINR is being post-processed by the MRC combiner. In this chapter, we elaborate more on the difference TAS strategies induce in terms of the outage performance with a special inclination towards the so-called SINR-driven TAS strategy. Our cognitive MIMO relay setup consists of three multi-antenna secondary nodes: a transmitter, a receiver and a DF relay node acting in a half-duplex incremental mode, whereas the primary transmitter and receiver nodes are equipped with a single antenna. The more realistic CSI scenario of acquiring only a partial CSI about the interfering channels on the primary system is adopted by the secondary transmitting nodes. In this context, our contributions are twofold. Firstly, we target the direct-link (i.e. first hop) secondary system outage performance and derive new *accurate* statistics of the received SINR with respect to the SINR-driven TAS strategy while putting previous works on the SNR-driven one within the same framework. Secondly, both TAS strategies are extended to operate during the second hop and the corresponding MRC-combined SINRs are neatly expressed prior to addressing the end-to-end outage performance of the newly built virtual cognitive MIMO setup. Here, we also derive a comprehensive yet insightful mathematical framework that serves in the accurate overall secondary system outage analysis. Our analytical results for both relaying hops are confirmed by monte-carlo

simulations and compared for both TAS strategies while always revealing the superiority and optimality of the SINR-driven TAS. Before concluding, we discuss implementation prospects of both TAS strategies in future large-scale cognitive MIMO relay systems.

4.2 Framework Description

4.2.1 System Model

Our cognitive MIMO relay system consists of a secondary s_t-antenna transmitter (S-Tx) and an s_r-antenna receiver (S-Rx), both nodes share the same spectrum band with a primary single-antenna transmitter (P-Tx) and receiver (P-Rx). To ensure a highly reliable and spectrally efficient secondary system transmission, a single r_e-antenna relay node (Re) operating in a half-duplex decode-and-forward incremental relaying mode is supposed to assist S-Tx in its transmission towards S-Rx. As shown in the table above, $h_{l,k}^{a\to b}$ denotes the coefficient of the frequency-flat fading channel connecting the kth transmit antenna at node of index $a \in \{p, s, r\}$ with the lth receive antenna at node of index $b \in \{p, s, r\}$. All channel coefficients in our cognitive MIMO relay system are assumed to be mutually independent and drawn from a zero-mean λ_{ab}-variance circularly symmetric complex Gaussian distribution. That is, $h_{l,k}^{a\to b} \sim \mathcal{CN}(0, \lambda_{ab})$. In a vector-wise form, the SIMO channel vector connecting the kth transmit antenna at node of index a with its respective receiving node of index b can be expressed as

$$\boldsymbol{h}_k^{i,a\to b} = \begin{bmatrix} h_{1,k}^{i,a\to b} \\ \vdots \\ h_{n,k}^{i,a\to b} \end{bmatrix} \in \mathbb{C}^{n\times 1} \tag{4.1}$$

where $n = r_e$ if $b = r$ whereas $n = s_r$ if $b = s$. The exponent $i \in \{1, 2\}$ in (4.1) is appended to $\boldsymbol{h}_k^{a\to b}$ as long as the link $\{a \to b\}$ is involved in transmission over two consecutive relaying hops. Implicitly, we consider that our cognitive MIMO relay channel undergoes a quasi-static fading change from one relaying hop to another. In the following, subscripts T and H denote transpose and Hermitian transpose, respectively. The CDF and PDF of a random vector X are denoted by $F_X(.)$ and $f_X(.)$, respectively. $|z|$ is the modulus of the complex number z while $\|\boldsymbol{z}\| = \boldsymbol{z}^H\boldsymbol{z}$ is the Frobenius norm of the column vector $\boldsymbol{z}$. $\mathcal{P}(.)$, $E(.)$ and $Var(.)$ denote the probability, expectation and variance operators, respectively.

Table 4.1: The coefficients of the frequency-flat quasi-static fading channels connecting the kth transmit antenna at node of index a with the lth receive antenna at node of index b.

	Receiving Nodes →		
Transmitting Nodes ↓	P-Rx ($b = p$)	S-Rx ($b = s$)	Re ($b = r$)
P-Tx ($a = p$)	$h_{1,1}^{p\to p}$	$h_{l,1}^{p\to s}$	$h_{l,k}^{p\to r}$
S-Tx ($a = s$)	$h_{1,k}^{s\to p}$	$h_{l,k}^{s\to s}$	$h_{l,k}^{s\to r}$
Re ($a = r$)	$h_{1,k}^{r\to p}$	$h_{l,k}^{r\to s}$	—

4.2.2 Power Allocation for S-Tx and R

Irrespective of the TAS criterion used by S-Tx and Re, both nodes have to keep their transmit power P under a maximum P_s and P_r, respectively, while transmitting alongside with P-Tx. Specifically, the interference caused by the secondary system at the level of the primary receiver must be limited so as not to violate its QoS. From an outage probability perspective, P_s and similarly P_r can be derived as the solution to the following system

$$\begin{aligned} &\text{maximize } P \\ &\text{subject to } \begin{cases} op_p \leq \varepsilon_p \\ P \leq \bar{P} \end{cases} \end{aligned} \quad . \tag{4.2}$$

In (4.2), op_p denotes the outage probability of the primary system, ε_p is an outage threshold that is defined by the primary system to maintain its QoS, and $\bar{P}$ is a practical power maximum that neither S-Tx nor Re can exceed. For the sake of simplicity and without loss of generality, we consider that $\bar{P}$ equals the primary system transmit power P_p. The interference channel coefficients $\boldsymbol{h}_k^{i,s\to p}$ for $k \in \{1,\ldots,s_t\}$ and $\boldsymbol{h}_k^{r\to p}$ for $k \in \{1,\ldots,r_e\}$ are assumed to be completely known to P-Rx, yet S-Tx and R can only acquire their second order statistics λ_{sp} and λ_{rp}, respectively. This scenario is more practical as it does not burden the primary system with feeding the secondary system with instantaneous channel estimates prior to each secondary system transmission. To resolve (4.2), it suffices to derive the primary system outage probability as

$$op_p = \int_0^{+\infty} \left(1 - e^{-\frac{\Phi_p(Pz+N_0)}{P_p\lambda_{pp}}}\right) \frac{e^{-\frac{z}{\lambda_{sp}}}}{\lambda_{sp}} dz = 1 - e^{-\frac{\Phi_p N_0}{P_p\lambda_{pp}}} \left(\frac{\Phi_p P\lambda_{sp}}{P_p\lambda_{pp}} + 1\right)^{-1} \tag{4.3}$$

where Φ_p denotes the received SINR threshold below which the primary system falls in outage and N_0 is the additive white Gaussian noise at the level of P-Rx and S-Rx. It follows then that the solution P to (4.2) is given by

$$P_s = \min\left\{\frac{Q_i N_0}{\lambda_{sp}}, P_p\right\} \tag{4.4}$$

where

$$Q_i = \frac{P_p \lambda_{pp}}{\Phi_p N_0}\left(\frac{e^{-\frac{\Phi_p N_0}{P_p \lambda_{pp}}}}{(1-\varepsilon_p)} - 1\right) \tag{4.5}$$

is interpreted as the maximum tolerated interference from S-Tx at P-Rx. The quantity Q_i must strictly be positive, i.e. the condition $e^{-\frac{\Phi_p N_0}{P_p \lambda_{pp}}} > (1-\varepsilon_p)$ in (4.5) must be satisfied. This means that S-Tx may stand idle with no transmission opportunity if the primary system settings are not favorable. Likewise, P_r is given by (4.4) where λ_{sp} is replaced by λ_{rp}.

4.2.2.1 Fixed Interference Threshold ($Q_i = \overline{Q}_i$)

In situations where the primary system fixes the interference threshold Q_i at a constant $\overline{Q}_i$ regardless of Φ_p, λ_{pp}, ε_p and P_p in (4.5), the primary system is viewed to be more selfish towards the secondary system. As a result,

$$P_s = \min\left\{\frac{\overline{Q}_i N_0}{\lambda_{sp}}, P_p\right\} \tag{4.6}$$

will not improve as the primary system QoS improves. Even if we operate at high primary system SNR ratios, i.e. $P_p/N_0 \to +\infty$, $\overline{Q}_i$ will be regarded as a constant that must not be exceeded anyway. This power allocation method leads to severe performance degradation of the secondary system.

4.2.2.2 Adaptive Interference Threshold

In the opposite case, when the primary system adapts Q_i (4.5) according to Φ_p, λ_{pp}, ε_p and P_p, the interference constraint put on P_s will be relaxed as P_p increases. Thus, more degrees of freedom will be given to S-Tx to transmit at a high P_s. Nevertheless, due to the spectrum sharing compromise of limiting P_s (4.4), the secondary system performance will

still be impacted. In what follows, we are more interested in scenarios where the secondary system adapts its transmit power to the primary system QoS.

4.3 TAS/MRC Strategies for Cognitive MIMO DF Relaying

4.3.1 Relaying Protocol and MRC-Combined SINRs

We adopt an incremental cognitive DF relaying protocol that spans one hop or at most two relaying hops if necessary. During the first hop, S-Tx broadcasts its symbol x_s through a given (say arbitrary chosen for now) transmit antenna $k \in \{1, \ldots, s_t\}$ while all receiving nodes S-Rx, P-Rx and Re are listening. The received baseband signals at S-Rx *before* and *after* MRC are successively given by

$$\begin{cases} \boldsymbol{y}_k^1 = \sqrt{P_s}\boldsymbol{h}_k^{1,s\to s} x_s + \sqrt{P_p}\boldsymbol{h}_1^{1,p\to s} x_p^1 + \boldsymbol{n}_s^1 \\ z_k = \boldsymbol{w}_k^H \boldsymbol{y}_k^1 \end{cases} \tag{4.7}$$

where $\boldsymbol{w}_k = \boldsymbol{h}_k^{1,s\to s} / \left\| \boldsymbol{h}_k^{1,s\to s} \right\| \in \mathbb{C}^{s_r \times 1}$ is the MRC weighting vector, x_p^1 is the transmitted symbol by P-Tx, and $\boldsymbol{n}_s^1$ is the AWGN noise vector at S-Rx with zero mean and variance equals to N_0 per each element. Considering that x_s and x_p^1 have zero mean and unit variance each, and that S-Rx has perfect knowledge of the channel coefficients $\boldsymbol{h}_k^{1,s\to s}$ and $\boldsymbol{h}_1^{1,p\to s}$, the conditional variance of the interference plus noise component in $\boldsymbol{y}_k^1$ equals to $P_p \left| \boldsymbol{w}_k^H \boldsymbol{h}_1^{1,p\to s} \right|^2 + N_0$. Therefore, the received combined SINR at S-Rx can be expressed as

$$\gamma_k^{s\to s} = \frac{P_s \left\| \boldsymbol{h}_k^{1,s\to s} \right\|^2}{P_p \frac{\left| \boldsymbol{h}_k^{1,s\to s^H} \boldsymbol{h}_1^{1,p\to s} \right|^2}{\left\| \boldsymbol{h}_k^{1,s\to s} \right\|^2} + N_0}. \tag{4.8}$$

The received SINR at Re after MRC can, following the same approach, be expressed as

$$\gamma_k^{s\to r} = \frac{P_s \left\| \boldsymbol{h}_k^{s\to r} \right\|^2}{P_p \frac{\left| \boldsymbol{h}_k^{s\to r^H} \boldsymbol{h}_1^{p\to r} \right|^2}{\left\| \boldsymbol{h}_k^{s\to r} \right\|^2} + N_0}. \tag{4.9}$$

In the case of $\gamma_k^{s\to s}$ in (4.8) is greater than a certain threshold Φ_s, S-Tx will move on to the next symbol transmission. Otherwise, S-Rx checks if successful decoding is detected at Re, i.e., $\gamma_k^{s\to r}$ in (4.9) is greater than a threshold Φ_r. If so, Re will be asked to retransmit x_s

during the second hop via its selected transmit antenna. In the worst case of the link $\{s \to r\}$ connecting S-Tx with Re falls in outage, i.e., $\gamma_k^{s\to r} < \Phi_r$, S-Rx asks S-Tx to retransmit x_s instead of Re but probably through a different transmit antenna.

Therefore, in the case of successful decoding at Re, the second-hop received signal at S-Rx *before* MRC is given by

$$\boldsymbol{y}_{k'}^2 = \sqrt{P_r}\boldsymbol{h}_{k'}^{r\to s} x_s + \sqrt{P_p}\boldsymbol{h}_1^{2,p\to s} x_p^2 + \boldsymbol{n}_s^2, \tag{4.10}$$

where $k' \in \{1, \ldots, r_e\}$ is the index of the transmit antenna used by Re while x_p^2 and $\boldsymbol{n}_s^2$ are the newly transmitted symbol by P-Tx and AWGN vector at S-Rx during the second hop, respectively. Their statistics are similar to those of x_p^1 and $\boldsymbol{n}_s^1$ in (4.7). Note that the secondary system transmit powers P_s and P_r are explicitly derived in the previous section. S-Rx then performs MRC over the received replicas $\boldsymbol{y}_k^1$ and $\boldsymbol{y}_{k'}^2$ during both relaying hops as if x_s was virtually sent in one shot and received by $2s_r$ receive antennas. Hence, the equivalent received signal at S-Rx after signal grouping and MRC is

$$z_{k,k'} = \boldsymbol{w}_{k,k'}^H \begin{bmatrix} \boldsymbol{y}_k^1 \\ \boldsymbol{y}_{k'}^2 \end{bmatrix} = \boldsymbol{w}_{k,k'}^H \left[\begin{bmatrix} \sqrt{P_s}\boldsymbol{h}_k^{1,s\to s} \\ \sqrt{P_r}\boldsymbol{h}_{k'}^{r\to s} \end{bmatrix} x_s + \sqrt{P_p} \begin{bmatrix} \boldsymbol{h}_1^{1,p\to s} x_p^1 \\ \boldsymbol{h}_1^{2,p\to s} x_p^2 \end{bmatrix} + \begin{bmatrix} \boldsymbol{n}_s^1 \\ \boldsymbol{n}_s^2 \end{bmatrix} \right], \tag{4.11}$$

where the second-hop MRC weighting vector $\boldsymbol{w}_{k,k'}$ applied on the newly built-up signal vector is constructed as

$$\boldsymbol{w}_{k,k'} = \frac{\begin{bmatrix} \boldsymbol{h}_k^{1,s\to s} \\ \boldsymbol{h}_{k'}^{r\to s} \end{bmatrix}}{\sqrt{\left\|\boldsymbol{h}_k^{1,s\to s}\right\|^2 + \left\|\boldsymbol{h}_{k'}^{r\to s}\right\|^2}}. \tag{4.12}$$

The indices k and k' in $z_{k,k'}$ and $\boldsymbol{w}_{k,k'}$ refer to the antennas used by S-Tx and Re during the first and second-hop transmissions, respectively. From (4.10) and (4.12), we deduce that the second-hop received SINR at S-Rx *after* MRC is given by

$$\gamma_{k,k'}^{s,r\to s} = \frac{P_s \left\|\boldsymbol{h}_k^{1,s\to s}\right\|^2 + P_r \left\|\boldsymbol{h}_{k'}^{r\to s}\right\|^2}{P_p \frac{\left|\boldsymbol{h}_k^{1,s\to s H}\boldsymbol{h}_1^{1,p\to s} + \boldsymbol{h}_{k'}^{r\to s H}\boldsymbol{h}_1^{2,p\to s}\right|^2}{\left\|\boldsymbol{h}_k^{1,s\to s}\right\|^2 + \left\|\boldsymbol{h}_{k'}^{r\to s}\right\|^2} + N_0}. \tag{4.13}$$

However, if unsuccessful decoding is detected at Re, S-Rx asks S-Tx to retransmit x_s during the second hop. In which case, the received SINR after MRC can similarly to (4.13) be

written as

$$\gamma_{k,k'}^{s,s\to s}=\frac{P_s\left\|\boldsymbol{h}_k^{1,s\to s}\right\|^2+P_s\left\|\boldsymbol{h}_{k'}^{2,s\to s}\right\|^2}{P_p\frac{\left|\boldsymbol{h}_k^{1,s\to s^H}\boldsymbol{h}_1^{1,p\to s}+\boldsymbol{h}_{k'}^{2,s\to s^H}\boldsymbol{h}_1^{2,p\to s}\right|^2}{\left\|\boldsymbol{h}_k^{1,s\to s}\right\|^2+\left\|\boldsymbol{h}_{k'}^{2,s\to s}\right\|^2}+N_0}, \tag{4.14}$$

where k' now refers to the used antenna by S-Tx during the second hop. Finally, depending on which node Re or S-Tx is selected for retransmission, S-Rx checks if the SINR in (4.13) or (4.14) is greater than Φ_s prior to deciding if the decoding outcome is positive or negative. In the positive case, S-Tx moves on to the next symbol while, in the negative case, the protocol starts anew until successful decoding is detected. In this Subsection, we assume that the indices k and k' in the SINRs (4.8), (4.9), (4.13) and (4.14) are arbitrary chosen. Next, Subsection 4.3.2 and Subsection 4.3.3 present the SNR and SINR-driven TAS strategies, respectively, where it becomes clear how k and k' in the aforementioned SINRs are selected.

4.3.2 SNR-driven TAS/MRC Strategy

The SNR-driven TAS has been widely adopted as a simple strategy that reduces to picking up k that maximizes (4.8) and then k' that maximizes (4.13) or (4.14) wherein all P_p is set to zero. Accordingly, the transmit antenna index k at S-Tx during the first relaying hop is selected as

$$\dot{s}_1=\arg\max_{k\in\{1,\ldots,s_t\}}\left\{\left\|\boldsymbol{h}_k^{1,s\to s}\right\|^2\right\} \tag{4.15}$$

while k' is selected at Re or S-Tx depending on the selected node for retransmission as

$$\begin{cases}\dot{r}=\arg\max_{k'\in\{1,\ldots,r_e\}}\left\{\left\|\boldsymbol{h}_{k'}^{r\to s}\right\|^2\right\}\\ \dot{s}_2=\arg\max_{k'\in\{1,\ldots,s_t\}}\left\{\left\|\boldsymbol{h}_{k'}^{2,s\to s}\right\|^2\right\}\end{cases}. \tag{4.16}$$

Under this TAS strategy, (4.8), (4.9), (4.14) and (4.13) should be rewritten as $\gamma_{\dot{s}_1}^{s\to s}$, $\gamma_{\dot{s}_1}^{r\to s}$, $\gamma_{\dot{s}_1,\dot{r}}^{s,r\to s}$ and $\gamma_{\dot{s}_1,\dot{s}_2}^{s,s\to s}$, respectively. Clearly, the SNR-driven TAS is not optimal in the sense that it does not take into account the interference caused by the primary system. However, it is regarded as a sub-optimal strategy realizing a reasonable complexity-performance tradeoff. We deduce from (4.15) and (4.16) that the antenna selection is disjointly carried over both relaying hops.

4.3.3 SINR-driven TAS/MRC Strategy

For the first time, we extend the operating mode of the SINR-driven TAS into an incremental cognitive MIMO relaying setup to optimally leverage the inherited temporal, spatial and relaying diversities. During the first hop, the index k leading to the highest $\gamma_k^{s\to s}$ is selected as

$$\ddot{s}_1 \quad = \arg \max_{k\in\{1,\ldots,s_t\}} \{\gamma_k^{s\to s}\}. \tag{4.17}$$

Unlike (4.15) and (4.16), the antenna selection during the second hop is based on the combined SINR at S-Rx resulting from the combination of both received replicas of the same transmitted symbol. As a result, the selected antenna $\ddot{r}$ at Re or s_2 at S-Tx are successively given by

$$\begin{cases} \ddot{r} = \arg \max\limits_{k'\in\{1,\ldots,r_e\}} \left\{\gamma_{\ddot{s}_1,k'}^{s,r\to s}\right\} \\ \ddot{s}_2 = \arg \max\limits_{k'\in\{1,\ldots,s_t\}} \left\{\gamma_{\ddot{s}_1,k'}^{s,s\to s}\right\} \end{cases}. \tag{4.18}$$

It is worth noting here that when S-Rx is equipped with a single antenna [45], i.e., $s_r = 1$, we have $\ddot{s}_1 = \dot{s}_1$ yet the following equalities $\ddot{r} = \dot{r}$ and $\ddot{s}_2 = \dot{s}_2$ do not hold true. Under the SINR-driven TAS strategy, (4.8), (4.9), (4.14) and (4.13) should alternatively be rewritten as $\gamma_{\ddot{s}_1}^{s\to s}$, $\gamma_{\ddot{s}_1}^{r\to s}$, $\gamma_{\ddot{s}_1,\ddot{r}}^{s,r\to s}$ and $\gamma_{\ddot{s}_1,\ddot{s}_2}^{s,s\to s}$, respectively, with the difference in the number of the dots on top of the indices s_1, s_2 and r compared to the SNR-driven TAS strategy.

4.4 Direct Transmission Outage Performance

The probability that the direct link of our cognitive MIMO secondary system fails in outage during the first relaying hop equals the CDF of $\gamma_k^{s\to s}$ at a certain threshold Φ_s. The selected transmit antenna k at S-Tx corresponds to $\dot{s}_1$ (4.15) or $\ddot{s}_1$ (4.17) depending on the adopted TAS/MRC strategy.

4.4.1 Received SINR Statistics for the SNR-driven TAS/MRC

4.4.1.1 CDF Derivation of $\gamma_{\dot{s}_1}^{s\to s}$

If antenna k at S-Tx is selected according to (4.15) meaning that $k = \dot{s}_1$, we have

$$F_{\gamma_{\dot{s}_1}^{s\to s}}(\gamma) = \mathcal{P}\left(\frac{P_s X_{\dot{s}_1}^1}{P_p Z_{\dot{s}_1}^1 + N_0} < \gamma\right), \tag{4.19}$$

where

$$X_{\dot{s}_1}^1 \;=\; \left\|\boldsymbol{h}_{\dot{s}_1}^{1,s\to s}\right\|^2 \tag{4.20}$$

and

$$Z_{\dot{s}_1}^1 = \frac{\left|\boldsymbol{h}_{\dot{s}_1}^{1,s\to s^H}\boldsymbol{h}^{1,p\to s}\right|^2}{\left\|\boldsymbol{h}_{\dot{s}_1}^{1,s\to s}\right\|^2}. \tag{4.21}$$

To evaluate $F_{\gamma_k^{s\to s}}(.)$ in the context of a conventional SIMO system with co-channel interference, *Shah and al.* [65] demonstrated a-priori that X_k^1 and Z_k^1 are independent because basically $\boldsymbol{h}_k^{1,s\to s}$and $\boldsymbol{h}^{1,p\to s}$ are independent and the latter entries are independent and identically distributed complex Gaussian variables. Since both conditions also apply on $\boldsymbol{h}_k^{1,s\to s}$ and $\boldsymbol{h}^{1,p\to s}$ for $k = \dot{s}_1$ (4.15), we deduce that $X_{\dot{s}_1}^1$ and $Z_{\dot{s}_1}^1$ are independent. Furthermore, because $E\left(\boldsymbol{h}^{1,p\to s}\right) = \mathbf{0}$, $Z_{s_1}^1$ is an Exponential variable with parameter λ_{ps} whereas the CDF and PDF of $X_{s_1}^1$ are given by

$$X_{\dot{s}_1}^1(x) = \overline{\gamma}\left(s_r, \frac{x}{\lambda_{ss}}\right)^{s_t} U(x) \tag{4.22}$$

and

$$f_{X_{\dot{s}_1}^1}(x) = \frac{s_t x^{s_r-1}}{\lambda_{ss}^{s_r}\Gamma(s_r)} e^{-\frac{x}{\lambda_{ss}}}\overline{\gamma}\left(s_r, \frac{x}{\lambda_{ss}}\right)^{s_t-1} U(x), \tag{4.23}$$

respectively, where $\overline{\gamma}(n,x)$=$\gamma(n,x)/\Gamma(n)$ with $\Gamma(n) = (n-1)!$ for an integer n is the regularized lower incomplete Gamma [71, Eq. 8.352.1] and $U(.)$ is the unit step function. It follows by conditioning $F_{\gamma_{\dot{s}_1}^{s\to s}}(.)$ on $Z_{\dot{s}_1}^1$ that (4.19) develops to

$$F_{\gamma_{\dot{s}_1}^{s\to s}}(\gamma) = \int_0^{+\infty} \overline{\gamma}\left(s_r, \frac{\gamma\left(P_p z + N_0\right)}{P_s\lambda_{ss}}\right)^{s_t} \frac{e^{-\frac{z}{\lambda_{ps}}}}{\lambda_{ps}} dz. \tag{4.24}$$

Lemma 3: At an early stage of our analysis, we introduce a simple yet tractable expansion of $\overline{\gamma}(l,x)$ to the power of k as follows

$$\overline{\gamma}(l,x)^k = \sum_{\substack{0\leq i_1\leq k \\ 0\leq i_2\leq i_1(l-1)}} \psi_{i_1,i_2}^{k,l} e^{-i_1 x} x^{i_2} \tag{4.25}$$

where the coefficients $\psi_{i_1,i_2}^{k,l}$ for $i_1 \in \{0,\ldots,k\}$ and $i_2 \in \{0,\ldots,i_1(l-1)\}$ with $l,k \in \mathbb{N}^*$ are governed by the following recursion

$$\begin{cases} \psi_{i_1,0}^{k,l} = \binom{k}{i_1}(-1)^{i_1} & , i_2 = 0 \\ \psi_{i_1,i_2}^{k,l} = \dfrac{1}{i_2}\displaystyle\sum_{i_3=1}^{\min(i_2,l-1)} \dfrac{(i_3 i_1 - i_2 + i_3)}{i_3!}\psi_{i_1,i_2-i_3}^{k,l} & , 1\leq i_2 \end{cases}. \tag{4.26}$$

See Appendix E.

By replacing (4.25) into (4.24), and using [71, 3.382.4], the CDF of the first-hop received SINR $\gamma_{\dot{s}_1}^{s\to s}$ when adopting an SNR-based TAS/MRC scheme is given by

$$F_{\gamma_{\dot{s}_1}^{s\to s}}(\gamma) = \frac{e^{\frac{N_0}{P_p\lambda_{ps}}}}{\lambda_{ps}} \sum_{\substack{0\leq i_1\leq s_t \\ 0\leq i_2\leq i_1(s_r-1)}} \frac{\psi_{i_1,i_2}^{s_t,s_r}\left(\frac{\gamma P_p}{P_s\lambda_{ss}}\right)^{i_2}}{\left(\frac{i_1\gamma P_p}{P_s\lambda_{ss}}+\frac{1}{\lambda_{ps}}\right)^{i_2+1}}\Gamma\left(i_2+1, \frac{\gamma N_0 i_1}{P_s\lambda_{ss}}+\frac{N_0}{P_p\lambda_{ps}}\right)U(\gamma) \tag{4.27}$$

where $\Gamma(n,x)$ is the upper incomplete Gamma function [71, 8.352.2] for an integer n and real x.

4.4.1.2 PDF Derivation of $\gamma_{\dot{s}_1}^{s\to s}$

An important consequence of deriving $F_{\gamma_{\dot{s}_1}^{s\to s}}(.)$ (4.27) is that it can serve for calculating the PDF of $\gamma_{\dot{s}_1}^{s\to s}$, as $f_{\gamma_{\dot{s}_1}^{s\to s}}(\gamma) = \partial F_{\gamma_{\dot{s}_1}^{s\to s}}(\gamma)/\partial\gamma$. From (4.24), we deduce that

$$\begin{aligned} f_{\gamma_{\dot{s}_1}^{s\to s}}(\gamma) &= s_t \int_0^{+\infty} \overline{\gamma}\left(s_r, \frac{\gamma(P_p z+N_0)}{P_s\lambda_{ss}}\right)^{s_t-1} \frac{\partial}{\partial\gamma}\overline{\gamma}\left(s_r, \frac{\gamma(P_p z+N_0)}{P_s\lambda_{ss}}\right) \frac{e^{-\frac{z}{\lambda_{ps}}}}{\lambda_{ps}}dz \\ &= \frac{s_t e^{\frac{N_0}{P_p\lambda_{ps}}}}{\Gamma(s_r)\lambda_{ps}} \sum_{\substack{0\leq i_1\leq s_t-1 \\ 0\leq i_2\leq i_1(s_r-1)}} \frac{\psi_{i_1,i_2}^{k,l}\left(\frac{\gamma P_p}{P_s\lambda_{ss}}\right)^{i_2+s_r-1}}{\left(\frac{\gamma P_p(i_1+1)}{P_s\lambda_{ss}}+\frac{1}{\lambda_{ps}}\right)^{i_2+s_r}}\Gamma\left(i_2+s_r, \frac{\gamma N_0(i_1+1)}{P_s\lambda_{ss}}+\frac{N_0}{P_p\lambda_{ps}}\right)U(\gamma). \end{aligned} \tag{4.28}$$

4.4.2 Direct Transmission Outage Probability for the SNR-driven TAS/MRC

We deduce from (4.27) that the first-hop outage probability when our cognitive MIMO system adopts an SNR-driven TAS/MRC strategy equals $op^1_{s,snr} = F_{\gamma^{s\to s}_{\ddot{s}_1}}(\Phi_s)$. In particular, if the secondary system is allowed to regulate its transmit power P_s in an adaptive manner as described in subsection 4.2.2.2, $op^1_{s,snr}$ will converge to a floor, $opF^1_{s,snr}$, for $\frac{P_p}{N_0} \to +\infty$ that is given by

$$opF^1_{s,snr} = \sum_{\substack{0\le i_1\le s_t \\ 0\le i_2\le i_1(s_r-1)}} \frac{\psi^{s_t,s_r}_{i_1,i_2}\left(\frac{\Phi_s}{\eta\lambda_{ss}}\right)^{i_2}\Gamma(i_2+1)}{\left(\frac{i_1\Phi_s}{\eta\lambda_{ss}}+\frac{1}{\lambda_{ps}}\right)^{i_2+1}} \tag{4.29}$$

where η is deduced from (4.4) and (4.5) for $\frac{P_p}{N_0} \to +\infty$ as

$$\eta = \frac{P_s}{P_p} = \min\left\{\frac{\lambda_{pp}}{\Phi_p\lambda_{sp}}\left(\frac{\varepsilon_p}{(1-\varepsilon_p)}\right), 1\right\}. \tag{4.30}$$

4.4.3 Received SINR Statistics for the SINR-driven TAS/MRC

4.4.3.1 CDF Derivation of $\gamma^{s\to s}_{\ddot{s}_1}$

Herein, if antenna $\ddot{s}_1$ at S-Tx is rather selected according to (4.17), the CDF of the received MRC combiner output SINR is given by

$$F_{\gamma^{s\to s}_{\ddot{s}_1}}(\gamma) = \mathcal{P}\left(\frac{P_s X^1_{\ddot{s}_1}}{P_p Z^1_{\ddot{s}_1}+N_0} < \gamma\right) \tag{4.31}$$

where the variables $X^1_{\ddot{s}_1}$ and $Z^1_{\ddot{s}_1}$ are constructed such as

$$\underbrace{\frac{P_s X^1_{\ddot{s}_1}}{P_p Z^1_{\ddot{s}_1}+N_0}}_{\gamma^{s\to s}_{\ddot{s}_1}} = \max_{k\in\{1,\ldots,s_t\}} \underbrace{\left\{\frac{P_s X^1_k}{P_p Z^1_k+N_0}\right\}}_{\gamma^{s\to s}_k} \tag{4.32}$$

Contrary to the SNR-based TAS strategy, $X^1_{\ddot{s}_1}$ and $Z^1_{\ddot{s}_1}$ are now dependent variables whose PDFs are not known although X^1_k and Z^1_k, for a given $k \in \{1,\ldots,s_t\}$, are independent and their PDFs are known to follow Gamma and Exponential distributions, respectively. Under the assumption of independent per-transmit-antenna received SINRs (i.e. $\gamma^{s\to s}_1,\ldots,\gamma^{s\to s}_{s_t}$ are mutually independent), the CDF of $\gamma^{s\to s}_{\ddot{s}_1}$ (4.32) was derived in [47] and

later in [48] and [49] as

$$F_{\gamma_{\tilde{s}_1}^{s\to s}}(\gamma) = F_{\gamma_k^{s\to s}}(\gamma)^{s_t} \tag{4.33}$$

where $F_{\gamma_k^{s\to s}}(.)$ for a given $k \in \{1,\ldots,s_t\}$ is deduced from (4.27) by letting $s_t = 1$ before being replaced into (4.33).

A deeper look into $\gamma_k^{s\to s}$ (4.32) especially Z_k^1 as in the middle of (4.35), we realize that this assumption can not hold true in our case of study because of the interference channel $\boldsymbol{h}^{1,p\to s}$ appearing across the denominator of all $\gamma_k^{s\to s}$s. Indeed, the correlation between the received SINRs is a direct outcome of applying the MRC at S-Rx despite the interference channel $\boldsymbol{h}^{1,p\to s}$ is being independent of the SIMO channels $\boldsymbol{h}_k^{1,s\to s}$. Therefore, the equality (4.33) should consistently be rewritten as

$$F_{\gamma_{\tilde{s}_1}^{s\to s}}(\gamma) \approx F_{\gamma_k^{s\to s}}(\gamma)^{s_t} \tag{4.34}$$

and it becomes worth investigating whether (4.34) holds as a tight approximation or not. To the best of the authors knowledge, an exact derivation of (4.31) has not been addressed yet in the literature. To proceed with its accurate derivation, we rewrite the variable Z_k^1 in the right-hand side of (4.32) as

$$Z_k^1 \;=\; \frac{\left|\boldsymbol{h}_k^{1,s\to s^H}\boldsymbol{h}^{1,p\to s}\right|^2}{\left\|\boldsymbol{h}_k^{1,s\to s}\right\|^2} = \frac{Y_k^1}{X_k^1}V \tag{4.35}$$

where $Y_k^1 = \left|\boldsymbol{h}_k^{1,s\to s^H}\boldsymbol{h}^{1,p\to s}\right|^2/V$, $V = \left\|\boldsymbol{h}^{1,p\to s}\right\|^2$ and $X_k^1 = \left\|\boldsymbol{h}_k^{1,s\to s}\right\|^2$. Note that X_k^1 and the newly introduced variable Y_k^1 are still dependent variables following Gamma and Exponential distributions, respectively. However, to get rid of the maximum operator in (4.32) after being plug into (4.31), it suffices to condition the variable Z_k^1 on V because the latter appears to be the cause of dependence between the received SINRs, $\gamma_k^{s\to s} = P_s X_k^1/\left(P_p Z_k^1 + N_0\right)$ for $k \in \{1,\ldots,s_t\}$. Therefore, (4.31) can now precisely be expressed as

$$F_{\gamma_{\tilde{s}_1}^{s\to s}}(\gamma) = \int_0^{+\infty} \mathcal{P}\left(\frac{P_s X_k^1}{P_p \frac{Y_k^1}{X_k^1} v + N_0} < \gamma\right)^{s_t} f_V(v)\, dv \tag{4.36}$$

where the PDF of the Gamma variable V is given by

$$f_V(v) = \frac{v^{s_r-1}e^{-\frac{v}{\lambda_{ps}}}}{\lambda_{ps}^{s_r}\Gamma(s_r)}U(v). \tag{4.37}$$

The difference between (4.33) and (4.36) lies in the exponent s_t that is now correctly appearing inside the integral.

Because the following quadratic inequality

$$\frac{\boldsymbol{h}^{1,p\to s^H}\boldsymbol{h}_k^{1,s\to s}\boldsymbol{h}_k^{1,s\to s^H}\boldsymbol{h}^{1,p\to s}}{\left\|\boldsymbol{h}^{1,p\to s}\right\|^2} \leq \left\|\boldsymbol{h}_k^{1,s\to s}\right\|^2 \tag{4.38}$$

holds true in general for any arbitrary channel vectors $\boldsymbol{h}_k^{1,s\to s}$ and $\boldsymbol{h}^{1,p\to s} \neq \mathbf{0}$, we prove in Appendix XX that the joint PDF of X_k^1 and $Y_k^1|v$, $f_{X_k^1,Y_k^1|v}(,)$, coincides with the McKay's bivariate Gamma distribution [73] that is given by

$$f_{X_k^1,Y_k^1|v}(x,y) = \frac{(x-y)^{s_r-2}\,e^{-\frac{x}{\lambda_{ss}}}}{\lambda_{ss}^{s_r}\Gamma(s_r-1)}U(x-y) \tag{4.39}$$

for a number of receive antennas $s_r \geq 2$. It is apparent from (4.39) that X_k^1 and Y_k^1 are jointly independent from V. Hence, the probability inside (4.36), after carefully defining our integration regions, can be rewritten as

$$\mathcal{P}\left(\gamma_k^{s\to s}\middle|v<\gamma\right) = \underbrace{\int_0^{\frac{\gamma N_0}{P_s}}\int_0^{x}\frac{(x-y)^{s_r-2}\,e^{-\frac{x}{\lambda_{ss}}}}{\lambda_{ss}^{s_r}\Gamma(s_r-1)}dydx}_{\mathcal{J}_1(\gamma)}$$
$$+\underbrace{\int_{\frac{\gamma N_0}{P_s}}^{\frac{\gamma}{P_s}(P_pv+N_0)}\int_{\frac{-\gamma N_0 x+P_s x^2}{\gamma P_p v}}^{x}\frac{(x-y)^{s_r-2}\,e^{-\frac{x}{\lambda_{ss}}}}{\lambda_{ss}^{s_r}\Gamma(s_r-1)}dydx}_{\mathcal{J}_2(\gamma,v)}. \tag{4.40}$$

It can be shown with the help of [71, 3.351.1] that the first term $\mathcal{J}_1(\gamma)$ of the right-hand side of (4.40) is the regularized lower incomplete Gamma function,

$$\mathcal{J}_1(\gamma) = \overline{\gamma}\left(s_r, \frac{\gamma N_0}{P_s\lambda_{ss}}\right), \tag{4.41}$$

while the first integral in the second term $\mathcal{J}_2(\gamma, v)$ can further be developed as

$$\mathcal{J}_2(\gamma, v) = \int_{\frac{\gamma N_0}{P_s}}^{\frac{\gamma}{P_s}(P_p v + N_0)} \frac{x^{s_r-1} e^{-\frac{x}{\lambda_{ss}}}}{\Gamma(s_r)} \left(\frac{P_s}{\gamma P_p v} \left(\frac{\gamma}{P_s}(P_p v + N_0) - x \right) \right)^{s_r-1} dx. \quad (4.42)$$

After making the change of variable $t = \frac{\gamma}{P_s}(P_p v + N_0) - x$, (4.42) can be evaluated by expanding the resulting binomial inside the integral and using [71, 3.351.1] as

$$\mathcal{J}_2(\gamma, v) = \frac{(-1)^{s_r} e^{-\frac{\gamma N_0}{P_s \lambda_{ss}}}}{\Gamma(s_r)} \sum_{k=0}^{s_r-1} \binom{s_r - 1}{k} \left(\frac{P_s \lambda_{ss}}{\gamma} \right)^k \times e^{-\frac{\gamma P_p v}{P_s \lambda_{ss}}} \frac{(P_p v + N_0)^{s_r-1-k}}{(P_p v)^{s_r-1}} \gamma \left(s_r + k, -\frac{\gamma P_p v}{P_s \lambda_{ss}} \right). \quad (4.43)$$

Once we replace (4.41) and (4.43) into (4.40), raised to the power of s_t, the result can be treated as a binomial whose expansion can be expressed as

$$\begin{aligned} \mathcal{P}\left(\gamma_k^{s \to s} \middle| v < \gamma \right)^{s_t} &= \overline{\gamma}\left(n_r, \frac{\gamma N_0}{P_s \lambda_{ss}} \right)^{s_t} + \sum_{l=1}^{s_t} \binom{s_t}{l} \overline{\gamma}\left(n_r, \frac{\gamma N_0}{P_s \lambda_{ss}} \right)^{s_t - l} \\ &\times \frac{(-1)^{l s_r} e^{-\frac{\gamma N_0 l}{P_s \lambda_{ss}}}}{\Gamma(s_r)^l} \left(\frac{P_s \lambda_{ss}}{\gamma} \right)^{\sum_{i=1}^{l} k_i} \sum_{0 \le k_1, \ldots, k_l \le s_r - 1} \prod_{i=1}^{l} \binom{s_r - 1}{k_i} (P_p v)^{l(s_r-1)} \\ &\times (P_p v + N_0)^{l(s_r-1) - \sum_{i=1}^{l} k_i} e^{-\frac{\gamma P_p v l}{P_s \lambda_{ss}}} \prod_{i=1}^{l} \gamma\left(s_r + k_i, \frac{-\gamma P_p v}{P_s \lambda_{ss}} \right) \end{aligned} \quad (4.44)$$

where we pulled out to the right the terms containing the variable v. Prior to carrying the integration over v as in (4.36), the product of the lower incomplete Gamma functions in the last line of (4.44) is evaluated with the help of [71, 8.354.1] as

$$\prod_{i=1}^{l} \gamma\left(s_r + k_i, \frac{-\gamma P_p v}{P_s \lambda_{ss}} \right) = \sum_{n=0}^{+\infty} \mathcal{A}_{l,n}^{s_r}(k_1, \ldots, k_l) \left(-\frac{\gamma P_p v}{P_s \lambda_{ss}} \right)^{\sum_{i=1}^{l} k_i + l s_r + n} \quad (4.45)$$

where the coefficients $\mathcal{A}_{l,n}^{s_r}(.,\ldots,.)$ for an integer $n \geq 0$ are given by

$$\mathcal{A}_{l,n}^{s_r}(k_1,\ldots,k_l) = (-1)^n \sum_{m_1=0}^{n} \sum_{m_2=0}^{n-m_1} \cdots \sum_{m_{l-1}=0}^{n-m_1-\cdots-m_{l-2}} \frac{1}{\prod_{i=1}^{l-1} m_i!} \times \frac{1}{(k_i+s_r+m_i)\left(k_l+s_r+n-\sum_{i=1}^{l-1} m_i\right)}. \tag{4.46}$$

Finally, by replacing (4.45) into (4.44), we obtain a closed-form expression of the CDF of $\gamma_{\ddot{s}_1}^{s\to s}$ (4.47) in terms of the Tricomi confluent hypergeometric function $\mathcal{U}(.,.,.)$ [74] which is implemented in famous mathematical softwares such as Mathematica thereby can serve for accurately evaluating (4.47).

$$\begin{aligned} F_{\gamma_{\ddot{s}_1}^{s\to s}}(\gamma) &= \overline{\gamma}\left(s_r, \frac{\gamma N_0}{P_s\lambda_{ss}}\right)^{s_t} + \frac{1}{\Gamma(s_r)}\left(\frac{N_0}{P_p\lambda_{ps}}\right)^{s_r} \sum_{l=1}^{s_t} \binom{s_t}{l} \\ &\times \overline{\gamma}\left(s_r, \frac{\gamma N_0}{P_s\lambda_{ss}}\right)^{s_t-l} \frac{(-1)^{ls_r}}{\Gamma(s_r)^l} e^{-\frac{\gamma N_0 l}{P_s\lambda_{ss}}} \sum_{0\leq k_1,\ldots,k_l\leq s_r-1} \prod_{i=1}^{l} \binom{s_r-1}{k_i} \\ &\times (-1)^{\sum_{i=1}^{l} k_i} \sum_{n=0}^{+\infty} \mathcal{A}_{l,n}^{s_r}(k_1,\ldots,k_l) \left(\frac{-\gamma N_0}{P_s\lambda_{ss}}\right)^{ls_r+n} \Gamma\left(l+\sum_{i=1}^{l} k_i + s_r + n\right) \\ &\times \mathcal{U}\left(l+\sum_{i=1}^{l} k_i + s_r + n, s_r(l+1)+n+1, \frac{N_0}{P_p}\left(\frac{\gamma P_p l}{P_s\lambda_{ss}} + \frac{1}{\lambda_{ps}}\right)\right). \end{aligned} \tag{4.47}$$

4.4.3.2 PDF Derivation of $\gamma_{\ddot{s}_1}^{s\to s}$

To proceed with the PDF derivation of the received SINR, $\gamma_{\ddot{s}_1}^{s\to s}$, it follows from (4.36) that

$$f_{\gamma_{\ddot{s}_1}^{s\to s}}(\gamma) = s_t \int_0^{+\infty} \mathcal{P}\left(\gamma_k^{s\to s} \middle| v < \gamma\right)^{s_t-1} \left(\mathcal{DJ}_1(\gamma) + \mathcal{DJ}_2(\gamma, v)\right) f_V(v)\, dv \tag{4.48}$$

where $\mathcal{DJ}_1$ is evaluated as

$$\mathcal{DJ}_1 = \frac{\partial}{\partial\gamma}\overline{\gamma}\left(s_r, \frac{\gamma N_0}{P_s\lambda_{ss}}\right) = \frac{\gamma^{s_r-1} e^{-\frac{\gamma N_0}{P_s\lambda_{ss}}}}{\left(\frac{P_s\lambda_{ss}}{N_0}\right)^{s_r}\Gamma(s_r)} \tag{4.49}$$

and

$$\mathcal{D}\mathcal{J}_2(\gamma,v)=\frac{\partial}{\partial\gamma}\int_{\frac{\gamma N_0}{P_s}}^{\frac{\gamma}{P_s}(P_pv+N_0)}\frac{x^{s_r-1}e^{-\frac{x}{\lambda_{ss}}}}{\lambda_{ss}^{s_r}\Gamma(s_r)}\left(\frac{P_s}{\gamma P_pv}\left(\frac{\gamma}{P_s}(P_pv+N_0)-x\right)\right)^{s_r-1}dx. \quad (4.50)$$

Using the general Leibniz rule for partial derivative of integrals and identical steps used to derive $\mathcal{J}_2(v)$ (4.43), $\mathcal{D}\mathcal{J}_2(v)$ can be expressed as

$$\mathcal{D}\mathcal{J}_2(\gamma,v)=-\frac{\gamma^{s_r-1}e^{-\frac{\gamma N_0}{P_s\lambda_{ss}}}}{\left(\frac{P_s\lambda_{ss}}{N_0}\right)^{s_r}\Gamma(s_r)}+\frac{(-1)^{s_r-1}e^{-\frac{\gamma N_0}{\lambda_{ss}P_s}}}{\lambda_{ss}\Gamma(s_r-1)P_s}$$
$$\times\sum_{k=0}^{s_r}\binom{s_r}{k}\left(\frac{P_s\lambda_{ss}}{\gamma}\right)^k e^{-\frac{\gamma P_pv}{\lambda_{ss}P_s}}\frac{(P_pv+N_0)^{s_r-k}}{(P_pv)^{s_r-1}}\gamma\left(s_r+k-1,-\frac{P_pv\gamma}{P_s\lambda_{ss}}\right). \quad (4.51)$$

Adding $\mathcal{D}\mathcal{J}_2(\gamma,v)$ to $\mathcal{D}\mathcal{J}_1(v)$ and replacing the result into (4.48), it follows from applying the same approach used to derive $F_{\gamma_{\ddot{s}_1}^{s\to s}}(.)$ that the PDF of $\gamma_{\ddot{s}_1}^{s\to s}$ is given by

$$f_{\gamma_{\ddot{s}_1}^{s\to s}}(\gamma)=\frac{s_t\left(\frac{N_0}{P_s\lambda_{ss}}\right)^{s_r}\gamma^{s_r-1}e^{-\frac{\gamma N_0}{P_s\lambda_{ss}}}}{\Gamma(s_r-1)\Gamma(s_r)}\overline{\gamma}\left(n_r,\frac{\gamma N_0}{P_s\lambda_{ss}}\right)^{s_t-1}\sum_{\substack{0\le i\le s_r\\0\le j\le s_r-j}}\binom{s_r}{i}\binom{s_r-i}{j}(-1)^i$$
$$\times\left(\frac{P_p\lambda_{ps}}{N_0}\right)^{i+j}\frac{\Gamma(s_r+i+j)}{(s_r+i-1)}{}_2F_1\left(1,s_r+i+j;s_r+i;-\frac{\gamma P_p\lambda_{ps}}{P_s\lambda_{ss}}\right)+$$
$$\frac{s_tN_0\left(\frac{N_0}{P_p}\right)^{s_r}}{\Gamma(s_r-1)P_s\lambda_{ss}\lambda_{ps}^{s_r}}\sum_{l=1}^{s_t-1}\binom{s_t-1}{l}\frac{(-1)^{s_r(l+1)-1}e^{-\frac{\gamma N_0(l+1)}{P_s\lambda_{ss}}}}{\Gamma(s_r)^{l+1}}\overline{\gamma}\left(n_r,\frac{\gamma N_0}{P_s\lambda_{ss}}\right)^{s_t-1-l}$$
$$\sum_{\substack{0\le k\le s_r\\0\le k_1,\ldots,k_l\le s_r-1}}\binom{s_r}{k}\prod_{i=1}^{l}\binom{s_r-1}{k_i}(-1)^{\left(k+\sum_{i=1}^{l}k_i\right)}\sum_{n=0}^{+\infty}\mathcal{A}_{l+1,n}^{s_r}(k_1,\ldots,k_l,k-1)$$
$$\times\left(\frac{-\gamma N_0}{P_s\lambda_{ss}}\right)^{(l+1)s_r+n-1}\Gamma\left(l+k+\sum_{i=1}^{l}k_i+s_r+n\right)$$
$$\times\mathcal{U}\left(l+k+\sum_{i=1}^{l}k_i+s_r+n,s_r(l+2)+n+1,\frac{N_0}{P_p}\left(\frac{\gamma(l+1)P_p}{P_s\lambda_{ss}}+\frac{1}{\lambda_{ps}}\right)\right) \quad (4.52)$$

where ${}_2F_1(.,.;.;.)$ is the Gauss hypergeometric function [71, 9.142] resulting from [71, Eq. 6.455.2]. Together with $\mathcal{U}(.,.,.)$, both can accurately be evaluated using Mathematica for instance.

4.4.4 Direct Transmission Outage Probability for the SINR-driven TAS/MRC

The first-hop outage probability of our cognitive MIMO system when an SINR-driven TAS/MRC strategy is adopted, $op^1_{s,sinr}$, can finally be deduced from (4.47) as $op^1_{s,sinr} = F_{\gamma^{s\to s}_{\tilde{s}_1}}(\Phi_s)$. In particular, if the secondary system transmit power allocation is adapted to the primary system QoS as is the case in 4.2.2.2, $op^1_{s,sinr}$ converges for $\frac{P_p}{N_0} \to +\infty$ to an outage probability floor $opF^1_{s,sinr}$. Pertaining to (4.36), we have

$$opF^1_{s,sinr} = \int_0^{+\infty} \mathcal{P}\left(\eta {X_k^1}^2 < \Phi_s Y_k^1 v\right)^{s_t} f_V(v)\, dv \tag{4.53}$$

where η is given by (4.30). The conditional probability inside the integral in (4.53) now reduces from (4.40) to

$$\begin{aligned}\mathcal{P}\left(\eta {X_k^1}^2 < \Phi_s Y_k^1 v\right) &= \left(\frac{\eta}{\Phi_s v}\right)^{s_r-1} \int_0^{\frac{\gamma v}{\eta}} \frac{x^{s_r-1} e^{-\frac{x}{\lambda_{ss}}}}{\Gamma(s_r)} \left(\frac{\Phi_s v}{\eta} - x\right)^{s_r-1} dx \\ &= \lambda_{ss}^{s_r} \sqrt{\frac{\pi v \Phi_s}{\eta \lambda_{ss}}} e^{-\frac{v\gamma}{2\lambda_{ss}\eta}} I_{s_r-\frac{1}{2}}\left(\frac{\pi v \Phi_s}{2\eta\lambda_{ss}}\right)\end{aligned} \tag{4.54}$$

where the last line (4.54) follows from [71, 3.383.2] with $I_{s_r-\frac{1}{2}}(.)$ is the modified Bessel function of the first kind. Similar to the derivation approach of $op^1_{s,sinr}$, (4.54) can also be expressed as

$$\mathcal{P}\left(\eta {X_k^1}^2 < \Phi_s Y_k^1 v\right) = \frac{(-1)^{s_r} e^{-\frac{\Phi_s v}{\eta\lambda_{ss}}}}{\Gamma(s_r)} \sum_{k=0}^{s_r-1} \binom{s_r-1}{k} \left(\frac{\eta\lambda_{ss}}{\Phi_s v}\right)^k \gamma\left(s_r+k, -\frac{\Phi_s v}{\eta\lambda_{ss}}\right). \tag{4.55}$$

After, raising (4.55) to the power of s_t, and then substituted into (4.53), we finally obtain a closed-form expression of $opF^1_{s,sinr}$ that is explicitly given by

$$opF^1_{s,sinr} = \frac{(-1)^{s_t s_r}\, e^{-\frac{\Phi_s v s_t}{\eta \lambda_{ss}}}}{\Gamma(s_r)^{s_t}} \sum_{l=1}^{s_t} \binom{s_t}{l} \sum_{0\leq k_1,\ldots,k_l\leq s_r-1} \prod_{i=1}^{l} \binom{s_r-1}{k_i} (-1)^{\sum_{i=1}^{l} k_i} \sum_{n=0}^{+\infty} \mathcal{A}^{s_r}_{l,n}(k_1,\ldots,k_l) \left(\frac{-\Phi_s}{\eta\lambda_{ss}}\right)^{l s_r+n} \frac{\Gamma((l+1)s_r+n)}{\left(\frac{\Phi_s s_t}{\eta\lambda_{ss}}+\frac{1}{\lambda_{ps}}\right)^{(l+1)s_r+n}}. \quad (4.56)$$

4.5 End-to-End Transmission Outage Probability

In this section, we are keen on the exact derivation of the end-to-end second-hop outage probability of the proposed cognitive MIMO relaying system. Using the total probability law, it is given by [33, Eq. 7-8]

$$op^2_s = \underbrace{\mathcal{P}\left(\gamma_k^{s\to s} < \Phi_s; \gamma_{k,k}^{s,s\to s} < \Phi_s\right)}_{A_3} \underbrace{\mathcal{P}\left(\gamma_k^{s\to r} < \Phi_s\right)}_{A_1} + \underbrace{\mathcal{P}\left(\gamma_k^{s\to s} < \Phi_s; \gamma_{k,k}^{s,r\to s} < \Phi_s\right)}_{A_2} \underbrace{\mathcal{P}\left(\gamma_k^{s\to r} \geq \Phi_s\right)}_{1-A_1} \quad (4.57)$$

where the transmit antenna indices at S-Tx and the relay Re are selected depending on the TAS/MRC strategy being utilized.

4.5.1 Derivation of A_1

Due to the independence between the random channel vectors $\boldsymbol{h}_k^{1,s\to s}$ and $\boldsymbol{h}_k^{s\to r}$ for $k \in \{1,\ldots,s_t\}$, the TAS criterion used by S-Tx does not impact the derivation of A_1 in (4.57). Therefore, A_1 can be deduced from (4.27) as $A_1 = F_{\gamma_{\hat{s}_1}^{s\to s}}(\Phi_s)$ after making the following change of parameters $\lambda_{ss} = \lambda_{sr}$, $\lambda_{pr} = \lambda_{ps}$, $s_t = 1$ and $s_r = r_e$.

4.5.2 Derivation of A_3

The probability A_3 in (4.57) can be viewed as a particular case of A_2 since $A_3 = A_2$ when $r_e = s_t$, $\lambda_{rs} = \lambda_{ss}$ and $\lambda_{rp} = \lambda_{sp}$. The latter equality implies that $P_r = P_s$ (4.4). Therefore, we proceed with the derivation of A_2 according to both TAS/MRC strategies for

an arbitrary r_e, λ_{rs} and λ_{rp}. Then, we deduce A_3 from the final expression of A_2 by making the aforementioned change of parameters.

4.5.3 Derivation of A_2 for the SNR-driven TAS Strategy

According to (4.15) and (4.16), $A_2 = \dot{A}_2$ can be expressed as

$$\dot{A}_2 = \mathcal{P}\left(\frac{P_s X^1_{\dot{s}_1}}{P_p Z^1_{\dot{s}_1} + N_0} < \Phi_s; \frac{P_s X^1_{\dot{s}_1} + P_r X_{\dot{r}}}{P_p Z^2_{\dot{s}_1,\dot{r}} + N_0} < \Phi_s\right) \tag{4.58}$$

where $X^1_{\dot{s}_1}$ (4.20) and $X_{\dot{r}} = \left\|\boldsymbol{h}^{r\to s}_{\dot{r}}\right\|^2$ are independent but not identically distributed variables. The CDF of $X_{\dot{r}}$ is given by (4.22) where s_t and λ_{ss} are being replaced by r_e and λ_{rs}, respectively. On the contrary, $Z^1_{\dot{s}_1}$ (4.21) and

$$Z^2_{\dot{s}_1,\dot{r}} = \frac{\left|\boldsymbol{h}^{1,s\to s^H}_{\dot{s}_1}\boldsymbol{h}^{1,p\to s} + \boldsymbol{h}^{r\to s^H}_{\dot{r}}\boldsymbol{h}^{2,p\to s}\right|^2}{\left\|\boldsymbol{h}^{1,s\to s}_{\dot{s}_1}\right\|^2 + \left\|\boldsymbol{h}^{r\to s}_{\dot{r}}\right\|^2} \tag{4.59}$$

are dependent yet identically distributed λ_{sp}-mean Exponential variables. Given the distribution of the marginals, it is not necessarily true to deduce that the joint PDF of $Z^1_{\dot{s}_1}$ and $Z^2_{\dot{s}_1,\dot{r}}$ follows a bivariate Exponential distribution. Indeed, this implication does not hold true in our case. However, conditioned on $\boldsymbol{h}^{1,s\to s}_{\dot{s}_1}$ and $\boldsymbol{h}^{r\to s}_{\dot{r}}$, the generating complex Gaussian variables of $Z^1_{\dot{s}_1}$,

$$\frac{\boldsymbol{h}^{1,s\to s^H}_{\dot{s}_1}\boldsymbol{h}^{1,p\to s}}{\left\|\boldsymbol{h}^{1,s\to s}_{\dot{s}_1}\right\|}, \tag{4.60}$$

and $Z^2_{\dot{s}_1,\dot{r}}$,

$$\frac{\boldsymbol{h}^{1,s\to s}_{\dot{s}_1}\boldsymbol{h}^{1,p\to s} + \boldsymbol{h}^{r\to s}_{\dot{r}}\boldsymbol{h}^{2,p\to s}}{\sqrt{\left\|\boldsymbol{h}^{1,s\to s}_{\dot{s}_1}\right\|^2 + \left\|\boldsymbol{h}^{r\to s}_{\dot{r}}\right\|^2}}, \tag{4.61}$$

appear to arise from nonsingular linear combinations of independent Gaussian variables. Therefore, they jointly follow a bivariate complex Gaussian distribution. As a result, the joint PDF of $Z^1_{\dot{s}_1}$ and $Z^2_{\dot{s}_1,\dot{r}}$ conditioned on $X^1_{\dot{s}_1} = x_1$ and $X_{\dot{r}} = x_2$ is a bivariate Exponential that can be expressed as

$$f_{Z^1_{\dot{s}_1},Z^2_{\dot{s}_1,\dot{r}}\left|x_1,x_2\right.}(z_1,z_2)=\frac{e^{-\frac{(z_1+z_2)}{\lambda_{ps}(1-\rho_x^2)}}}{\lambda_{ps}^2\left(1-\rho_x^2\right)}I_0\left(\frac{2\rho_x\sqrt{z_1z_2}}{\lambda_{ps}\left(1-\rho_x^2\right)}\right)U(z_1)U(z_2) \tag{4.62}$$

where ρ_x^2 is the conditional correlation coefficient between $Z^1_{\dot{s}_1}$ and $Z^2_{\dot{s}_1,\dot{r}}$ conditioned on $X^1_{\dot{s}_1}=x_1$ and $X_{\dot{r}}=x_2$, and $I_0\left(.\right)$ is the zeroth-order modified Bessel function of the first kind whose series expansion equals

$$I_0\left(z\right)=\sum_{i=0}^{+\infty}\frac{\left(\frac{1}{4}z^2\right)^i}{i!^2}. \tag{4.63}$$

Lemma 4: The conditional correlation coefficient between $Z^1_{\dot{s}_1}$ and $Z^2_{\dot{s}_1,\dot{r}}$ is given by

$$\rho_x^2=\frac{x_1}{x_1+x_2}, \tag{4.64}$$

while its averaged variant $\rho^2=E\left[X^1_{\dot{s}_1}/\left(X^1_{\dot{s}_1}+X_{\dot{r}}\right)\right]$ can be expressed as[1]

$$\begin{aligned}\rho^2=&\frac{s_tr_e}{\Gamma\left(s_r\right)^2}\sum_{\substack{0\le i_1\le n_t-1\\0\le i_2\le i_1(n_r-1)}}\frac{\psi^{s_t-1,s_r}_{i_1,i_2}}{\lambda_{ss}^{i_2+s_t}}\Gamma\left(s_r+i_2+1\right)\\&\times\sum_{\substack{0\le i_3\le r_e-1\\0\le i_4\le i_1(s_r-1)}}\frac{\psi^{r_e-1,s_r}_{i_3,i_4}}{\lambda_{rs}^{i_4+s_r}}\frac{\Gamma\left(s_r+i_4\right)}{\left(2s_r+i_2+i_4\right)}\frac{1}{\left(\frac{i_3+1}{\lambda_{rs}}\right)^{2s_r+i_2+i_4}}\\&\times{}_2F_1\left(s_r+i_2+1,2s_r+i_2+i_4,2s_r+i_2+i_4+1,1-\frac{\lambda_{rs}\left(i_1+1\right)}{\lambda_{ss}\left(i_3+1\right)}\right).\end{aligned} \tag{4.65}$$

Proof: See Appendix F.

[1]In the particular case of $X^1_{\dot{s}_1}$ and $X^2_{\dot{r}}$ are identically distributed in addition to being independent, we would have easily obtained $\rho^2=E\left[X^1_{\dot{s}_1}/\left(X^1_{\dot{s}_1}+X_{\dot{r}}\right)\right]=E\left[X_{\dot{r}}/\left(X_{\dot{r}}+X^1_{\dot{s}_1}\right)\right]=\frac{1}{2}$ compared to the general expression (4.65). This case arises in the calculation of A_3 (4.57) reflecting the event in which S-Tx transmits during both relaying hops.

We proceed now with the derivation of $\dot{A}_2$ starting from equation (4.58). It can be rewritten as

$$\dot{A}_2 = \iiiint_{\mathcal{R}} f_{Z^1_{\dot{s}_1}, Z^2_{\dot{s}_1,\dot{r}}\left|x_1,x_2\right.}(z_1,z_2)\, f_{X_{\dot{r}}}(x_2)\, f_{X^1_{\dot{s}_1}}(x_1)\, dx_1 dx_2 dz_1 dz_2 \tag{4.66}$$

$$= \frac{s_t r_e}{(\lambda_{ss}\lambda_{rs})^{s_r}\,\Gamma(s_r)^2}\left[\mathcal{I}_{\mathcal{R}_1} + \mathcal{I}_{\mathcal{R}_2} + \sum_{i=0}^{+\infty}\frac{\mathcal{I}_{\mathcal{R}_3}(i)}{i!^2}\right] \tag{4.67}$$

where $\mathcal{R} = \{\mathcal{R}_1 \cup \mathcal{R}_2 \cup \mathcal{R}_3\}$ is our four-dimensional integration region that can be subdivided into three distinct regions

$$\begin{cases} \mathcal{R}_1 = & \big\{(x_1,x_2,z_1,z_2)\in\mathbb{R}^{+4}\,|0<x_1<\beta, \\ & 0<x_2<\frac{1}{\delta}(\beta-x1), 0<z_1, 0<z_2\big\} \\ \mathcal{R}_2 = & \big\{(x_1,x_2,z_1,z_2)\in\mathbb{R}^{+4}\,|0<x_1<\beta, \\ & \frac{1}{\delta}(\beta-x1)<x_2, 0<z_1, \\ & \frac{1}{\alpha}(-\beta+x_1+\delta x_2)<z_2\big\} \\ \mathcal{R}_3 = & \big\{(x_1,x_2,z_1,z_2)\in\mathbb{R}^{+4}\,|\beta<x_1, \\ & 0<x_2, \frac{1}{\alpha}(-\beta+x_1)<z_1, \\ & \frac{1}{\alpha}(-\beta+x_1+\delta x_2)<z_2\big\} \end{cases} \tag{4.68}$$

over each the integral in (4.66) will be carried on. In (4.68), $\alpha = \frac{\Phi_s P_p}{P_s}$, $\beta = \frac{\Phi_s N_0}{P_s}$ and $\delta = \frac{P_r}{P_s}$. Given (4.23), the first quadruple integral $\mathcal{I}_{\mathcal{R}_1}$ in (4.67) over the region $\mathcal{R}_1$ is given by

$$\mathcal{I}_{\mathcal{R}_1} = \int_0^{\beta}\int_0^{\frac{1}{\delta}(\beta-x1)} (x_1x_2)^{s_r-1}\, e^{-\frac{x_1}{\lambda_{ss}}-\frac{x_2}{\lambda_{rs}}}\,\overline{\gamma}\left(s_r,\frac{x_1}{\lambda_{ss}}\right)^{s_t-1}\overline{\gamma}\left(s_r,\frac{x_2}{\lambda_{rs}}\right)^{r_e-1} dx_2 dx_1. \tag{4.69}$$

It can further be developed using the result of Lemma 1, [71, Eq. 3.351.1] and [71, Eq. 3.383.1] to obtain

$$\mathcal{I}_{\mathcal{R}_1} = \sum_{\substack{0\leq i_1\leq s_t-1\\ 0\leq i_2\leq i_1(s_r-1)}} \frac{\psi_{i_1,i_2}^{s_t-1,s_r}}{\lambda_{ss}^{i_2}} \sum_{\substack{0\leq i_3\leq r_e-1\\ 0\leq i_4\leq i_3(s_r-1)}} \frac{\psi_{i_3,i_4}^{r_e-1,s_r}}{\lambda_{rs}^{i_4}} \frac{\Gamma(s_r+i_4)\,\Gamma(s_r+i_2)}{\left(\frac{i_3+1}{\lambda_{rs}}\right)^{s_r+i_4}} \times$$
$$\left[\left(\frac{\lambda_{ss}}{i_1+1}\right)^{s_r+i_2} \overline{\gamma}\left(s_r+i_2, \frac{(i_1+1)\,\beta}{\lambda_{ss}}\right) e^{-\frac{\beta(i_3+1)}{\lambda_{rs}\delta}} \sum_{m=0}^{s_r+i_4-1} \left(\frac{i_3+1}{\lambda_{rs}\delta}\right)^m \beta^{s_r+i_2+m}\right.$$
$$\left. -\Gamma(m+1)\,{}_1F_1\left(s_r+i_2; s_r+i_2+m+1; \beta\left(\frac{i_3+1}{\lambda_{rs}\delta}-\frac{i_1+1}{\lambda_{ss}}\right)\right)\right] \tag{4.70}$$

where ${}_1F_1(.;.;.)$ denotes the Kummer confluent hypergeometric function [71, Eq. 9.210.1]. Following the same steps, $\mathcal{I}_{\mathcal{R}_2}$ and $\mathcal{I}_{\mathcal{R}_3}(i)$ can also be derived using [71, Eq. 3.351.2] (instead of [71, Eq. 3.351.1] in the $\mathcal{I}_{\mathcal{R}_1}$ derivation case) and (4.62) as

$$\mathcal{I}_{\mathcal{R}_2} = \sum_{\substack{0\leq i_1\leq s_t-1\\ 0\leq i_2\leq i_1(s_r-1)}} \frac{\psi_{i_1,i_2}^{s_t-1,s_r}}{\lambda_{ss}^{i_2}} \sum_{\substack{0\leq i_3\leq r_e-1\\ 0\leq i_4\leq i_3(s_r-1)}} \frac{\psi_{i_3,i_4}^{r_e-1,s_r}}{\lambda_{rs}^{i_4}} \frac{\Gamma(s_r+i_4)\,\Gamma(s_r+i_2)}{\left(\frac{i_3+1}{\lambda_{rs}}+\frac{\delta}{\lambda_{ps}\alpha}\right)^{s_r+i_4}}$$
$$\times e^{-\beta\left(\frac{i_3+1}{\lambda_{rs}\delta}+\frac{1}{\lambda_{ps}\alpha}\right)} \sum_{m=0}^{s_r+i_4-1} \Gamma(m+1)\left(\frac{i_3+1}{\lambda_{rs}\delta}+\frac{1}{\lambda_{ps}\alpha}\right)^m$$
$$\times\beta^{s_r+i_2+m}\,{}_1F_1\left(s_r+i_2; s_r+i_2+m+1; \beta\left(\frac{i_3+1}{\lambda_{rs}\delta}-\frac{i_1+1}{\lambda_{ss}}\right)\right) \tag{4.71}$$

and

$$\mathcal{I}_{\mathcal{R}_3}(i) = \sum_{\substack{0\leq i_1\leq s_t-1\\ 0\leq i_2\leq i_1(s_r-1)}} \frac{\psi_{i_1,i_2}^{s_t-1,s_r}}{\lambda_{ss}^{i_2}} \sum_{\substack{0\leq i_3\leq r_e-1\\ 0\leq i_4\leq i_3(s_r-1)}} \frac{\psi_{i_3,i_4}^{r_e-1,s_r}}{\lambda_{rs}^{i_4}} \int_{\beta}^{+\infty}\int_{0}^{+\infty} \frac{x_1^{s_r-1+i+i_2}}{(x_1+x_2)^{i+1}}$$
$$\times x_2^{s_r+i_4} e^{-\frac{(i_1+1)x_1}{\lambda_{ss}}-\frac{(i_3+1)x_2}{\lambda_{rs}}} \Gamma\left(1+i, \frac{(x_1+x_2)}{\lambda_{ps}x_2}\frac{(-\beta+x_1)}{\alpha}\right)$$
$$\times\Gamma\left(1+i, \frac{(x_1+x_2)}{\lambda_{ps}x_2}\frac{(-\beta+x_1+\delta x_2)}{\alpha}\right) dx_2 dx_1, \tag{4.72}$$

respectively. To the best of the authors knowledge, the double integral in (4.72) cannot be resolved in closed form. Yet, it can accurately be calculated via numerical integration using Mathematica for instance.

At this stage, we conclude with the derivation of the end-to-end outage probability of our cognitive MIMO relay system, $op^2_{s,snr} = \dot{A}_3 A_1 + \dot{A}_2 (1 - A_1)$, using an SNR-driven TAS/MRC strategy. The outage probability floor $opF^2_{s,snr}$ appearing for $\frac{P_p}{N_0} \to +\infty$ can be deduced from the final expression of $op^2_{s,snr}$ by setting $\alpha = \Phi_s/\eta$, $\beta = 0$ and $\delta = \frac{\kappa}{\eta}$ where κ is given by η (4.30) with λ_{sp} being replaced by $\lambda_{rp}.\frac{P_p}{N_0} = 5\,\mathrm{dB} d_{ss}$.

4.5.4 Derivation of A_2 for the SINR-driven TAS Strategy

It follows from the SINR-driven TAS/MRC criterion proposed in (4.17) and (4.18), that $A_2 = \ddot{A}_2$ can be expressed as

$$\ddot{A}_2 = \mathcal{P}\left(\frac{P_s X^1_{\ddot{s}_1}}{P_p Z^1_{\ddot{s}_1} + N_0} < \Phi_s; \frac{P_s X^1_{\ddot{s}_1} + P_r X_{\ddot{r}}}{P_p Z^2_{\ddot{s}_1,\ddot{r}} + N_0} < \Phi_s \right). \tag{4.73}$$

The derivation of $\ddot{A}_2$ is too involved because of the correlation linking most the variables in (4.73). A summary of the relationship between all pairs of variables in our system is shown in table 4.2. Despite, we develop $\ddot{A}_2$ in a general integral format, then to get much intuition into its exact derivation, we proceed by considering the particular case of single receive-antenna at S-Rx, i.e. $s_r = 1$.

The right-hand side event of (4.73) can be rewritten as

$$\frac{P_s X^1_{\ddot{s}_1} + P_r X_{\ddot{r}}}{P_p Z^2_{\ddot{s}_1,\ddot{r}} + N_0} = \max_{k \in \{1,\ldots,r_e\}} \left\{ \frac{P_s X^1_{\ddot{s}_1} + P_r X_k}{P_p Z^2_{\ddot{s}_1,k} + N_0} \right\}. \tag{4.74}$$

Variables		**SNR-driven TAS** $(s_i = \dot{s}_i\,, r = \dot{r})$	**SINR-driven TAS** $(s_i = \ddot{s}_i\,, r = \ddot{r})$
$X^1_{s_1}$	$X^2_{s_2}$	$\perp$	$\propto$
$X^1_{s_1}$	$Z^1_{s_1}$	$\perp$	$\propto$
$X^1_{s_1}$	$Z^2_{s_1,r}$ or $Z^2_{s_1,s_2}$	$\perp$	$\propto$
$X^2_{s_2}$	$Z^1_{s_1}$	$\perp$	$\propto$
$X^2_{s_2}$	$Z^2_{s_1,r}$ or $Z^2_{s_1,s_2}$	$\perp$	$\propto$
$Z^1_{s_1}$	$Z^2_{s_1,r}$or $Z^2_{s_1,s_2}$	$\propto$	$\propto$

TABLE 4.2: The relationship between each two variables resulting from the use of both TAS/MRC strategies. $\perp$ and $\propto$ denote for the independence and dependence, respectively.

To expand $\ddot{A}_2$, we condition both events in (4.73) on $X^1_{\ddot{s}_1}$ and $Z^1_{\ddot{s}_1}$. Consequently, we obtain (4.82) where the conditional probability $\ddot{A}_2(x,z)$ can in turn be expressed as

$$\ddot{A}_2(x,z) = \int_0^{+\infty} \mathcal{P}\left(\frac{P_s x + P_r X_k}{P_p \frac{Z^2_{\ddot{s}_1,k}\big|x,z,v}{x+X_k} + N_0} < \Phi_s \right)^{r_e} f_V(v)\, dv \tag{4.75}$$

where $V = \left\| \boldsymbol{h}^{2,p\to s} \right\|^2$. Expression (4.75) has resulted from applying the same approach used in Subsection 4.4.3. In (4.75), the variable $Z^2_{\ddot{s}_1,k}\big|x,z,v$ for $k \in \{1,\ldots,r_e\}$ is given by

$$Z^2_{\ddot{s}_1,k}\big|x,z,v = \left| \sqrt{xz} + \boldsymbol{h}_k^{r\to s^H} \boldsymbol{h}^{2,p\to s} e^{-\mathrm{i}\theta} \right|^2 v \tag{4.76}$$

where the random variable θ corresponds to the argument of $\boldsymbol{h}_{\ddot{s}_1}^{1,s\to s^H} \boldsymbol{h}^{1,p\to s}$ that is independent of $\boldsymbol{h}_k^{r\to s^H} \boldsymbol{h}^{2,p\to s}$. After being properly scaled, it turns out that $Z^2_{\ddot{s}_1,k}\big|x,z,v$ follows a non-central Chi-squared distribution. In fact, the derivation of $\ddot{A}_2(x,z)$ involves knowing the bivariate PDF of $2X_k \setminus \lambda_{rs}$ and $2Z^2_{\ddot{s}_1,k}\big|x,z,v \setminus v\lambda_{rs}$ as central and non-central chi-squared random variables, respectively, with different degrees of freedom and noncentrality parameters.

To the best of our knowledge, the bivariate PDF in question has not been derived yet in the literature. As a starting point, we resort to the single receive antenna case at S-Rx in order to get some insights into the derivation of $\ddot{A}_2$ (4.73) as the latter appears to be too complex to evaluate in a closed-form expression for an arbitrary receive antennas s_r at S-Rx.

Theorem 2: The bivariate PDF of X_k and $Z^2_{\ddot{s}_1,k}\big|x,z,v$ in the case of an arbitrary non-negative reals x, z and v, and $s_r = 1$ is given by

$$f_{X_k, Z^2_{\ddot{s}_1,k}\big|x,z,v}(x_2,z_2) = \begin{cases} \dfrac{e^{-x_2/\lambda_{rs}}}{\lambda_{rs}\pi\sqrt{4xzx_2v - (z_2 - (xz + x_2v))^2}}; \\ \left(\sqrt{xz} - \sqrt{x_2v}\right)^2 < z_2 < \left(\sqrt{xz} + \sqrt{x_2v}\right)^2 \\ 0; \ \text{Otherwise} \end{cases} \tag{4.77}$$

See Appendix G.

Also, the joint PDF in (4.82), $f_{X^1_{\ddot{s}_1},Z^1_{\ddot{s}_1}}(.,.)$, now reduces for $s_r = 1$, $x \geq 0$ and $z \geq 0$ to

$$f_{X^1_{\ddot{s}_1},Z^1_{\ddot{s}_1}}(x,z) = s_t \left(1 - e^{-\frac{x}{\lambda_{ss}}}\right)^{s_t-1} \frac{e^{-\frac{x}{\lambda_{ss}}}}{\lambda_{ss}} \frac{e^{-\frac{z}{\lambda_{ps}}}}{\lambda_{ps}} \tag{4.78}$$

because both variables $X^1_{\ddot{s}_1}$ and $Z^1_{\ddot{s}_1}$ becomes independent. Let the probability inside (4.75) before raised to the power of r_e be denoted by $\ddot{A}_2(x,z,v)$. As a result of Theorem 1, it can now be expressed as

$$\ddot{A}_2(x,z,v) = \iint_{\mathcal{T}} f_{X_k,Z^2_{\ddot{s}_1,k}\big|x,z,v}(x_2,z_2)\, dx_2 dz_2 \tag{4.79}$$

where $\mathcal{T} = \{\mathcal{T}_1 \cup \mathcal{T}_2 \cup \mathcal{T}_3\}$ is a two-dimensional region that, for a given $z \geq 0$ and $0 \leq x \leq \Phi_s(P_p z + N_0)/P_s$, defines the sub-regions over which the inequality $(P_s x + P_r x_2 - \Phi_s N_0) \leq z_2 \Phi_s P_p/(x + x_2)$ holds true. It can be divided into three distinct sub-regions as

$$\begin{cases} \mathcal{T}_1 = & \big\{(x_2,z_2) \in \mathbb{R}^{+2} \,|0 \leq z, 0 \leq x \leq \beta, \\ & 0 \leq x_2 \leq \frac{1}{\delta}(\beta - x), 0 \leq z_2\big\} \\ \mathcal{T}_2 = & \big\{(x_2,z_2) \in \mathbb{R}^{+2} \,|0 \leq z, 0 \leq x \leq \beta, \\ & \frac{1}{\delta}(\beta - x) < x_2, \frac{1}{\alpha}(-\beta + x_1 + \delta x_2) < z_2\big\} \\ \mathcal{T}_3 = & \big\{(x_2,z_2) \in \mathbb{R}^{+2} \,|0 \leq z, \beta < x \leq \beta + \alpha z \\ & 0 \leq x_2, \frac{1}{\alpha}(-\beta + x + \delta x_2) < z_2\big\} \end{cases} \tag{4.80}$$

where the parameters α, β and δ are similarly defined as in previous section. Note that it becomes not trivial to precise $\mathcal{T}$ if we add the definition domain of the bivariate distribution in (4.77) to the system of inequalities (4.80) as it will involve solving quartic inequalities. Indeed, we replace (4.77) as is into (4.79) and carry out the double integration over $\mathcal{T}_1$, $\mathcal{T}_2$ and $\mathcal{T}_3$. After usual mathematical manipulation, we derive $\ddot{A}_2(x,z,v)$ as shown in (4.83) where the function $\mathcal{G}(.)$ is given by

$$\mathcal{G}(u) = \begin{cases} 1 & ; \ u \leq -1 \\ \arccos(u) & ; \ -1 \leq u \leq 1 \\ 0 & ; \ \text{Otherwise} \end{cases}. \tag{4.81}$$

Finally, we substitute $\ddot{A}_2(x,z,v)$ (4.83) into $\ddot{A}_2(x,z)$ which in turn being raised to the power of r_e (4.75) before replaced in

$$\ddot{A}_2 = \int_0^{+\infty} \int_0^{\frac{\Phi_s}{P_s}(P_p z + N_0)} f_{X^1_{\ddot{s}_1}, Z^1_{\ddot{s}_1}}(x,z) \times \underbrace{\mathcal{P}\left(\frac{P_s x + P_r X_1}{P_p Z^2_{\ddot{s}_1,1} | x, z+N_0} < \Phi_s; \ldots; \frac{P_s x + P_r X_{r_e}}{P_p Z^2_{\ddot{s}_1,r_e} | x, z+N_0} < \Phi_s \right)}_{\ddot{A}_2(x,z)} dx dz. \tag{4.82}$$

The resulting expression of $\ddot{A}_2$ is a three-dimensional integration over v, x and z, successively, without counting the integral over x_2 in

$$\ddot{A}_2(x,z,v) = \begin{cases} \left(1 - e^{-\frac{1}{\delta}(\beta - x)}\right) + \int_{\frac{1}{\delta}(\beta-x)}^{+\infty} \frac{e^{-\frac{x_2}{\lambda_{rs}}}}{\lambda_{rs}} \times \\ \mathcal{G}\left(\frac{(-\beta + x + \delta x_2) - \alpha(xz + x_2 v)}{2\alpha\sqrt{xzvx_2}} \right) dx_2 & ; 0 \le x \le \beta \\ \int_0^{+\infty} \frac{e^{-\frac{x_2}{\lambda_{rs}}}}{\lambda_{rs}} \times \\ \mathcal{G}\left(\frac{(-\beta + x + \delta x_2) - \alpha(xz + x_2 v)}{2\alpha\sqrt{xzvx_2}} \right) dx_2 & ; \beta < x \le \beta + \alpha z \\ 0 & ; \text{Otherwise} \end{cases}. \tag{4.83}$$

Clearly, it is difficult to evaluate $\ddot{A}_2$ in a closed form for the SINR-driven TAS/MRC strategy even in the single receive antenna case at S-Rx. However, thanks to powerful mathematical softwares such as Mathematica, $\ddot{A}_2$ and consequently the end-to-end outage probability $op^2_{s,sinr} = \ddot{A}_3 A_1 + \ddot{A}_2(1 - A_1)$ can accurately be computed via numerical integration and double-checked with monte-carlo simulations. The same applies to the calculation of the outage probability floor $opF^2_{s,sinr}$ occurring in high primary system SNR ratios. It can be deduced from $op^2_{s,sinr}$ as pointed out in the SNR-driven TAS/MRC strategy.

4.6 Simulation Results and Implementation Prospects

In this section, we confirm the correctness of the outage probability analysis we carried out in the previous two sections. Furthermore, we conduct an accurate outage performance comparison between the SNR and SINR-driven TAS/MRC strategies for different system settings and scenarios. Finally, we give more insights on our results and discuss implementation prospects of both TAS/MRC strategies in future cognitive MIMO relaying systems.

4.6.1 PDF of the First-Hop Received SINR at S-Rx for both TAS/MRC strategies and Some Insights on Approximation (4.34)

Fig. 4.1 shows the curves of the derived PDFs (4.28) and (4.52) for both TAS/MRC strategies, thereby confirming the exactitude of our findings in subsection 4.4. As the receive antenna number s_r increases, as illustrated in Fig. 1(b), the approximation (4.34) leading to

$$f_{\gamma_{\tilde{s}_1}^{s\to s}}(\gamma) \approx s_t F_{\gamma_k^{s\to s}}(\gamma)^{s_t-1} f_{\gamma_k^{s\to s}}(\gamma) \tag{4.84}$$

becomes tight because the correlation between the received MRC output SINRs $\gamma_k^{s\to s}$ weakens. The evidence of this claim is justified by evaluating the correlation coefficient ζ^2 between the variables Z_k^1 (4.35) that is found to be inversely proportional to s_r and exactly equaling $\zeta^2 = 1/s_r$. Hence, a typical scenario for which (4.84) holds as a tight approximation arises if a large-scale receive antenna array is deployed at S-Rx. This reasoning is valid only for the direct-link transmission, otherwise (4.84) is not adequate to approximate the PDF of the equivalent received SINR during the second-hop transmission as the correlation between the resulting system variables become much more involved. From Fig. 4.2, we point out that the PDFs corresponding to both TAS/MRC strategies tend to approach each other for low values of λ_{ps}, and got clearly separated for high values of λ_{ps} reflecting the dominance of the interference from P-Tx on S-Rx. If the primary system interference on the secondary system is neglected, i.e. $\lambda_{ps} \to 0$, the SINR-driven TAS/MRC strategy reduces to its SNR-driven counterpart. Therefore, the former is viewed as an optimal interference-aware strategy that outperforms the latter over the entire primary system SNR ratio and for any arbitrary secondary system settings.

4.6.2 First-Hop Outage Probability

In Fig. 4.3(a), the analytical expressions of the first-hop outage probability for both TAS/MRC schemes are depicted and compared to those found by Monte-Carlo simulations, whereas in Fig 4.3(b), we separately plot the outage probability floors appearing at high primary system SNR ratios using an adaptive secondary system power allocation method. Our curves are generated for different antenna configurations. Once again, our findings are confirmed by simulations to be exact and accurate. Pertaining to Fig. 4.3(a), the secondary system transmit power P_s is allocated either in a fixed (4.6) or adaptive manner as described in section 4.2.2. Apparently, the former leads to severe performance degradation as opposed to the latter which leads to a proportional outage performance enhancement with the primary system QoS. In the adaptive power allocation scenario, the condition $Q_i > 0$ from (4.5) must hold or equivalently the primary system SNR ratio P_p/N_0 is required to be greater than a certain threshold $Q_{th}\,\mathrm{dB}$, i.e.

$$\frac{P_p}{N_0} > \frac{\Phi_p}{\lambda_{pp} \log\left(\frac{1}{1-\varepsilon_p}\right)} = 10^{\frac{Q_{th}}{10}},$$

so as the secondary system can coexist with the primary system on the same spectrum. Our simulations in Fig. (4.3) are conducted with $Q_{th} = -0.1\,\mathrm{dB}$ in order for the x-axis to be defined starting from $P_p/N_0 = 0\,\mathrm{dB}$, and $\varepsilon_p = 0.01$. The value of Q_{th} can arbitrary be modified as a function of the primary system settings Φ_p, λ_{pp} and ε_p.

4.6.2.1 Impact of Antenna Configuration

Fig 4.3(b) shows the gap between both TAS/MRC strategies in terms of the outage probability floors (4.29) and (4.56) for different antenna configurations in the case of an adaptive power allocation is used by S-Tx. Clearly, the superiority of the SINR-driven TAS/MRC gets more pronounced as our MIMO system gets larger reflecting its interference cancellation capability against its SNR-driven counterpart. For instance, the outage probability floors for a 6×6 cognitive MIMO system are $opF^1_{s,snr} = 1.43251 \times 10^{-9}$ and much less $opF^1_{s,sinr} = 1.0784 \times 10^{-15}$. We mention that this gap limit is attained in the high primary system SNR regime although the beginning of its appearance starts from low values of P_p/N_0 as captured by Fig. 4.3(a).

4.6.2.2 Impact of the Second-Order Statistic λ_{ps}

Alternatively, in Fig. 4.4, we plot the outage probability floors $opF^1_{s,snr}$ and $opF^1_{s,sinr}$ but now as function of $1/\lambda_{ps}$. When large-scale variations of the interference channel between P-Tx and S-Rx are taken into account, λ_{ps} can be viewed as inversely proportional to the distance between P-Tx and S-Rx. This means that the greater $1/\lambda_{ps}$ is the farther P-Tx is seen from S-Rx. As captured Fig. 4.4, the outage probability floors $opF^1_{s,snr}$ and $opF^1_{s,sinr}$ decrease as P-Tx goes far from S-Rx thus causing less interference impact on the secondary system. Once again, the gap between both TAS/MRC strategies widens for loaded cognitive MIMO configurations as the SINR-driven TAS/MRC strategy leverages all available cognitive MIMO system diversities to optimally reducing the primary system interference impact on the secondary system.

Kindly note that the general nature of our derived analytical results can serve as a framework to evaluate the secondary system outage performance under different system settings and scenarios for both TAS/MRC strategies under consideration.

4.6.3 End-to-End Outage Performance

During the second-hop, our cognitive $s_t \times s_r$ MIMO relay system can be viewed as a virtual $s_t \times 2s_r$ cognitive MIMO system, hence, most of the insights we gave in the previous subsection hold true herein as well. However, we are here keen on assessing the end-to-end outage performance of our system, in particular, evaluating the advantage of relaying and transmit diversities that are jointly targeted in the proposed SINR-driven TAS/MRC strategy.

4.6.3.1 Impact of Antenna Configuration

In Fig. 4.5(a), our derived analytical results of the end-to-end outage probability (4.57) for both TAS/MRC strategies under focus are compared and double-checked by simulations. Note that the curves representing the SINR-driven TAS/MRC in the case of $s_r = 1$ corresponds to the end-to-end outage analysis carried out in subsections 4.5.4, 4.5.2 and 4.5.1. As already pointed out, for situations where $s_r \geq 2$, the end-to-end outage probability when an SINR-driven TAS/MRC strategy is adopted becomes too complex to evaluate analytically, therefore, we resort to monte-carlo simulations as depicted in green solid lines in both pictures of Fig. 4.5.

4.6.3.2 Impact of Relay Location

Fig. 4.5(b) shows the end-to-end outage probability as a function of the distance between S-Tx and Re. For simplicity, we consider a two-dimensional squared geometry [39] of our cognitive MIMO relay system where P-Tx, P-Rx, S-Tx and S-Rx are positioned at locations of coordinates (1,0), (1,1), (0,0), (0,1), respectively, and the relay Re moves across the line between S-Tx and S-Rx. Our path-loss model is assumed to be exponentially decaying such that $\lambda_{ab} = d_{ab}^{-\kappa}$ where d_{ab} is the distance between the transmitting node of index a and the receiving node of index b, and κ is the path-loss coefficient. From Fig 4.5(b), we observe that the optimal relay location is centered around $d_{ss} = 0.5$, but tends to shrink as s_r increases and enlarges as s_r decreases. This is true whether the secondary system is operating at low or moderate-to-high primary system SNR ratios.

4.6.4 Implementation Prospects of both TAS/MRC Strategies

4.6.4.1 Antenna Index Feedback Load

During both relaying hops, the secondary system transmitting nodes need to identify the index of their transmit antenna. This index is assumed to be selected by S-Rx and fed back to either S-Tx or Re via an error-free load of $\max\left\{\lceil \log_2(s_t) \rceil, \lceil \log_2(r_e) \rceil\right\}$ binary bits where $\lceil u \rceil$ refers to the smallest integer greater than or equals u. In this regard, both TAS/MRC strategies are alike.

4.6.4.2 CSI Acquisition and Antenna Selection

Assuming the secondary system receiving node S-Rx is capable of acquiring complete CSI about its forwarding channels, it can simply identify the index of the selected transmit antenna at either S-Tx or Re according to the SNR-driven TAS/MRC strategy. Yet, for packet decoding purposes, S-Rx is required to also acquire complete CSI about its respective interference channel and determine the primary and secondary transmit power levels in addition to the AWGN power spectral density. Altogether, these parameters are the prerequisites of the SINR-driven TAS/MRC strategy. Hence, while the SNR-driven TAS/MRC strategy can be applied at an early stage of the packet decoding process at S-Rx, its SINR-driven counterpart requires additional parameters at an advanced stage in the received symbol packet processing. This justifies the performance/complexity tradeoff by which both TAS/MRC strategies are governed.

4.6.4.3 TAS in Future Wireless Communications

TAS has been used in LTE/LTE-A as a means to reduce system complexity and power consumption at the transmitter side while reaping the benefits of multi-antenna systems especially at the user equipment side. Its flexibility and adaptability to be used with different MIMO variants such as spatial division multiplexing and space-time block codes [68] makes it a potential candidate for the 5G and beyond. TAS can also be envisaged for large-scale cognitive MIMO systems in an attempt to combat/exploit co-channel interference in a more sophisticated way [69]. However, particular efforts should be paid to lower the complexity of the antenna selection algorithm in use.

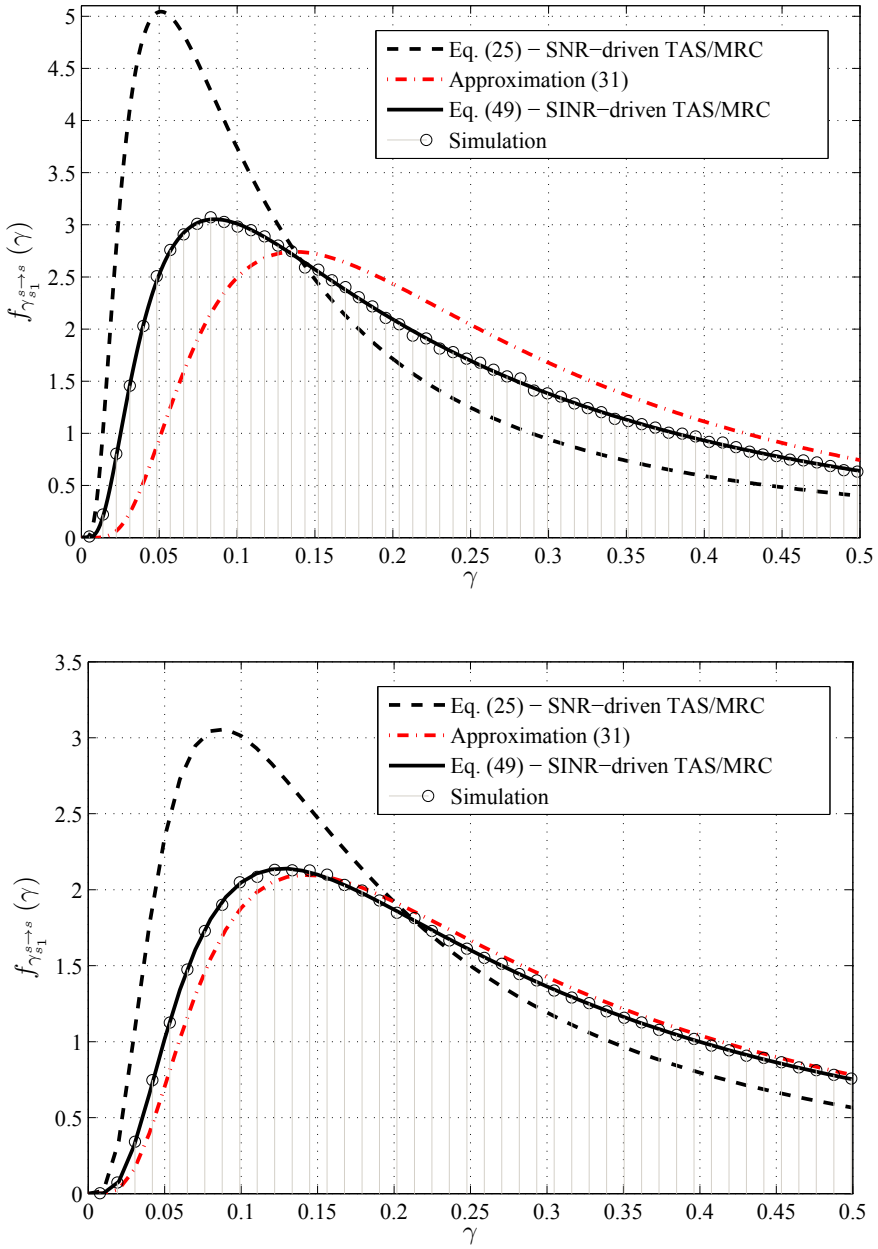

Figure 4.1: The MRC combiner output SINR PDFs (4.28) and (4.52) when the SNR and SINR-driven TAS/MRC strategies are adopted, respectively. Both PDFs are compared against the one generated according to approximation (4.34). For both figures, we have taken $\lambda_{ss} = \lambda_{sp} = \lambda_{ps} = 1$, $P_p/N_0 = 10\,\text{dB}$ and $Q_i = -5\,\text{dB}$ as practical system settings that can arbitrary be modified. The figure on the Top (a) is generated for $s_t = 5$ and $s_r = 2$, whereas the figure on the Bottom (b) is generated for $s_t = 2$ and $s_r = 5$. The index s_1 in $f_{\gamma_{s_1}^{s\to s}}(\gamma)$ equals either $\dot{s}_1$ or $\ddot{s}_1$ depending on the TAS/MRC strategy being utilized.

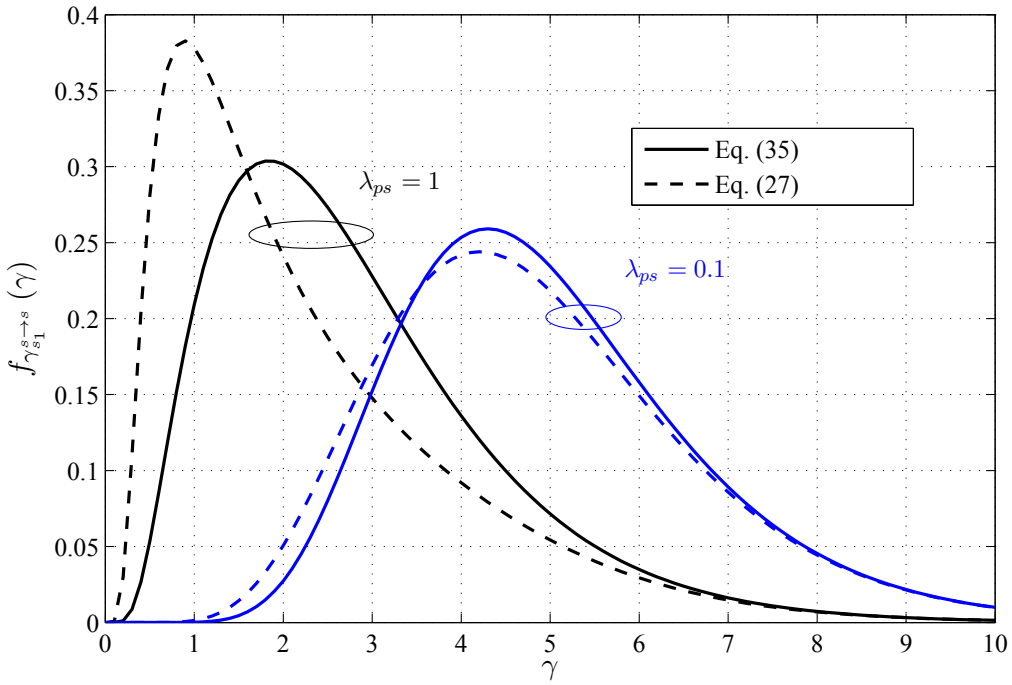

Figure 4.2: Comparison between the received SINR PDFs when an SNR and SINR-driven TAS/MRC strategies are adopted, respectively. It is assumed that $\lambda_{ss} = \lambda_{sp} = 1$, $P_p/N_0 = 5\,\text{dB}$, $Q_i = 0\,\text{dB}$ and s_1 in $f_{\gamma_{s_1}^{s\to s}}(\gamma)$ equals either $\dot{s}_1$ or $\ddot{s}_1$ depending on the TAS/MRC strategy being utilized.

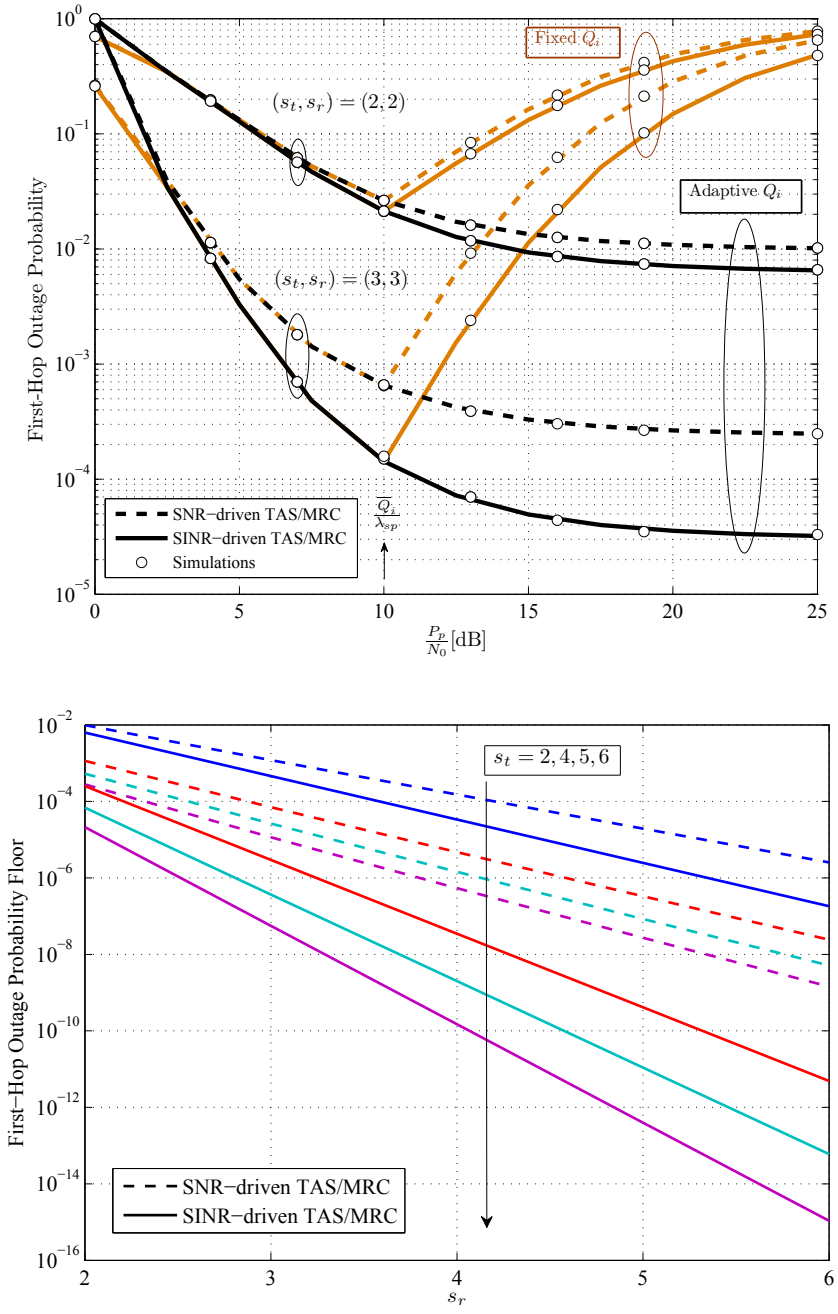

Figure 4.3: Top (a): The first-hop outage probability $op^1_{s,snr}$ and $op^1_{s,sinr}$ at a certain threshold $\Phi_s = 2^2 - 1$ versus the primary system SNR ratio P_p/N_0 while having $\lambda_{ss} = 1$, $\lambda_{sp} = \lambda_{ps} = 0.1$ and $\overline{Q}_i = 0\,\text{dB}$ fixed. Down (b): The outage probability floor gap between (4.29) and (4.56), appearing when $P_p/N_0 \to +\infty$, is calculated for different antenna configurations.

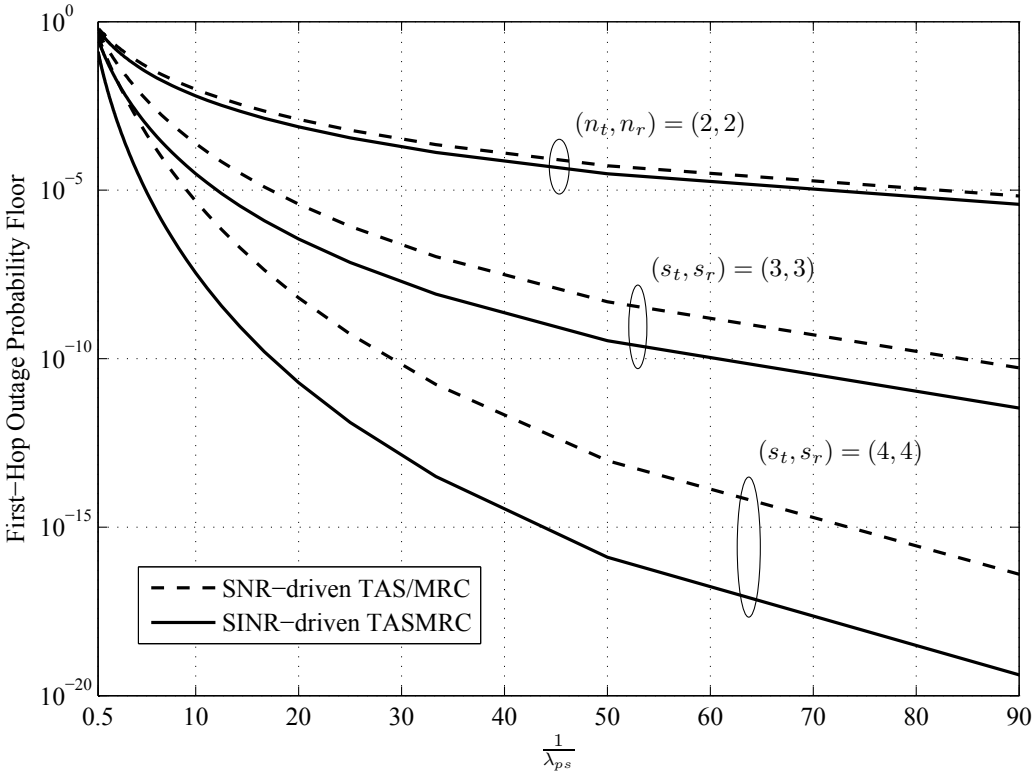

Figure 4.4: The first-hop outage probability floor for both TAS/MRC strategies versus the inverse of λ_{ps} for different antenna configurations. The parameters $\lambda_{ss} = 1$, $\lambda_{sp} = 0.1$, $Q_{th} = -0.1\,\mathrm{dB}$ and $\varepsilon_p = 0.01$ are being fixed.

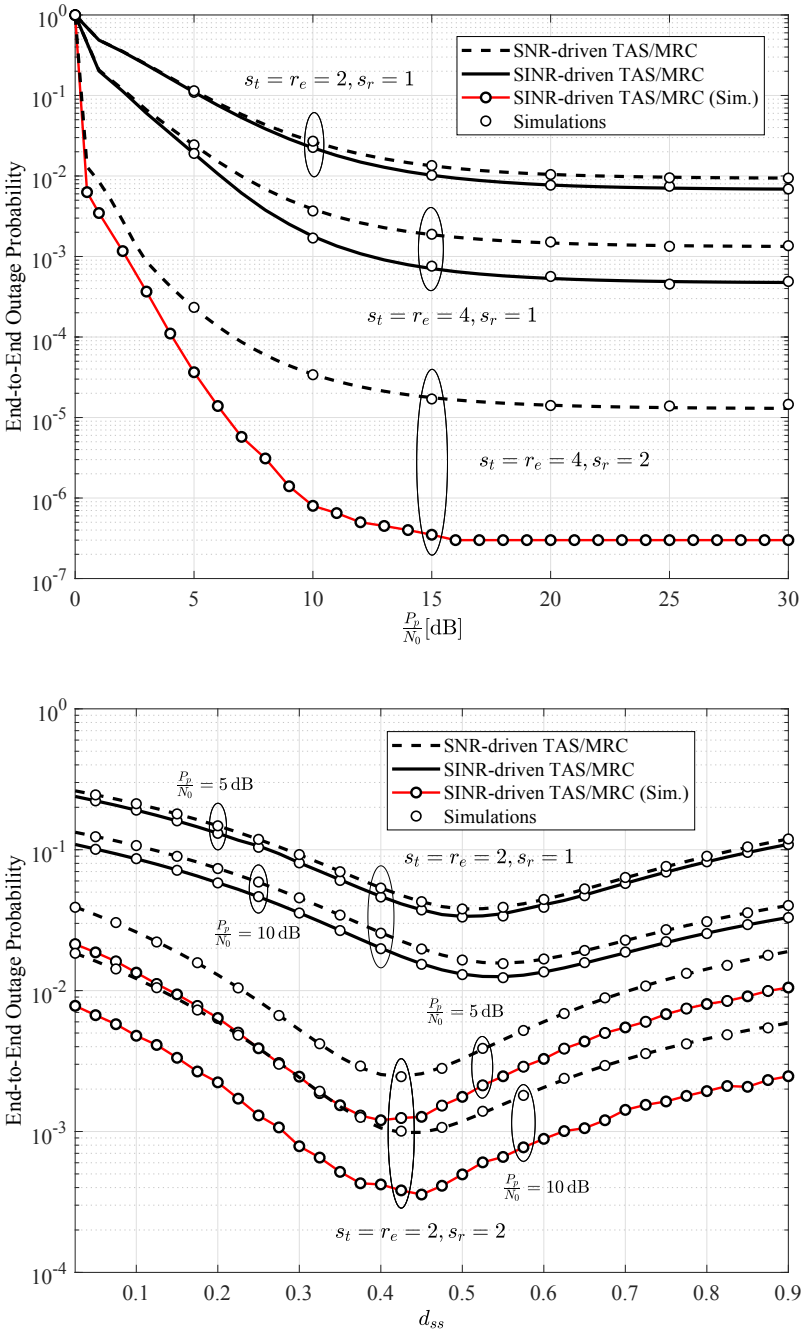

Figure 4.5: Top (a): Comparison of the derived end-to-end outage probability (4.57) for both TAS/MRC strategies under different MIMO relay system configurations while the parameters $\lambda_{ss} = 1$, $\lambda_{sr} = \lambda_{rs} = 0.4$, $\lambda_{sp} = \lambda_{ps} = 0.1$, $\lambda_{pr} = 0.6$, $\lambda_{rp} = 0.5$, $\Phi_s = 2^2 - 1$, $\varepsilon_p = 0.01$ and $Q_{th} = -0.1\,\text{dB}$ are being fixed as exemplary parameters. Down (b): The end-to-end outage probability (4.57) versus d_{ss} for both TAS/MRC strategies.

Chapter 5

Conclusion

In this this dissertation, we focused on the design of spectrum-efficient cognitive MIMO relaying schemes from a practical perspective. We made three key contributions that can be summarized as follows. We firstly focused on spectrum-efficient relay ARQ transmissions over broadband cooperative MIMO channels. We considered a two-slot transmission strategy that, combined with signal-level sub-packet combining at the the destination side, enables to achieve attractive system average throughput compared with conventional ARQ-based cooperative relaying protocols. We also addressed the computational load of the proposed turbo receiver scheme, and provide an efficient recursive implementation that considerably reduces both the receiver's complexity and memory requirements. Secondly, we investigated the impact of interference CSI acquisition in underlay cognitive SIMO relaying. To this end, in the second chapter, we have derived expressions of the outage probability for SIMO relay-aided secondary systems under strict primary system outage constraints. Both partial and complete I-CSI-based interference channel acquisition are considered for the secondary system transmitting nodes. In addition, depending on the primary system interference constraint, either fixed or proportional to the primary system transmit power, we derived an asymptotic analysis of the outage probability. Then, we have provided the diversity-and-multiplexing tradeoff that characterizes the secondary system communications. The analytical results are validated by simulations, and discussed for several cognitive radio system settings. As a result, cooperative relaying and the deployment of multiple antennas at the primary and secondary receivers are two gainful facts that can boost the outage performance and considerably enhance the spectral efficiency of a cognitive radio system in a spectrum sharing underlay context. Capitalizing on the result

of the second chapter, in the third chapter, an exact outage probability analysis of cognitive MIMO incremental DF relaying with TAS is conducted for two antenna selection strategies based on maximizing either the received MRC-combined SNR or SINR ratios. For each relaying hop and each TAS strategy, we thoroughly analyzed the statistical behavior of the secondary system post-processed received SINR under different system settings and various power allocation scenarios. Finally, our analytical and simulation results are evaluated while revealing the accuracy of our developments and optimality of the SINR-driven TAS/MRC strategy.

Appendix A

Proof of Proposition 2

Different from the first transmit power adaptation scenario, neither P-Tx nor S-Tx can now acquire complete I-CSI about the interference channel $\mathbf{h}_{\mathrm{sp}}$. Consequently, one may derive of the primary system $\mathrm{OP_p}$ as,

$$\begin{aligned}\mathrm{OP_p} &= P_{\mathrm{rob}}\left(\frac{\bar{\mathrm{P}}_{\mathrm{p}} z_{\mathrm{pp}}}{\mathrm{P_s}z_{\mathrm{sp}}+N_0} < \Phi_{\mathrm{p}}\right) = \int_0^{+\infty} \overline{\gamma}\left(N_{\mathrm{p}}, \frac{\Phi_{\mathrm{p}}\left(\mathrm{P_s x}+N_0\right)}{\bar{\mathrm{P}}_{\mathrm{p}}\lambda_{\mathrm{pp}}}\right)\frac{\mathrm{x}^{(N_{\mathrm{p}}-1)}\boldsymbol{e}^{-\mathrm{x}/\lambda_{\mathrm{sp}}}}{\lambda_{\mathrm{sp}}^{N_{\mathrm{p}}}\Gamma(N_{\mathrm{p}})}\mathrm{dx} \\ &= 1-\frac{1}{\Gamma\left(N_{\mathrm{p}}\right)}\frac{\boldsymbol{e}^{-\frac{\Phi_{\mathrm{p}}N_0}{\bar{\mathrm{P}}_{\mathrm{p}}\lambda_{\mathrm{pp}}}}}{\left(\frac{\Phi_{\mathrm{p}}\mathrm{P_s}\lambda_{\mathrm{sp}}}{\bar{\mathrm{P}}_{\mathrm{p}}\lambda_{\mathrm{pp}}}+1\right)^{N_{\mathrm{p}}}}\sum_{\mathrm{i}_1=0}^{N_{\mathrm{p}}-1}\frac{1}{\mathrm{i}_1!}\left(\frac{\Phi_{\mathrm{p}}N_0}{\bar{\mathrm{P}}_{\mathrm{p}}\lambda_{\mathrm{pp}}}\right)^{\mathrm{i}_1}\sum_{\mathrm{i}_2=0}^{\mathrm{i}_1}\binom{\mathrm{i}_1}{\mathrm{i}_2}\frac{\Gamma(\mathrm{i}_2+N_{\mathrm{p}})}{\left(\frac{\Phi_{\mathrm{p}}N_0}{\bar{\mathrm{P}}_{\mathrm{p}}\lambda_{\mathrm{pp}}}+\frac{N_0}{\mathrm{P_s}\lambda_{\mathrm{sp}}}\right)^{\mathrm{i}_2}},\end{aligned} \tag{A.1}$$

where the second line is deduced from the fact that when the first argument of the normalized lower incomplete Gamma function, $\overline{\gamma}\left(\mathrm{n},\mathrm{x}\right)=\gamma\left(\mathrm{n},\mathrm{x}\right)/\Gamma(\mathrm{n})$, is a positive integer, the latter can be rewritten in its serial form as [71, Eq. 8.352.1],

$$\overline{\gamma}\left(\mathrm{n},\mathrm{x}\right)=1-e^{-\mathrm{x}}\sum_{\mathrm{i}=0}^{\mathrm{n}-1}\frac{\mathrm{x}^{\mathrm{i}}}{\mathrm{i}!}. \tag{A.2}$$

After some manipulations, it turns out that the first constraint of our optimization problem (3.2), $\mathrm{OP_p}(\mathrm{P_s})\leq\varepsilon_{\mathrm{p}}$, is equivalent to the following inequality,

$$\mathrm{P}(\alpha)=(\varepsilon_{\mathrm{p}}-1)\alpha^{2N_{\mathrm{p}}}+\frac{\boldsymbol{e}^{-\frac{\Phi_{\mathrm{p}}N_0}{\bar{\mathrm{P}}_{\mathrm{p}}\lambda_{\mathrm{pp}}}}}{\Gamma\left(N_{\mathrm{p}}\right)}\sum_{\mathrm{i}_1=0}^{N_{\mathrm{p}}-1}\sum_{\mathrm{i}_2=0}^{\mathrm{i}_1}\frac{\Gamma\left(\mathrm{i}_2+N_{\mathrm{p}}\right)}{\mathrm{i}_2!(\mathrm{i}_1-\mathrm{i}_2)!}\left(\frac{\Phi_{\mathrm{p}}N_0}{\bar{\mathrm{P}}_{\mathrm{p}}\lambda_{\mathrm{pp}}}\right)^{\mathrm{i}_1-\mathrm{i}_2}(\alpha-1)^{\mathrm{i}_2}\,\alpha^{N_{\mathrm{p}}-\mathrm{i}_2}\geq 0$$

where $\alpha = \left(\Phi_{\mathrm{p}} \mathrm{P}_{\mathrm{s}} \lambda_{\mathrm{sp}} / \bar{\mathrm{P}}_{\mathrm{p}} \lambda_{\mathrm{pp}}\right) + 1$. For high values of α, i.e. $\alpha \to +\infty$, the above $2N_{\mathrm{p}}-$degree polynomial $\mathrm{P}(.)$ tends continuously to $-\infty$. In resolving the inequality $\mathrm{P}(\alpha) \geq 0$, we therefore have to find the greatest root of $\mathrm{P}(.)$ (there exists at least one, that is zero), $\mathrm{O}_{\max}$, leading to the exact knowledge of the maximum transmit power $\mathrm{P}_{\text{s-max}}$ the secondary transmitter can attain.

Appendix B

Proof of Lemma 1

Irrespective of the relay indices belonging to the subset $\mathcal{S}$, we will clearly see in the following that, due to the clustered structure of the relays, the conditional CDF $F_{\mathbf{rs}||\mathcal{S}|}(.)$ of the received SNR $\gamma_{\mathbf{rs}}$ at S-Rx during the second-hop, in the case of $|\mathcal{S}| \neq 0$, depends only on the cardinal $|\mathcal{S}|$. In fact, we can without loss of generality consider that $\mathcal{S} = \left\{R_1, \ldots, R_{|\mathcal{S}|-1}, R_{|\mathcal{S}|}\right\}$. Therefore, the conditional CDF, $F_{\mathbf{rs}||\mathcal{S}|}(.)$, can be expressed as

$$\begin{aligned} F_{\mathbf{rs}||\mathcal{S}|}(z) &= \prod_{\mathrm{k}=1}^{|\mathcal{S}|} P_{\mathrm{rob}}\left[\min\left\{\frac{\mathrm{I}}{z_{\mathrm{kp}}}, \frac{\bar{\mathrm{P}}_{\mathrm{s}}}{N_0}\right\} z_{\mathrm{ks}} \leq z\right] \\ &= \prod_{\mathrm{k}=1}^{|\mathcal{S}|}\left[\int_0^{\mathrm{I}N_0/\bar{\mathrm{P}}_{\mathrm{s}}} P_{\mathrm{rob}}\left(\frac{\bar{\mathrm{P}}_{\mathrm{s}}}{N_0} z_{\mathrm{ks}} \leq z\right) \mathrm{f}_{z_{\mathrm{kp}}}(\mathrm{x})\,\mathrm{dx} + \int_{\mathrm{I}N_0/\bar{\mathrm{P}}_{\mathrm{s}}}^{+\infty} P_{\mathrm{rob}}\left(\frac{\mathrm{I}}{\mathrm{x}} z_{\mathrm{ks}} \leq z\right) \mathrm{f}_{z_{\mathrm{kp}}}(\mathrm{x})\,\mathrm{dx}\right], \end{aligned} \tag{B.1}$$

where $\mathrm{f}_{z_{\mathrm{kp}}}(.)$ refers to the probability distribution function (PDF) of z_{kp} which follows a Gamma distribution with shape N_{p} and scale λ_{rp}. Using the serial representation of the lower incomplete Gamma function, (B.1) can be rewritten as,

$$\begin{aligned} F_{\mathbf{rs}||\mathcal{S}|}(z) = \Bigg[1 - \overline{\gamma}\left(N_{\mathrm{p}}, \frac{\mathrm{I}N_0}{\bar{\mathrm{P}}_{\mathrm{s}}\lambda_{\mathrm{rp}}}\right)\overline{\Gamma}\left(N_{\mathrm{s}}, \frac{zN_0}{\bar{\mathrm{P}}_{\mathrm{s}}\lambda_{\mathrm{rs}}}\right) - \\ \frac{1}{\lambda_{\mathrm{rp}}^{N_{\mathrm{p}}}\Gamma(N_{\mathrm{p}})}\sum_{\mathrm{m}=0}^{N_{\mathrm{s}}-1}\frac{\left(\frac{z}{\mathrm{I}\lambda_{\mathrm{rs}}}\right)^{\mathrm{m}}}{\mathrm{m}!}\frac{\Gamma\left(N_{\mathrm{p}}+\mathrm{m}, \frac{\mathrm{I}N_0}{\bar{\mathrm{P}}_{\mathrm{s}}}\left(\frac{z}{\mathrm{I}\lambda_{\mathrm{rs}}}+\frac{1}{\lambda_{\mathrm{rp}}}\right)\right)}{\left(\frac{z}{\mathrm{I}\lambda_{\mathrm{rs}}}+\frac{1}{\lambda_{\mathrm{rp}}}\right)^{N_{\mathrm{p}}+\mathrm{m}}}\Bigg]^{|\mathcal{S}|}. \end{aligned} \tag{B.2}$$

In a preliminary step towards a more tractable formula of the outage probability of the proposed SIMO relay-aided cognitive radio system, we would like to decouple the variable

z in (B.2) from the rest of the terms. So, we begin by substituting the upper incomplete Gamma functions by their serial expressions. Then, the result is treated as a binomial whose expansion is given by,

$$F_{\mathbf{rs}||\mathcal{S}|}(z) = \sum_{\mathrm{u}=0}^{|\mathcal{S}|} \binom{|\mathcal{S}|}{\mathrm{u}} \left[-\overline{\gamma}\left(N_{\mathrm{p}}, \frac{\mathrm{I}N_0}{\bar{\mathrm{P}}_{\mathrm{s}}\lambda_{\mathrm{rp}}}\right)\right]^{\mathrm{u}} \frac{\boldsymbol{e}^{-\frac{zN_0\mathrm{u}}{\mathrm{P}_{\mathrm{s}}\lambda_{\mathrm{rs}}}}}{\left(\frac{z}{\mathrm{I}\lambda_{\mathrm{rs}}}+\frac{1}{\lambda_{\mathrm{rp}}}\right)^{\mathrm{u}(N_{\mathrm{s}}+N_{\mathrm{p}}-1)}} \left[\sum_{\mathrm{m}=0}^{N_{\mathrm{s}}-1} \sum_{\mathrm{n}=N_{\mathrm{s}}-1-\mathrm{m}}^{N_{\mathrm{s}}+N_{\mathrm{p}}+\mathrm{m}-1} \frac{\varphi_{\mathrm{m,n}}}{\mathrm{m}!}\left(\frac{z}{\mathrm{I}\lambda_{\mathrm{rs}}}+\frac{1}{\lambda_{\mathrm{rp}}}\right)^{\mathrm{n}}\right]^{\mathrm{u}} \tag{B.3}$$

where the coefficients $\varphi_{\mathrm{m,n}}$ for $\mathrm{m} \in \{0, \ldots, N_{\mathrm{s}}-1\}$ and $\mathrm{n} \in \{N_{\mathrm{s}}-1-\mathrm{m}, \ldots, N_{\mathrm{s}}+N_{\mathrm{p}}+\mathrm{m}-1\}$ can be expressed as,

$$\varphi_{\mathrm{m,n}} = \sum_{\mathrm{s}=0}^{\min\{\mathrm{n},\mathrm{m}\}} \binom{\mathrm{m}}{\mathrm{s}} \left(-\frac{1}{\lambda_{\mathrm{rp}}}\right)^{\mathrm{m}-\mathrm{s}} \mathcal{B}_{\mathrm{m,n}-\mathrm{s}}. \tag{B.4}$$

In turn, the coefficients $\mathcal{B}_{\mathrm{m,w}}$ in (B.4) for $\mathrm{w} \in \{N_{\mathrm{s}}-1-\mathrm{m}, \ldots, N_{\mathrm{s}}+N_{\mathrm{p}}-2\}$ are given by

$$\begin{cases} \mathcal{B}_{\mathrm{m,w}} = \dfrac{\Gamma(N_{\mathrm{p}}+\mathrm{m})\,\boldsymbol{e}^{-\frac{\mathrm{I}N_0}{\bar{\mathrm{P}}_{\mathrm{s}}\lambda_{\mathrm{rp}}}}}{\gamma\left(N_{\mathrm{p}}, \frac{\mathrm{I}N_0}{\bar{\mathrm{P}}_{\mathrm{s}}\lambda_{\mathrm{rp}}}\right)\lambda_{\mathrm{rp}}^{N_{\mathrm{p}}}} \left(\dfrac{\mathrm{I}N_0}{\bar{\mathrm{P}}_{\mathrm{s}}}\right)^{\mathrm{w}+\mathrm{m}-N_{\mathrm{s}}+1} & , \; N_{\mathrm{s}}-1-\mathrm{m} \le \mathrm{w} \le N_{\mathrm{s}}+N_{\mathrm{p}}-1 \\ \mathcal{B}_{\mathrm{m,w}} = \left(\dfrac{\mathrm{I}N_0}{\bar{\mathrm{P}}_{\mathrm{s}}}\right)^{\mathrm{m}} & , \; \mathrm{w} = N_{\mathrm{s}}+N_{\mathrm{p}}-2 \\ \mathcal{B}_{\mathrm{m,w}} = 0 & , \; \text{otherwise} \end{cases} . \tag{B.5}$$

Furthermore, the double summation in (B.3) can further be developed and rewritten as,

$$\sum_{\mathrm{m}=0}^{N_{\mathrm{s}}-1} \sum_{\mathrm{n}=N_{\mathrm{s}}-1-\mathrm{m}}^{N_{\mathrm{s}}+N_{\mathrm{p}}+\mathrm{m}-1} \frac{\varphi_{\mathrm{m,n}}}{\mathrm{m}!}\left(\frac{z}{\mathrm{I}\lambda_{\mathrm{rs}}}+\frac{1}{\lambda_{\mathrm{rp}}}\right)^{\mathrm{n}} = \sum_{\mathrm{i}=0}^{2N_{\mathrm{s}}+N_{\mathrm{p}}-2} \mathcal{D}_{\mathrm{i}}\left(\frac{z}{\mathrm{I}\lambda_{\mathrm{rs}}}+\frac{1}{\lambda_{\mathrm{rp}}}\right)^{\mathrm{i}}, \tag{B.6}$$

where the coefficients $\mathcal{D}_{\mathrm{i}}$ for $\mathrm{i} \in \{0, \ldots, 2N_{\mathrm{s}}+N_{\mathrm{p}}-2\}$ are given by,

$$\begin{cases} \mathcal{D}_{\mathrm{i}} = \displaystyle\sum_{\mathrm{m}=N_{\mathrm{s}}-1-\mathrm{i}}^{N_{\mathrm{s}}-1} \frac{\varphi_{\mathrm{m},N_{\mathrm{s}}-1-\mathrm{m}}}{\mathrm{m}!} & , \; 0 \le \mathrm{i} \le N_{\mathrm{s}}-2 \\ \mathcal{D}_{\mathrm{i}} = \displaystyle\sum_{\mathrm{m}=0}^{N_{\mathrm{s}}-1} \frac{\varphi_{\mathrm{m,i}}}{\mathrm{m}!} & , \; N_{\mathrm{s}-1} \le \mathrm{i} \le N_{\mathrm{s}}+N_{\mathrm{p}}-1 \\ \mathcal{D}_{\mathrm{i}} = \displaystyle\sum_{\mathrm{m}=\mathrm{i}-(N_{\mathrm{s}}+N_{\mathrm{p}}-1)}^{N_{\mathrm{s}}-1} \frac{\varphi_{\mathrm{m},N_{\mathrm{s}}+N_{\mathrm{p}}-1+\mathrm{m}}}{\mathrm{m}!} & , \; N_{\mathrm{s}}+N_{\mathrm{p}}-2 \le \mathrm{i} \le 2N_{\mathrm{s}}+N_{\mathrm{p}}-2 \end{cases} . \tag{B.7}$$

Consequently, the conditional CDF $F_{\mathbf{rs}||\mathcal{S}|}(.)$ can finally be expressed as,

$$F_{\mathbf{rs}||\mathcal{S}|}(z) = \sum_{\mathrm{u}=0}^{|\mathcal{S}|} \boldsymbol{e}^{-\frac{zN_0\mathrm{u}}{\mathrm{P_s}\lambda_{\mathrm{rs}}}} \sum_{\mathrm{v}=0}^{\mathrm{u}(2N_{\mathrm{s}}+N_{\mathrm{p}}-2)} \mathcal{E}_{\mathrm{u,v}} \left(\frac{z}{\mathrm{I}\lambda_{\mathrm{rs}}} + \frac{1}{\lambda_{\mathrm{rp}}}\right)^{\mathrm{v}-\mathrm{u}(\mathrm{N_s}+\mathrm{N_p}-1)}, \tag{B.8}$$

where the terms $\mathcal{E}_{\mathrm{u,v}}$ for $\mathrm{u} \in \{0, \ldots, |\mathcal{S}|\}$ and $\mathrm{v} \in \{0, \ldots, \mathrm{u}(2N_{\mathrm{s}} + N_{\mathrm{p}} - 2)\}$ are recursively computed with the help of [71, Eq. 0.314] as,

$$\mathcal{E}_{\mathrm{u,v}} = \begin{cases} (-1)^{\mathrm{u}N_{\mathrm{s}}} \binom{|\mathcal{S}|}{\mathrm{u}} \frac{\boldsymbol{e}^{-\frac{\mathrm{u}\mathrm{I}N_0}{\mathrm{P_s}\lambda_{\mathrm{rp}}}}}{\lambda_{\mathrm{rp}}^{\mathrm{u}(N_{\mathrm{p}}+N_{\mathrm{s}}-1)}} \left[\frac{\Gamma(N_{\mathrm{p}}+N_{\mathrm{s}}-1)}{\Gamma(N_{\mathrm{s}})\Gamma(N_{\mathrm{p}})}\right]^{\mathrm{u}} & , \ \mathrm{v}=0 \\ \frac{1}{\mathrm{v}\mathcal{D}_0} \sum_{\mathrm{w}=1}^{\min\{2N_{\mathrm{s}}+N_{\mathrm{p}}-2,\mathrm{v}\}} (\mathrm{wu}-\mathrm{v}+\mathrm{w})\,\mathcal{D}_{\mathrm{v}}\mathcal{E}_{\mathrm{u,v-w}} & , \ 1 \le \mathrm{v} \le \mathrm{u}(2N_{\mathrm{s}}+N_{\mathrm{p}}-2) \end{cases}. \tag{B.9}$$

Appendix C

Proof of Lemma 2

In the case of the relay nodes can only acquire a partial I-CSI about their interference channels, the conditional CDF, $F_{\mathbf{rs}||\mathcal{S}|}(.)$, can easily be shown to be equal to

$$F_{\mathbf{rs}||\mathcal{S}|}(z) = \left[\overline{\gamma}\left(N_{\mathrm{s}}, \frac{zN_0}{\lambda_{\mathrm{rs}}\mathrm{P}_{\text{r-max}}}\right)\right]^{|\mathcal{S}|}, \tag{C.1}$$

which, after writing the regularized lower incomplete Gamma function in its serial form, can be treated as a binomial and shown to be given by,

$$F_{\mathbf{rs}||\mathcal{S}|}(z) = \sum_{\mathrm{u}=0}^{|\mathcal{S}|}\binom{|\mathcal{S}|}{\mathrm{u}}(-1)^{\mathrm{u}}\boldsymbol{e}^{-\frac{z\mathrm{u}N_0}{\lambda_{\mathrm{rs}}\mathrm{P}_{\text{r-max}}}}\left[\sum_{\mathrm{v}=0}^{N_{\mathrm{s}}-1}\underbrace{\frac{1}{\mathrm{v}!\left(\lambda_{\mathrm{rs}}\mathrm{P}_{\text{r-max}}/N_0\right)^{\mathrm{v}}}}_{\mathcal{A}_{\mathrm{v}}}z^{\mathrm{v}}\right]^{\mathrm{u}}. \tag{C.2}$$

Since $\left[\sum_{\mathrm{v}=0}^{(N_{\mathrm{s}}-1)}\mathcal{A}_{\mathrm{v}}z^{\mathrm{v}}\right]$ to the u^{th} power is also a $\mathrm{u}(N_{\mathrm{s}}-1)$-degree polynomial, the coefficients of the resulting polynomial, $\mathcal{E}_{\mathrm{u,v}}$, can be expressed with the help of [71, Eq. 0.314] as a recursion similarly to (B.8). Finally, $F_{\mathbf{rs}||\mathcal{S}|}(.)$ can be rewritten in a compact formula as (3.17).

Appendix D

Proof of theorem 1

Let us begin by considering the first scenario for which the secondary system transmitting nodes are able to acquire complete I-CSI about their interference channels. In this case, the probability $\mathcal{P}_1(z)$ expressed in (3.23) can be approximated for $\bar{\mathrm{P}}_{\mathrm{s}} \to +\infty$ by

$$\begin{cases} \mathcal{P}_1^{\infty}(z) \approx \dfrac{\left(\dot{\Phi}_{\mathrm{s}} - z\right)^{N_{\mathrm{s}}}}{N_{\mathrm{s}}! \lambda_{\mathrm{sp}}^{N_{\mathrm{p}}} \Gamma\left(N_{\mathrm{p}}\right)} \dfrac{\lambda_{\mathrm{sp}}^{N_{\mathrm{p}}+N_{\mathrm{s}}+\mathrm{K}}}{\left(\xi\lambda_{\mathrm{ss}}\right)^{N_{\mathrm{s}}} \bar{\mathrm{P}}_{\mathrm{s}}^{\upsilon(N_{\mathrm{s}}+\mathrm{K})}} \left(\dfrac{\dot{\Phi}_{\mathrm{s}}}{\xi\lambda_{\mathrm{sr}}}\right)^{\mathrm{K}} \Gamma\left(N_{\mathrm{p}}+N_{\mathrm{s}}+\mathrm{K}\right) & , 0 < \upsilon < 1 \\ \mathcal{P}_1^{\infty}(z) \approx \dfrac{\left(\dot{\Phi}_{\mathrm{s}} - z\right)^{N_{\mathrm{s}}}}{N_{\mathrm{s}}! \bar{\mathrm{P}}_{\mathrm{s}}^{N_{\mathrm{s}}+\mathrm{K}}} \left(\dfrac{N_0}{\lambda_{\mathrm{ss}}}\right)^{N_{\mathrm{s}}} \left(\dfrac{\dot{\Phi}_{\mathrm{s}} N_0}{\lambda_{\mathrm{sr}}}\right)^{\mathrm{K}} & , 1 < \upsilon \\ \mathcal{P}_1^{\infty}(z) \approx \dfrac{\left(\dot{\Phi}_{\mathrm{s}} - z\right)^{N_{\mathrm{s}}}}{N_{\mathrm{s}}! \bar{\mathrm{P}}_{\mathrm{s}}^{N_{\mathrm{s}}+\mathrm{K}}} \left[\left(\dfrac{N_0}{\lambda_{\mathrm{ss}}}\right)^{N_{\mathrm{s}}} \overline{\gamma}\left(N_{\mathrm{p}}, \dfrac{\xi N_0}{\lambda_{\mathrm{sp}}}\right) \left(\dfrac{\dot{\Phi}_{\mathrm{s}} N_0}{\lambda_{\mathrm{sr}}}\right)^{\mathrm{K}} \right. & \\ \left. \quad + \dfrac{1}{\Gamma\left(N_{\mathrm{p}}\right)} \dfrac{\lambda_{\mathrm{sp}}^{N_{\mathrm{s}}+\mathrm{K}}}{\left(\xi\lambda_{\mathrm{ss}}\right)^{N_{\mathrm{s}}}} \left(\dfrac{\dot{\Phi}_{\mathrm{s}}}{\xi\lambda_{\mathrm{sr}}}\right)^{\mathrm{K}} \Gamma\left(N_{\mathrm{p}}+N_{\mathrm{s}}+\mathrm{K}, \dfrac{\xi N_0}{\lambda_{\mathrm{sp}}}\right) \right] & , \upsilon = 1 \end{cases}, \tag{D.1}$$

exploiting the fact that when $\mathrm{n} \in \mathbb{N}^*$, $\mathrm{a} \in \mathbb{R}^{*+}$, and $\mathrm{x} \to +\infty$, we have $\overline{\gamma}\left(\mathrm{n}, \frac{\mathrm{a}}{\mathrm{x}}\right) \approx \left(\frac{\mathrm{a}}{\mathrm{x}}\right)^{\mathrm{n}}/\mathrm{n}!$, $\overline{\Gamma}\left(\mathrm{n}, \frac{\mathrm{a}}{\mathrm{x}}\right) \approx 1$, and $\left(1 - \boldsymbol{e}^{-\frac{\mathrm{a}}{\mathrm{x}}}\right)^{\mathrm{n}} \simeq \left(\frac{\mathrm{a}}{\mathrm{x}}\right)^{\mathrm{n}}$. In (D.1), ξ equals to $\sigma\lambda_{\mathrm{pp}}\gamma^{-1}(N_{\mathrm{p}}, \varepsilon_{\mathrm{p}})/(\Phi_{\mathrm{p}} N_0)$.

Similarly, the CDF $F_{\rm ss}(.)$ expressed in (3.12) can be approximated for $\bar{\rm P}_{\rm s} \to +\infty$ by,

$$\begin{cases} F_{\rm ss}^{\infty}(z) \approx \dfrac{z^{N_{\rm s}}}{N_{\rm s}!\Gamma\left(N_{\rm p}\right)} \dfrac{\lambda_{\rm sp}^{N_{\rm s}}}{\left(\xi\lambda_{\rm ss}\right)^{N_{\rm s}} \bar{\rm P}_{\rm s}^{\upsilon N_{\rm s}}} \Gamma\left(N_{\rm p}+N_{\rm s}\right) & , \ 0<\upsilon<1 \\ F_{\rm ss}^{\infty}(z) \approx \dfrac{z^{N_{\rm s}}}{N_{\rm s}!\bar{\rm P}_{\rm s}^{N_{\rm s}}} \left(\dfrac{N_0}{\lambda_{\rm ss}}\right)^{N_{\rm s}} & , \ 1<\upsilon \\ F_{\rm ss}^{\infty}(z) \approx \dfrac{z^{N_{\rm s}}}{N_{\rm s}!\bar{\rm P}_{\rm s}^{N_{\rm s}}} \left[\left(\dfrac{N_0}{\lambda_{\rm ss}}\right)^{N_{\rm s}} \overline{\gamma}\left(N_{\rm p}, \dfrac{\xi N_0}{\lambda_{\rm sp}}\right)\right. & \\ \left. \quad + \dfrac{1}{\Gamma\left(N_{\rm p}\right)} \dfrac{\lambda_{\rm sp}^{N_{\rm s}}}{\left(\xi\lambda_{\rm ss}\right)^{N_{\rm s}}} \Gamma\left(N_{\rm p}+N_{\rm s}, \dfrac{\xi N_0}{\lambda_{\rm sp}}\right)\right] & , \ \upsilon=1 \end{cases} . \tag{D.2}$$

Combining (D.1) and (D.2), one may re-write the first term of the end-to-end secondary system outage probability for high values of $\bar{\rm P}_{\rm s}$ as,

$$\mathrm{OP}_{\rm s}^{(1)}\left(\rho, \mathcal{R}_{\rm s}\right) \approx - \int_{\dot{\Phi}_{\rm s}-\Phi_{\rm s}}^{\dot{\Phi}_{\rm s}} \frac{\mathrm{d}}{\mathrm{d}z}\left(\mathcal{P}_1^{\infty}(z)\right) F_{\rm ss}^{\infty}(z)\mathrm{d}z, \tag{D.3}$$

resulting in the following compact expressions of the first outage probability terms,

$$\begin{cases} \mathrm{OP}_{\rm s}^{(1)}\left(\rho, \mathcal{R}_{\rm s}\right) \approx \dfrac{N_{\rm s}}{\left(N_{\rm s}!\right)^2 \Gamma\left(N_{\rm p}\right)} \dfrac{\lambda_{\rm sp}^{2N_{\rm s}+{\rm K}}}{\left(\xi\lambda_{\rm ss}\right)^{N_{\rm s}} \bar{\rm P}_{\rm s}^{\upsilon(2N_{\rm s}+{\rm K})}} \left(\dfrac{\dot{\Phi}_{\rm s}}{\sigma\lambda_{\rm sr}}\right)^{\rm K} & \\ \quad \dfrac{\Gamma\left(N_{\rm p}+N_{\rm s}+{\rm K}\right)\Gamma\left(N_{\rm p}+N_{\rm s}\right)}{\Gamma\left(N_{\rm p}\right)\left(\xi\lambda_{\rm ss}\right)^{N_{\rm s}}} \displaystyle\int_{\dot{\Phi}_{\rm s}-\Phi_{\rm s}}^{\dot{\Phi}_{\rm s}} z^{N_{\rm s}}\left(\dot{\Phi}_{\rm s}-z\right)^{N_{\rm s}-1}\mathrm{d}z, & , \ 0<\upsilon<1 \\ \mathrm{OP}_{\rm s}^{(1)}\left(\rho, \mathcal{R}_{\rm s}\right) \approx \dfrac{N_{\rm s}}{\left(N_{\rm s}!\right)^2 \bar{\rm P}_{\rm s}^{2N_{\rm s}+{\rm K}}} \left(\dfrac{N_0}{\lambda_{\rm ss}}\right)^{2N_{\rm s}} \left(\dfrac{\dot{\Phi}_{\rm s}N_0}{\lambda_{\rm sr}}\right)^{\rm K} \displaystyle\int_{\dot{\Phi}_{\rm s}-\Phi_{\rm s}}^{\dot{\Phi}_{\rm s}} z^{N_{\rm s}}\left(\dot{\Phi}_{\rm s}-z\right)^{N_{\rm s}-1}\mathrm{d}z & , \ 1<\upsilon \\ \mathrm{OP}_{\rm s}^{(1)}\left(\rho, \mathcal{R}_{\rm s}\right) \approx \dfrac{N_{\rm s}}{\left(N_{\rm s}!\right)^2 \bar{\rm P}_{\rm s}^{2N_{\rm s}+{\rm K}}} \left[\left(\dfrac{N_0}{\lambda_{\rm ss}}\right)^{N_{\rm s}} \overline{\gamma}\left(N_{\rm p}, \dfrac{\xi N_0}{\lambda_{\rm sp}}\right) + \dfrac{1}{\Gamma\left(N_{\rm p}\right)} \dfrac{\lambda_{\rm sp}^{N_{\rm s}}}{\left(\xi\lambda_{\rm ss}\right)^{N_{\rm s}}} \times\right. & \\ \quad \left.\Gamma\left(N_{\rm p}+N_{\rm s}, \dfrac{\xi N_0}{\lambda_{\rm sp}}\right)\right] \left[\left(\dfrac{N_0}{\lambda_{\rm ss}}\right)^{N_{\rm s}} \overline{\gamma}\left(N_{\rm p}, \dfrac{\xi N_0}{\lambda_{\rm sp}}\right)\left(\dfrac{\dot{\Phi}_{\rm s}N_0}{\lambda_{\rm sr}}\right)^{\rm K} + \dfrac{1}{\lambda_{\rm sp}^{N_{\rm p}}\Gamma\left(N_{\rm p}\right)}\right. & , \ \upsilon=1 \\ \quad \left.\dfrac{\lambda_{\rm sp}^{N_{\rm p}+N_{\rm s}+{\rm K}}}{\left(\xi\lambda_{\rm ss}\right)^{N_{\rm s}}} \left(\dfrac{\dot{\Phi}_{\rm s}}{\xi\lambda_{\rm sr}}\right)^{\rm K} \Gamma\left(N_{\rm p}+N_{\rm s}+{\rm K}, \dfrac{\xi N_0}{\lambda_{\rm sp}}\right)\right] \displaystyle\int_{\dot{\Phi}_{\rm s}-\Phi_{\rm s}}^{\dot{\Phi}_{\rm s}} z^{N_{\rm s}}\left(\dot{\Phi}_{\rm s}-z\right)^{N_{\rm s}-1}\mathrm{d}z & \end{cases} . \tag{D.4}$$

Following the same steps used to derive the above asymptotic expressions, we similarly approximate $\mathrm{OP}_{\mathrm{s,k}}^{(2)}\left(\rho,\mathcal{R}_{\mathrm{s}}\right)$ for high values of $\overline{\mathrm{P}}_{\mathrm{s}}$ as,

$$\begin{cases} \mathrm{OP}_{\mathrm{s,k}}^{(2)}\left(\rho,\mathcal{R}_{\mathrm{s}}\right) \approx \dfrac{N_{\mathrm{s}}}{N_{\mathrm{s}}!\Gamma\left(N_{\mathrm{p}}\right)} \dfrac{\lambda_{\mathrm{sp}}^{N_{\mathrm{s}}+\mathrm{K}-\mathrm{k}}\Gamma\left(N_{\mathrm{p}}+N_{\mathrm{s}}+\mathrm{K}-\mathrm{k}\right)}{\left(\xi\lambda_{\mathrm{ss}}\right)^{N_{\mathrm{s}}}\bar{\mathrm{P}}_{\mathrm{s}}^{\upsilon(\mathrm{K}-\mathrm{k}+N_{\mathrm{s}}+\mathrm{k}N_{\mathrm{s}})}} \left(\dfrac{\dot{\Phi}_{\mathrm{s}}}{\xi\lambda_{\mathrm{sr}}}\right)^{\mathrm{K}-\mathrm{k}} \\ \qquad \left[\dfrac{\Gamma\left(N_{\mathrm{p}}+N_{\mathrm{s}}\right)\lambda_{\mathrm{rp}}^{N_{\mathrm{s}}}}{N_{\mathrm{s}}!\Gamma\left(N_{\mathrm{p}}\right)\left(\xi\lambda_{\mathrm{rs}}\right)^{N_{\mathrm{s}}}}\right]^{\mathrm{k}} \int\limits_{\dot{\Phi}_{\mathrm{s}}-\Phi_{\mathrm{s}}}^{\dot{\Phi}_{\mathrm{s}}} z^{N_{\mathrm{s}}}\left(\dot{\Phi}_{\mathrm{s}}-z\right)^{N_{\mathrm{s}}-1}\mathrm{d}z \qquad , \ 0<\upsilon<1 \\ \mathrm{OP}_{\mathrm{s,k}}^{(2)}\left(\rho,\mathcal{R}_{\mathrm{s}}\right) \approx \dfrac{N_{\mathrm{s}}}{N_{\mathrm{s}}!\bar{\mathrm{P}}_{\mathrm{s}}^{\mathrm{K}-\mathrm{k}+N_{\mathrm{s}}+\mathrm{k}N_{\mathrm{s}}}} \left(\dfrac{N_0}{\lambda_{\mathrm{ss}}}\right)^{N_{\mathrm{s}}} \left[\dfrac{1}{N_{\mathrm{s}}!}\left(\dfrac{N_0}{\lambda_{\mathrm{rs}}}\right)^{N_{\mathrm{s}}}\right]^{\mathrm{k}} \\ \qquad \left(\dfrac{\dot{\Phi}_{\mathrm{s}}N_0}{\lambda_{\mathrm{sr}}}\right)^{\mathrm{K}-\mathrm{k}} \int\limits_{\dot{\Phi}_{\mathrm{s}}-\Phi_{\mathrm{s}}}^{\dot{\Phi}_{\mathrm{s}}} z^{N_{\mathrm{s}}}\left(\dot{\Phi}_{\mathrm{s}}-z\right)^{N_{\mathrm{s}}-1}\mathrm{d}z \qquad , \ 1<\upsilon. \\ \mathrm{OP}_{\mathrm{s,k}}^{(2)}\left(\rho,\mathcal{R}_{\mathrm{s}}\right) \approx \dfrac{N_{\mathrm{s}}}{N_{\mathrm{s}}!\bar{\mathrm{P}}_{\mathrm{s}}^{\mathrm{K}-\mathrm{k}+N_{\mathrm{s}}+\mathrm{k}N_{\mathrm{s}}}} \left[\dfrac{1}{N_{\mathrm{s}}!}\left(\dfrac{N_0}{\lambda_{\mathrm{rs}}}\right)^{N_{\mathrm{s}}}\overline{\gamma}\left(N_{\mathrm{p}},\dfrac{\xi N_0}{\lambda_{\mathrm{rp}}}\right)+\dfrac{1}{N_{\mathrm{s}}!\Gamma\left(N_{\mathrm{p}}\right)}\times\right. \\ \qquad \left.\dfrac{\lambda_{\mathrm{rp}}^{N_{\mathrm{s}}}}{\left(\xi\lambda_{\mathrm{rs}}\right)^{N_{\mathrm{s}}}}\Gamma\left(N_{\mathrm{p}}+N_{\mathrm{s}},\dfrac{\xi N_0}{\lambda_{\mathrm{rp}}}\right)\right]^{\mathrm{k}} \left[\left(\dfrac{N_0}{\lambda_{\mathrm{ss}}}\right)^{N_{\mathrm{s}}}\overline{\gamma}\left(N_{\mathrm{p}},\dfrac{\xi N_0}{\lambda_{\mathrm{sp}}}\right)\left(\dfrac{\dot{\Phi}_{\mathrm{s}}N_0}{\lambda_{\mathrm{sr}}}\right)^{\mathrm{K}-\mathrm{k}}+\dfrac{1}{\Gamma(N_{\mathrm{p}})}\times\right. \qquad , \ \upsilon=1 \\ \left.\dfrac{\lambda_{\mathrm{sp}}^{N_{\mathrm{p}}+N_{\mathrm{s}}+\mathrm{K}-1}}{\left(\xi\lambda_{\mathrm{ss}}\right)^{N_{\mathrm{s}}}}\left(\dfrac{\dot{\Phi}_{\mathrm{s}}}{\xi\lambda_{\mathrm{sr}}}\right)^{\mathrm{K}-\mathrm{k}}\Gamma\left(N_{\mathrm{p}}+N_{\mathrm{s}}+\mathrm{K}-\mathrm{k},\dfrac{\xi N_0}{\lambda_{\mathrm{sp}}}\right)\int\limits_{\dot{\Phi}_{\mathrm{s}}-\Phi_{\mathrm{s}}}^{\dot{\Phi}_{\mathrm{s}}} z^{N_{\mathrm{s}}}\left(\dot{\Phi}_{\mathrm{s}}-z\right)^{N_{\mathrm{s}}-1}\mathrm{d}z\right. \end{cases} \tag{D.5}$$

It is quiet important to note that the term that decays slowly in the overall summation (3.18) is the second one $\mathrm{KOP}_{\mathrm{s},1}^{(2)}\left(\rho,\mathcal{R}_{\mathrm{s}}\right)$. Thus, we conclude our analysis with the following asymptotic formula of the end-to-end outage probability of the secondary system with respect to scenario 1,

$$\begin{cases} \mathrm{OP_s}\left(\rho,\mathcal{R}_\mathrm{s}\right) \approx \dfrac{\mathrm{K}N_\mathrm{s}}{N_\mathrm{s}!\Gamma\left(N_\mathrm{p}\right)} \dfrac{\lambda_\mathrm{sp}^{N_\mathrm{s}+\mathrm{K}-1}\Gamma\left(N_\mathrm{p}+N_\mathrm{s}+\mathrm{K}-1\right)}{\left(\xi\lambda_\mathrm{ss}\right)^{N_\mathrm{s}}\bar{\mathrm{P}}_\mathrm{s}^{\upsilon(\mathrm{K}-1+2N_\mathrm{s})}} \left(\dfrac{1}{\xi\lambda_\mathrm{sr}}\right)^{\mathrm{K}-1} \\ \quad \left[\dfrac{\Gamma\left(N_\mathrm{p}+N_\mathrm{s}\right)\lambda_\mathrm{rp}^{N_\mathrm{s}}}{N_\mathrm{s}!\Gamma\left(N_\mathrm{p}\right)\left(\xi\lambda_\mathrm{rs}\right)^{N_\mathrm{s}}}\right] \dot{\Phi}_\mathrm{s}^{2N_\mathrm{s}+\mathrm{K}-1} \sum_{\mathrm{i}=0}^{N_\mathrm{s}-1} \binom{N_\mathrm{s}-1}{\mathrm{i}} \dfrac{(-1)^\mathrm{i}}{N_\mathrm{s}+1+\mathrm{i}} & , \ 0<\upsilon<1 \\ \mathrm{OP_s}\left(\rho,\mathcal{R}_\mathrm{s}\right) \approx \dfrac{\mathrm{K}N_\mathrm{s}}{N_\mathrm{s}!\bar{\mathrm{P}}_\mathrm{s}^{\mathrm{K}-1+2N_\mathrm{s}}} \left(\dfrac{N_0}{\lambda_\mathrm{ss}}\right)^{N_\mathrm{s}} \left[\dfrac{1}{N_\mathrm{s}!}\left(\dfrac{N_0}{\lambda_\mathrm{rs}}\right)^{N_\mathrm{s}}\right] \\ \quad \left(\dfrac{N_0}{\lambda_\mathrm{sr}}\right)^{\mathrm{K}-1} \dot{\Phi}_\mathrm{s}^{2N_\mathrm{s}+\mathrm{K}-1} \sum_{\mathrm{i}=0}^{N_\mathrm{s}-1} \binom{N_\mathrm{s}-1}{\mathrm{i}} \dfrac{(-1)^\mathrm{i}}{N_\mathrm{s}+1+\mathrm{i}} & , \ 1<\upsilon. \\ \mathrm{OP_s}\left(\rho,\mathcal{R}_\mathrm{s}\right) \approx \dfrac{\mathrm{K}N_\mathrm{s}}{N_\mathrm{s}!\bar{\mathrm{P}}_\mathrm{s}^{\mathrm{K}-1+2N_\mathrm{s}}} \left[\dfrac{1}{N_\mathrm{s}!}\left(\dfrac{N_0}{\lambda_\mathrm{rs}}\right)^{N_\mathrm{s}} \overline{\gamma}\left(N_\mathrm{p},\dfrac{\xi N_0}{\lambda_\mathrm{rp}}\right) + \dfrac{1}{N_\mathrm{s}!\Gamma\left(N_\mathrm{p}\right)} \dfrac{\lambda_\mathrm{rp}^{N_\mathrm{s}}}{\left(\xi\lambda_\mathrm{rs}\right)^{N_\mathrm{s}}}\right. \\ \quad \left.\Gamma\left(N_\mathrm{p}+N_\mathrm{s},\dfrac{\xi N_0}{\lambda_\mathrm{rp}}\right)\right] \left[\left(\tfrac{N_0}{\lambda_\mathrm{ss}}\right)^{N_\mathrm{s}} \overline{\gamma}\left(N_\mathrm{p},\tfrac{\xi N_0}{\lambda_\mathrm{sp}}\right)\left(\tfrac{N_0}{\lambda_\mathrm{sr}}\right)^{\mathrm{K}-1} + \tfrac{1}{\Gamma(N_\mathrm{p})} \tfrac{\lambda_\mathrm{sp}^{N_\mathrm{p}+N_\mathrm{s}+\mathrm{K}-1}}{\left(\xi\lambda_\mathrm{ss}\right)^{N_\mathrm{s}}}\right. & , \ \upsilon=1 \\ \quad \left.\left(\dfrac{1}{\xi\lambda_\mathrm{sr}}\right)^{\mathrm{K}-1} \Gamma\left(N_\mathrm{p}+N_\mathrm{s}+\mathrm{K}-1,\dfrac{\xi N_0}{\lambda_\mathrm{sp}}\right)\right] \dot{\Phi}_\mathrm{s}^{2N_\mathrm{s}+\mathrm{K}-1} \sum_{\mathrm{i}=0}^{N_\mathrm{s}-1} \binom{N_\mathrm{s}-1}{\mathrm{i}} \dfrac{(-1)^\mathrm{i}}{N_\mathrm{s}+1+\mathrm{i}} & \end{cases} \tag{D.6}$$

We point out that normalizing both SNR thresholds as $\dot{\Phi}_\mathrm{s} = \Phi_\mathrm{s} = 2^{\mathcal{R}_\mathrm{s}} - 1$ where $\mathcal{R}_\mathrm{s} = r\log_2\left(1+\rho\right) \overset{\rho\to\infty}{\approx} r\log_2\left(\rho\right)$, and r refers to the secondary system achievable multiplexing-gain, is essential because of the incremental nature of the proposed relaying scheme in which S-Tx might attain its target rate $\mathcal{R}_\mathrm{s}$ during the first relaying phase; therefore, refrains from transmitting during the second relaying phase. In which case, the secondary system will operate at full rate, that is, the multiplexing gain $r = 1$ is achieved. After replacing $\dot{\Phi}_\mathrm{s}$ by ρ^r in (D.6), we deduce that the diversity-and-multiplexing tradeoff governing the secondary communications is given by,

$$d(r) = \left(2N_\mathrm{s}+\mathrm{K}-1\right)\left(\min(\upsilon,1)-r\right)^+, \tag{D.7}$$

where $(.)^+$ stands for $\max\{.,0\}$. At this stage we conclude with the proof of theorem 1 with respect to scenario 1. Regarding the asymptotic analysis of the end-to-end outage probability in the case of scenario 2. We follow the same derivation steps used to derive (D.6). Thus, for brevity, we just provide our asymptotic results in this case, which can be expressed as,

$$\begin{cases} \mathrm{OP_s}\left(\rho,\mathcal{R}_\mathrm{s}\right) \approx \dfrac{\mathrm{K}N_\mathrm{s}}{\left(N_\mathrm{s}!\right)^2 \bar{\mathrm{P}}_\mathrm{s}^{\upsilon(\mathrm{K}-1+2N_\mathrm{s})}} \left[\left(\dfrac{\lambda_\mathrm{rp}}{\lambda_\mathrm{rs}\zeta}\right)^{N_\mathrm{s}}\right] \\ \qquad \left[\left(\dfrac{\lambda_\mathrm{sp}}{\lambda_\mathrm{ss}\zeta}\right)^{N_\mathrm{s}} \left(\dfrac{\lambda_\mathrm{sp}}{\lambda_\mathrm{sr}\zeta}\right)^{\mathrm{K}-1}\right] & , \ 0<\upsilon<1 \\ \qquad \dot{\Phi}_\mathrm{s}^{2N_\mathrm{s}+\mathrm{K}-1} \displaystyle\sum_{\mathrm{i}=0}^{N_\mathrm{s}-1} \binom{N_\mathrm{s}-1}{\mathrm{i}} \dfrac{(-1)^\mathrm{i}}{N_\mathrm{s}+1+\mathrm{i}} \\ \mathrm{OP_s}\left(\rho,\mathcal{R}_\mathrm{s}\right) \approx \dfrac{\mathrm{K}N_\mathrm{s}}{N_\mathrm{s}!\bar{\mathrm{P}}_\mathrm{s}^{\mathrm{K}-1+2N_\mathrm{s}}} \left(\dfrac{N_0}{\lambda_\mathrm{ss}}\right)^{N_\mathrm{s}} \left[\dfrac{1}{N_\mathrm{s}!}\left(\dfrac{N_0}{\lambda_\mathrm{rs}}\right)^{N_\mathrm{s}}\right] & , \ 1<\upsilon \qquad , \\ \qquad \left(\dfrac{N_0}{\lambda_\mathrm{sr}}\right)^{\mathrm{K}-1} \dot{\Phi}_\mathrm{s}^{2N_\mathrm{s}+\mathrm{K}-1} \displaystyle\sum_{\mathrm{i}=0}^{N_\mathrm{s}-1} \binom{N_\mathrm{s}-1}{\mathrm{i}} \dfrac{(-1)^\mathrm{i}}{N_\mathrm{s}+1+\mathrm{i}} \\ \mathrm{OP_s}\left(\rho,\mathcal{R}_\mathrm{s}\right) \approx \dfrac{\mathrm{K}N_\mathrm{s}}{\left(N_\mathrm{s}!\right)^2 \bar{\mathrm{P}}_\mathrm{s}^{\mathrm{K}-1+2N_\mathrm{s}}} \left[\left(\dfrac{1}{\lambda_\mathrm{rs}}\max\left\{\dfrac{\lambda_\mathrm{rp}}{\zeta},N_0\right\}\right)^{N_\mathrm{s}}\right] \\ \qquad \left[\left(\frac{1}{\lambda_\mathrm{ss}}\max\left\{\frac{\lambda_\mathrm{sp}}{\zeta},N_0\right\}\right)^{N_\mathrm{s}} \left(\frac{1}{\lambda_\mathrm{sr}}\max\left\{\frac{\lambda_\mathrm{sp}}{\zeta},N_0\right\}\right)^{\mathrm{K}-1}\right] & , \ \upsilon=1 \\ \qquad \dot{\Phi}_\mathrm{s}^{2N_\mathrm{s}+\mathrm{K}-1} \displaystyle\sum_{\mathrm{i}=0}^{N_\mathrm{s}-1} \binom{N_\mathrm{s}-1}{\mathrm{i}} \dfrac{(-1)^\mathrm{i}}{N_\mathrm{s}+1+\mathrm{i}} \end{cases} \tag{D.8}$$

where $\zeta = \left(\sigma\lambda_\mathrm{pp}(\mathrm{O}_\mathrm{max}^*-1)\right)/\left(\Phi_\mathrm{p}N_0\right)$, and $\mathrm{O}_\mathrm{max}^*$ is the greatest root of the following polynomial,

$$\mathrm{P}(\alpha) = (\varepsilon_\mathrm{p}-1)\alpha^{2N_\mathrm{p}} + \frac{1}{\Gamma\left(N_\mathrm{p}\right)} \sum_{\mathrm{i}_1=0}^{N_\mathrm{p}-1} \frac{\Gamma\left(N_\mathrm{p}+\mathrm{i}_1\right)}{\mathrm{i}_1!} \left(\alpha-1\right)^{\mathrm{i}_1} \alpha^{N_\mathrm{p}-\mathrm{i}_1}. \tag{D.9}$$

Clearly, the diversity-multiplexing tradeoff (D.7) is also achieved when scenario 2 is adopted. At this stage, we conclude with the proof of Theorem 1.

Appendix E

Derivation of Eq. (4.25)

By treating $\overline{\gamma}(l,x)^k$ as a binomial, we get

$$\overline{\gamma}(l,x)^k = \sum_{i_1=0}^{k} \binom{k}{i_1} (-1)^{i_1} e^{-x} \left(\sum_{i=0}^{l-1} \frac{x^i}{i!} \right)^{i_1} \tag{E.1}$$

$$= \sum_{i_1=0}^{k} \binom{k}{i_1} (-1)^{i_1} e^{-x} \sum_{i_2=0}^{i_1(l-1)} \varphi_{i_1,i_2}^{k,l} x^{i_2} \tag{E.2}$$

where, in (E.2), we explored the fact that the above $(l-1)$-degree polynomial to the power of i_1 is also a polynomial whose degree is $i_1(l-1)$. The resulting polynomial coefficients are given by

$$\varphi_{i_1,i_2}^{k,l} = \frac{1}{i_2!} \mathcal{D}_x \left[\left(\sum_{i=0}^{l-1} \frac{x^i}{i!} \right)^{i_1} \right]^{(i_2)} \Bigg|_{x=0} . \tag{E.3}$$

In (E.3), $\mathcal{D}_x [.]^{(i_2)}$ denotes the i_2th order derivative operator with respect to x. Hence, (E.3) can alternatively be expressed with the help of [71, 0.314] for $i_1 \in \{0, \ldots, k\}$ and $i_2 \in \{0, \ldots, i_1(l-1)\}$ in the form of the following recursion

$$\begin{cases} \varphi_{i_1,0}^{k,l} = 1 & , i_2 = 0 \\ \varphi_{i_1,i_2}^{k,l} = \dfrac{1}{i_2} \displaystyle\sum_{i_3=1}^{\min(i_2,l-1)} \dfrac{(i_3 i_1 - i_2 + i_3)}{i_3!} \varphi_{i_1,i_2-i_3}^{k,l} & , 1 \leq i_2 \end{cases} \tag{E.4}$$

resulting in (4.25) where $\psi_{i_1,i_2}^{k,l} = \binom{k}{i_1} (-1)^{i_1} \varphi_{i_1,i_2}^{k,l}$.

Appendix F

Derivation of ρ_x^2 and ρ^2

By definition, we have

$$\rho^2 = \frac{E\left[Z^1_{\dot{s}_1} Z^2_{\dot{s}_1,\dot{r}}\right] - \lambda^2_{ps}}{\lambda^2_{ps}}, \tag{F.1}$$

where $Z^1_{\dot{s}_1}$ and $Z^2_{\dot{s}_1,\dot{r}}$ are to be replaced by (4.21) and (4.59), respectively, into (F.1). Then, by carrying the expectation $E\left[Z^1_{\dot{s}_1} Z^2_{\dot{s}_1,\dot{r}}\right]$ firstly over $\boldsymbol{h}^{2,p\to s}$, we get

$$E\left[Z^1_{\dot{s}_1} Z^2_{\dot{s}_1,\dot{r}}\right] = E\left(\frac{Z^{1^2}_{\dot{s}_1} X^1_{\dot{s}_1}}{X^1_{\dot{s}_1} + X_{\dot{r}}} + \frac{\lambda_{ps} Z^1_{\dot{s}_1} X_{\dot{r}}}{X^1_{\dot{s}_1} + X_{\dot{r}}}\right) = \lambda^2_{ps} E\left(\frac{2X^1_{\dot{s}_1} + X_{\dot{r}}}{X^1_{\dot{s}_1} + X_{\dot{r}}}\right) \tag{F.2}$$

where the second line follows from carrying the expectation over $Z^1_{\dot{s}_1}$ in (F.2) recalling that $Z^1_{\dot{s}_1}$ alone is independent of $X^1_{\dot{s}_1}$ and $X_{\dot{r}}$. Hence, we have

$$\rho_x^2 = \frac{x_1}{(x_1 + x_2)} \tag{F.3}$$

and

$$\rho^2 = E\left[\frac{X^1_{\dot{s}_1}}{X^1_{\dot{s}_1} + X_{\dot{r}}}\right] = \int_0^{+\infty}\int_0^{+\infty} \frac{x_1}{x_1 + x_2} f_{X^1_{\dot{s}_1}}(x_1)\, f_{X_{\dot{r}}}(x_2)\, dx_1 dx_2, \tag{F.4}$$

where $f_{X^1_{\dot{s}_1}}(.)$ is given by (4.23) while $f_{X_{\dot{r}}}(.)$ is deduced from (4.23) by replacing s_t and λ_{ss} by r_e and λ_{rs}, respectively.

To calculate ρ^2, we expand both PDFs $f_{X^1_{\dot{s}_1}}(.)$ and $f_{X_{\dot{r}}}(.)$ using Lemma 1 before being substituted in (F.4). Then, with the help of [72, Vol 1: Eq. 3.1.3.5], we end up with (4.65).

Appendix G

Proof of Theorem 2

According to (4.76), $Z^2_{\ddot{s}_1,k}|x,z,v$ can be expanded for $s_r = 1$ as

$$Z^2_{\ddot{s}_1,k}|x,z,v = xz + X_k v + 2\sqrt{xzX_k v}\cos(\Omega) \tag{G.1}$$

where Ω is a random variable that is Uniformally distributed over $\left[-\pi,\pi\right[$. Hence, the derivative of the CDF $F_{\cos(\Omega)}(w) = F_{\Omega}(\arccos(w))$ with respect to w results in

$$f_{\cos(\Omega)}(w) = \begin{cases} \dfrac{1}{\pi\sqrt{1-w^2}};\ -1 < w < 1 \\ 0;\ \text{Otherwise} \end{cases}. \tag{G.2}$$

We deduce that $Z^2_{\ddot{s}_1,k}|x,z,v$ conditioned on $X_k = x_2$ for $k \in \{1,\ldots,r_e\}$ is drawn from the following distribution

$$f_{Z^2_{\ddot{s}_1,k}|x,z,v,x_2}(z_2) = \begin{cases} \dfrac{1}{\pi\sqrt{4xzx_2v - (z_2 - (xz + x_2v))^2}}; \\ \left(\sqrt{xz} - \sqrt{x_2v}\right)^2 < z_2 < \left(\sqrt{xz} + \sqrt{x_2v}\right)^2 \\ 0;\ \text{Otherwise} \end{cases}. \tag{G.3}$$

Since X_k is an Exponential random variable with parameter λ_{rs}, then by applying Bays rule, we obtain (4.77) and conclude with the proof of Theorem 1.

Bibliography

[1] E. Biglieri, R. Calderbank, A. Constantinides, A. Goldsmith, A. Paulraj, H. V. Poor, *MIMO Wireless Communications*, Cambridge University Press, 2007.

[2] H. El Gamal, A. R. Hammons, Y. Liu, M. P. Fitz, and O. Y. Takeshita, "On the design of space–time and space–frequency codes for MIMO frequency-selective fading channels," *IEEE Trans. Info. Theory*, vol. 49, no. 9, pp. 2277-2292, Sep. 2003.

[3] H. El Gamal, G. Caire, and M. O. Damen, "The MIMO ARQ Channel: Diversity-Multiplexing-Delay tradeoff," *IEEE Trans. Info. Theory*, vol. 52, no. 8, pp. 3601-3621, Aug. 2006.

[4] R. U. Nabar, H. Bolcskei, and F. W. Kneubuhler, "Fading relay channels: Performance limits and space-time signal design," *IEEE Journal on Sel. Areas in Comm.*, vol. 22, no. 6, pp. 1099-1109, Aug. 2004.

[5] Y. Fan, C. Wang, J. Thompson, and H.V. Poor, "Recovering multiplexing loss through successive relaying using repetition coding," *IEEE Trans. Wireless Commun.*, vol. 6, no. 12, pp. 4484 - 4493, Dec. 2007.

[6] R. Tannious and A. Nosratinia, "Spectrally efficient relay selection with limited feedback," *IEEE Journal on Sel. Areas in Comm.*, vol. 26, no. 8, pp. 1419-1428, Oct. 2008.

[7] R. Narasimhan, "Throughput-delay performance of half-duplex hybrid-ARQ relay channels," in *Proc. IEEE Intern. Conf. Commun. (ICC)*, Beijing, China, May 2008.

[8] T. Tabet, S. Dusad, and R. Knopp, "Achievable diversity-multiplexing-delay trade-off in half-duplex ARQ relay channels," in *Proc. IEEE ISIT*, Adelaide, Australia, Sep. 2005.

[9] Y. Qi, R. Hoshyar, and R. Tafazolli, "On the performance of HARQ with hybrid relaying schemes," in *Proc. IEEE Intern. Conf. Commun. (ICC)*, Dresden, Germany, Jun. 2009.

[10] H. Mheidat, M. Uysal, and N. Al-Dhahir, "Equalization techniques for distributed space-time block codes with amplify-and-forward relaying," *IEEE Trans. Signal Processing*, vol. 55, pp. 1839-1852, May 2007.

[11] H. Xiong and J. X. P. Wang, "Frequency-domain equalization and diversity combining for demodulate-and-forward cooperative systems," in *Proc. IEEE ICASSP*, Las Vegas, NV, Mar.-Apr. 2008.

[12] H. Chafnaji, T. Ait-Idir, H. Yanikomeroglu, and S. Saoudi, "On the design of turbo packet combining schemes for relay-assisted systems over multi-antenna broadband channels," in *Proc. IEEE Veh. Techn. Conf. (VTC)*, Taipei, Taiwan, May 2010.

[13] T. Ait-Idir, S. Saoudi, "Turbo packet combining strategies for the MIMO-ISI ARQ channel," *IEEE Trans. Comm.*, vol. 57, no. 12, pp. 3782-3793, Dec. 2009.

[14] T. Ait-Idir, H. Chafnaji, and S. Saoudi, "Turbo packet combining for broadband space-time BICM hybrid-ARQ systems with co-channel interference," *IEEE Trans. Wireless Commun.*, vol. 9, no. 5, pp. 1686-1697, May 2010.

[15] P. Kolodzy, "Spectrum policy task force," *Federal Comm. Commission*, Washington, DC, USA, Tech. Rep. ET Docket no. 02-135, Nov. 2002.

[16] J. Mitola and G. Q. Maguire, "Cognitive radio: Making software radios more personal," *IEEE Pers. Comm.*, vol. 6, no. 4, pp. 13–18, Aug. 1999.

[17] A. Glodsmith, S. A. Jafar, I. Marić, and S. Srinivasa, "Breaking spectrum gridlock with cognitive radios: An information theoretic perspective," *Proceedings of the IEEE*, vol. 97, no. 5, pp. 894–914, May 2009.

[18] A. M. Wyglinski, M. Nekovee, T. Hou, *Cognitive Radio Communications and Networks*, Academic Press, 2009.

[19] B. Makki, T. Eriksson, "On the average rate of HARQ-based quasi-static spectrum sharing networks," *IEEE Trans. on Wireless Comm.*, vol. 11, no. 1, pp. 65–77, Jan. 2012.

[20] L. Musavian, T. Le-Ngoc, "Cross-Layer Design for Cognitive Radios with Joint AMC and ARQ Under Delay QoS Constraint," in *Proc. Intern. Wireless Comm. and Mobile Comp. Conf.*, Cyprus, Turkey, Aug. 2012.

[21] G. Zhao, C. Yang, G. Y. Li, D. Li, and A. C. K. Soong, "Power and channel allocation for cooperative relay in cognitive radio networks," *IEEE Journal on Sel. Topics in Sig. Proc.*, vol. 5, no. 1, pp. 151–159, Feb. 2011.

[22] R. Zhang, Y.-C. Liang, "Exploiting multiantennas for opportunistic spectrum sharing in cognitive radio networks," *IEEE Journal on Sel. Topics in Signal Processing*, vol. 2, no. 1, pp. 88–102, Feb. 2008.

[23] H. Wang, J. Lee, S. Kim, and D. Hong, "Capacity enhancement of secondary links through spatial diversity in spectrum sharing," *IEEE Trans. on Wireless Comm.*, vol. 9, no. 2, pp. 494–499, Feb. 2010.

[24] J. Hong, B. Hong, T. W. Ban, and W. Choi, "On the Cooperative Diversity Gain in Underlay Cognitive Radio Systems," *IEEE Trans. on Comm.*, vol. 60, no. 1, pp. 209–219, Jan. 2012.

[25] W. Jaafar, W. Ajib, and D. Haccoun, "A novel relay-aided transmission scheme in cognitive radio networks," in *Proc. IEEE Global Comm. Conf.*, Houston, Texas, USA, Dec. 2011.

[26] J. Si, Z. Li, X. Chen, B. Hao, and Z. Liu, "On the performance of cognitive relay networks under primary user's outage constraint," *IEEE Communications Letters*, vol. 15, no. 4, pp. 422–424, Apr. 2011.

[27] Z. Yan, X. Zhang, and W. Wang, "Exact outage performance of cognitive relay networks with maximum transmit power limits," *IEEE Communications Letters*, vol. 15, no. 12, pp. 1317-1319, Dec. 2011.

[28] K. Tourki, K. A. Qaraqe, and M. Alouini, "Outage Analysis for Underlay Cognitive Networks Using Incremental Regenerative Relaying," *IEEE Trans. on Vehicular Technol.*, vol. 62, no. 2, pp. 721-734, Feb. 2013.

[29] Y. Zou, Y. Yao, and B. Zheng, "Diversity-Multiplexing tradeoff in selective cooperation for cognitive radio," *IEEE Trans. on Comm.*, vol. 60, no. 9, pp. 2467-2481, Sep. 2012.

[30] Z. El-Moutaouakkil, K. Tourki, K. A. Qaraqe, and S. Saoudi, "Exact Outage Probability Analysis for Relay-Aided Underlay Cognitive Communications," in *Proc. IEEE Vehicular Technol. Conf. Fall*, Québec City, Canada, Sep. 2012.

[31] Y. Zou, J. Zhu, B. Zheng, and Y.-D. Yao, "An adaptive cooperation diversity scheme with best-relay selection in cognitive radio networks," *IEEE Trans. on Signal Processing*, vol. 58, no. 10, pp. 5438 –5445, Oct. 2010.

[32] K. J. Kim, T. Q. Duong, and H. V. Poor, "Outage probability of single-carrier cooperative spectrum sharing systems with decode-and-forward relaying and selection combining," *IEEE Trans. on Comm.*, vol. 12, no. 2, pp. 806-817, Feb. 2013.

[33] R. Tannious, A. Nosratinia, "Spectrally-Efficient relay selection with limited feedback," *IEEE Journal on Sel Areas in Comm.*, vol. 26, no. 8, pp. 1419-1428, Oct 2008.

[34] Z. El-Moutaouakkil, K. Tourki, and S. Saoudi, "Spectrally-Efficient SIMO relay-aided underlay communications: An exact outage analysis," in *Proc. IEEE Intern. Conf. on Comm.*, Sydney, Australia, Jun. 2014.

[35] K. Huang, R. Zhang, "Cooperative feedback for multiantenna cognitive radio networks," *IEEE Trans. on Signal Proc*essing, vol. 59, no. 2, pp. 747-758, Feb. 2011.

[36] J. Lui, W. Chen, Z. Cao, and Y. J. Zhang, "Cooperative beamforming for cognitive radio networks: A cross-layer design," *IEEE Trans. on Wireless Comm.*, vol. 60, no. 5, pp. 1420–1431, May 2012.

[37] L. Sboui, H. Ghazzai, Z. Rezki, and M. S. Alouini, "Precoder design and power allocation for MIMO cognitive radio two-way relaying systems," *IEEE Trans. on Comm.*, vol. 64, no. 10, pp. 4111-4120, Oct. 2016.

[38] B. J. Lee, S. L. Ju, N. Kim, and K. S. Kim, "Enhanced transmit-antenna selection schemes for multiuser massive MIMO systems," *Wireless Comm. and Mobile Computing*, vol. 2017, Article ID 3463950, 6 pages, Jun. 2017.

[39] P. L. Yeoh, M. Elkashlan, K. J. Kim, T. Q. Duong, and G. K. Karagiannidis, "Transmit antenna selection in cognitive MIMO relaying with multiple primary transceivers," *IEEE Trans. on Veh. Tech.*, vol. 65, no. 1, pp. 483-489, Jan. 2016.

[40] P. L. Yeoh, M. Elkashlan, T. Q. Duong, N. Yang, and D. B. da Costa, "Transmit antenna selection for interference management in cognitive relay networks," *IEEE Trans. on Veh. Tech.*, vol. 63, no. 7, pp. 3250-3262, Sep. 2014.

[41] F. S. Al-Qahtani, R. M. Radaydeh, S. Hessien, T. Q. Duong, and H. Alnuweiri, "Underlay cognitive multihop MIMO networks with and without receive interference cancellation," *IEEE Trans. on Comm.*, vol. 65, no. 4, pp. 1477-1493, Apr. 2017.

[42] E. Erdogan, A. Afana, S. Ikki, and H. Yanikomeroglu, "Antenna selection in MIMO cognitive AF relay networks with mutual interference and limited feedback," *IEEE Comm. Letters*, vol. 21, no. 5, pp. 1111-1114, May 2017.

[43] K. Tourki, F. A. Khan, K. A. Qaraqe, H. C. Yang, and M. S. Alouini, "Exact performance analysis of MIMO cognitive radio systems using transmit antenna selection," *IEEE Journal on Sel. Areas in Comm.*, vol. 32, no. 3, pp. 425-438, Mar. 2014.

[44] F. A. Khan, K. Tourki, M. S. Alouini, and K. A. Qaraqe, "Performance analysis of a power limited spectrum sharing system with TAS/MRC," *IEEE Trans. on Signal Processing*, vol. 62, no. 4, pp. 954-967, Feb. 2014.

[45] M. Hanif, H. C. Yang, and M. S. Alouini, "Transmit antenna selection for power adaptive underlay cognitive radio with instantaneous interference constraint," *IEEE Trans. on Comm.*, vol. 65, no. 6, pp. 2357-2367, Jun. 2017.

[46] R. M. Radaydeh, "SNR and SINR-based selection combining algorithms in the presence of arbitrarily distributed co-channel interferers," *IET Comm.*, vol. 3, no. 1, pp. 57-66, Jan. 2009.

[47] R. M. Radaydeh, M. S. Alouini, "On the performance of arbitrary transmit selection for threshold-based receive MRC with and without co-channel interference," *IEEE Trans. on Comm.*, vol. 59, no. 11, pp. 3177-3191, Nov. 2011.

[48] A. A. AbdelNabi, F. S. Al-Qahtani, M. Shaqfeh, S. S. Ikki, and H. M. Alnuweiri, "Performance analysis of MIMO multi-hop system with TAS/MRC in poisson field of interferers," *IEEE Trans. on Comm.*, vol. 64, no. 2, pp. 525-540, Feb. 2016.

[49] A. A. AbdelNabi, F. S. Al-Qahtani, R. M. Radaydeh, and M. Shaqfeh, "Hybrid access femtocells in overlaid MIMO cellular networks with transmit selection under poisson field interference," *IEEE Trans. on Comm.*, no. 99, Sep. 2017.

[50] A. M. Tonello, "MIMO MAP equalization and turbo decoding in interleaved space-time coded systems," *IEEE Trans. Commun.*, vol. 51, pp. 155–160, Feb. 2003.

[51] H. Chafnaji, T. Ait-Idir, H. Yanikomeroglu, and S. Saoudi, "On the design of turbo packet combining schemes for relay-assisted systems over multi-antenna broadband channels," in *Proc. IEEE VTC Spring*, Taipei, Taiwan, May 2010.

[52] T. Ait-Idir and S. Saoudi, "Turbo packet combining strategies for the MIMO-ISI ARQ channel," *IEEE Trans. Commun.*, vol. 57 , no. 12, pp. 3782–3793, Dec. 2009.

[53] R.Visoz, A.O. Berthet, and S. Chtourou, "A new class of iterative equalizers for space-time BICM over MIMO block fading ISI AWGN channel," *IEEE Trans. Commun*, vol. 53, no. 12, pp. 2076-2091, Dec. 2005.

[54] Z. Zhang, T. M. Duman, and E. M. Kurtas, "Achievable information rates and coding for MIMO systems over ISI channels and frequency-selective fading channels," *IEEE Trans. Commun.*, vol. 52, no. 10, pp. 1698–1710, Oct. 2004.

[55] R. Wolff, *Stochastic Modeling and the Theory of Queues*, Upper Saddle River, NJ: Prentice-Hall, 1989.

[56] D. Tse and P. Viswanath, *Fundamentals of Wireless Communication,* Cambridge University Press, May 2005.

[57] G. Caire and D. Tuninetti, "The throughput of hybrid-ARQ protocols for the Gaussian collision channel," *IEEE Trans. Info. Theory*, vol. 47, no. 5, pp. 1971-1988, Jul. 2001.

[58] J. N. Laneman, G. W. Wornell, and D. N. C. Tse, "An efficient protocol for realizing cooperative diversity in wireless networks," in *Proc. IEEE ISIT*, Washington, DC, Jun. 2001.

[59] A. Sendonaris, E. Erkip, and B. Aazhang, "User cooperation diversity – Part I & Part II," *IEEE Trans. Commun.*, vol. 51, pp. 1927-1948, Nov. 2003.

[60] R. U. Nabar, H. Bolcskei, and F. W. Kneubuhler, "Fading relay channels: performance limits and space-time signal design," *IEEE Journal Select. Areas in Commun.*, vol. 22, no. 6, pp. 1099-1109, Aug. 2004.

[61] Z. El-Moutaouakkil, T. Ait-Idir, H. Yanikomeroglu, and S. Saoudi, "Relay ARQ strategies for single carrier MIMO broadband amplify-and-forward cooperative transmission," in *Proc. IEEE PIMRC*, Istanbul, Turkey, Sep. 2010.

[62] H. Chafnaji, H. Yanikomeroglu, T. Ait-Idir, and S. Saoudi, "Turbo packet combining techniques for multi-relay-assisted systems over multi-antenna broadband channels," in *Proc. ACM IWCMC*, Caen, France, Jun. 2010.

[63] A. Glodsmith, S. A. Jafar, I. Marić, and S. Srinivasa, "Breaking spectrum gridlock with cognitive radios: An information theoretic perspective," *Proceedings of the IEEE*, vol. 97, no. 5, pp. 894–914, May 2009.

[64] H. C. Yang and M. S. Alouini, "Outage probability of dual-branch diversity systems in presence of co-channel interference," *IEEE Trans. on Wireless Comm.*, vol. 2, no. 2, pp. 310-319, March 2003.

[65] A. Shah and A. M. Haimovich, "Performance analysis of maximal ratio combining and comparison with optimum combining for mobile radio communications with cochannel Interference," *IEEE Trans. on Vehicular Technol.*, vol. 49, no. 4, pp. 1417-1425, Aug. 2004.

[66] R. K. Mallik, "On multivariate rayleigh and exponential distributions," *IEEE Trans. on Inf. Theory*, vol. 49, no. 6, pp 1499 - 1515, Jun. 2003.

[67] R. Tannious and A. Nosratinia, "Spectrally-efficient relay selection with limited feedback," *IEEE Journal on Sel. Areas in Comm.*, vol. 26, no. 8, pp. 1419-1428, Oct. 2008.

[68] N. B. Mehta, S. Kashyap, and A. F. Molisch, "Antenna selection in LTE: from motivation to specification," *IEEE Comm. Mag.*, vol. 50, no. 10, pp. 144-150, October 2012.

[69] P. V. Amadori and C. Masouros, "Large scale antenna selection and precoding for interference exploitation," *IEEE Trans. on Comm.*, vol. 65, no. 10, pp. 4529-4542, Oct. 2017.

[70] J. Hong, B. Hong, T. W. Ban, and W. Choi, "On the cooperative diversity gain in underlay cognitive radio systems," *IEEE Trans. on Comm*, vol. 60, no. 1, pp. 209–219, Jan. 2012.

[71] I. S. Gradshteyn and I. M. Ryzhik, *Table of Integrals, Series, and Products*, 7th ed. San Diego, CA: Academic, 2007.

[72] A. P. Prudnikov, Y. A. Brychkov, and O. I. Marichev, *Integrals and Series*. New York: Gordon and Breach Science, 1986.

[73] A. T. McKay, "Sampling from batches," *Journal of the Royal Statistical Society*—Supplement 1, 1934, 207–216.

[74] http://functions.wolfram.com/HypergeometricFunctions/HypergeometricU/

[75] R. Visoz, A. O. Berthet, and S. Chtourou, "Frequency domain block turbo equalization for single carrier transmission over MIMO broadband wireless channel," *IEEE Trans. Commun.*, vol. 54, no. 12, Dec. 2006.

[76] S. Haykin, *Adaptive Filter Theory,* 3rd Ed. Upper Saddle River, NJ: Prentice-Hall, 1996.

[77] J. N. Laneman, G. W. Wornell, and D. N. C. Tse, "An efficient protocol for realizing cooperative diversity in wireless networks," in *Proc. IEEE Intern. Symp. Info. Theory (ISIT)*, Washington, DC, Jun. 2001.

[78] A. Sendonaris, E. Erkip, and B. Aazhang, "User cooperation diversity – Part I & Part II," *IEEE Trans. Commun.*, vol. 51, pp. 1927-1948, Nov. 2003.

[79] E. Zimmermann, P. Herhold, and G. Fettweis, "The impact of cooperation on diversity-exploiting protocols," in *Proc. IEEE Veh. Techn. Conf. (VTC)*, Milan, Italy, May 2004.

[80] K. Azarian, H. El Gamal, and P. Schniter, "On the achievable diversity-multiplexing trade-off in half-duplex cooperative channels," *IEEE Trans. Info. Theory*, vol. 51, pp. 4152-4172, Dec. 2005.

[81] J. Boyer, D. D. Falconer, and H. Yanikomeroglu, "Multihop diversity in wireless relaying channels," *IEEE Trans. Commun.*, vol. 52, pp. 1820- 1830, Oct. 2004.

[82] J. N. Laneman, D. Tse, and G. W. Wornell, "Cooperative diversity in wireless networks: Efficient protocols and outage behavior," *IEEE Trans. Info. Theory*, vol. 50, no. 12, pp. 3062-3080, Dec. 2004.

[83] G. Yu, Z. Zhang, and P. Qiu, "Cooperative ARQ in wireless networks: Protocols description and performance analysis," in *Proc. IEEE Intern. Conf. Commun. (ICC)*, Istanbul, Turkey, Jun. 2006.

[84] F. Atay Onat, H. Yanikomeroglu, and S. Periyalwar, "Relay-assisted spatial multiplexing in wireless fixed relay networks," in *Proc. IEEE GLOBECOM*, San Francisco, USA, Nov.- Dec. 2006.

[85] J. Lee, H.Wang, J. G. Andrews, and D. Hong, "Outage probability of cognitive relay networks with interference constraints," *IEEE Trans. on Wireless Communications*, vol. 10, no. 2, pp. 390–395, Feb. 2011.

[86] L. Luo, P. Zhang, G. Zhang, and J. Qin, "Outage performance for cognitive relay networks with underlay spectrum sharing," *IEEE Communications Letters*, vol. 15, no. 7, pp. 710–712, Jul. 2011.

[87] H. Ding, J. Ge, D. B. da Costa, and Z. Jiang, "Asymptotic analysis of cooperative diversity systems with relay selection in a spectrum-sharing scenario," *IEEE Trans. on Vehicular Technology*, vol. 60, no. 2, pp. 457–472, Feb. 2011.

[88] T. Q. Duong, V. N. Q. Bao, and H. J. Zepernick, "Exact outage probability of cognitive AF relaying with underlay spectrum sharing," *Electronics Letters*, vol. 47, no. 17, Aug. 2011.

[89] S. Ikki, M. Uysal, and M. H. Ahmed, "Performance analysis of incremental-best-relay amplify-and-forward technique," in *Proc. IEEE Global Commun. Conf.*, Honolulu, Hawaii, USA, Dec. 2009.

[90] A. Bletsas, A. Khisti, D. P. Reed, and A. Lippman, "A simple cooperative diversity method based on network path selection," *IEEE Journal on Selected Areas in Communications*, vol. 24, no. 3, pp. 659–672, Mar. 2006.

[91] P. J. Smith, P. A. Dmochowski, H. A. Suraweera, and M. Shafi, "The effects of limited channel knowledge on cognitive radio system capacity," *IEEE Trans. on Vehicular Technol.*, vol. 62, no. 2, pp. 927-933, Feb 2013.

UNIVERSITE BRETAGNE LOIRE / MATHSTIC

IMT Atlantique
Bretagne-Pays de la Loire
École Mines-Télécom

Titre : Le Relayage MIMO Cognitif à Grande Efficacité Spectrale : Une Perspective de Design Pratique

Mots clés : Radio cognitive, MIMO, relayage, TAS, MRC

Résumé : Le relayage cognitif *multiple-input multiple-output* (MIMO) hérite l'efficacité spectrale de la radio cognitive et les systèmes de relayage MIMO, apportant ainsi des gains prometteurs en termes de débit de données et de fiabilité pour les futures communications sans fil et mobiles. Dans cette thèse, nous concevons et évaluons des schémas pratiques d'émetteurs et de récepteurs pour des systèmes de relayage MIMO cognitifs qui peuvent être mis en œuvre à moindre coût. Tout d'abord, nous réduisons l'affaiblissement du débit du mode half-duplex du relayage MIMO *amplify-and-forward non-orthogonale* (NAF) large bande avec demande de répétition automatique (ARQ). Différemment des travaux de recherche existants, le protocole de relayage proposé ne nécessite que la durée de transmission d'un seul paquet sur des canaux sélectifs en fréquence. De plus, nous proposons une conception de réception itérative à complexité réduite pour cette classe de protocoles, entraînant ainsi une amélioration significative des performances de transmission de bout-en-bout.

Deuxièmement, nous nous concentrons sur les systèmes de relayage cognitive de partage du spectre *single-input multiple-output* (SIMO) et évaluons l'impact des contraintes d'interférence instantanée et statistique sur la qualité de leur probabilité de coupure. Nos résultats révèlent que l'imposition d'une contrainte statistique sur la puissance d'émission du système secondaire est plus favorable que son adversaire consommatrice de spectre. Troisièmement, nous capitalisons sur notre deuxième contribution pour étudier les systèmes de relayage MIMO *decode-and-forward* (DF) cognitifs utilisant la sélection d'antenne à l'émission (TAS) ainsi que le *maximum-ratio combining* (MRC) à la réception. Basés sur la maximisation du rapport signal-sur-bruit (SNR) ou du rapport signal-sur-interférence-plus-bruit (SINR), nos résultats de probabilité de coupure nouvellement dérivés pour les deux stratégies proposées de TAS démontre l'optimalité du système de sélection d'antenne basé sur le SINR par rapport aux effets néfastes d'interférence mutuelle dans les systèmes de relayage MIMO DF cognitifs.

Title : Spectrum-Efficient Cognitive MIMO Relay Systems: A Practical Design Perspective

Keywords : Cognitive radio, MIMO, Rlaying, TAS, MRC, SINR

Abstract : Cognitive multiple-input multiple-output (MIMO) relaying inherits the spectrum usage efficiency from both cognitive radio and MIMO relay systems, thereby bearing promising gains in terms of data rate and reliability for future wireless and mobile communications. In this dissertation, we design and evaluate practical transmitter and receiver schemes for cognitive MIMO relay systems that can readily be implemented at a lower cost. First, we reduce the multiplexing loss due the half-duplex operation in non-orthogonal amplify-and-forward (NAF) MIMO relay broadband transmissions with automatic repeat request (ARQ). Different from existing research works, the proposed relaying protocol requires only one packet duration to operate over frequency-selective block-fading relay channels. Further, we propose a low-complexity iterative receiver design for this class of protocols which results in significant enhancement of the end-to-end transmission performance.

Second, we focus on cognitive underlay single-input multiple-output (SIMO) relay systems and evaluate the impact of instantaneous and statistical interference constraints on their outage performance. Our results reveal that imposing a statistical interference constraint on the secondary system transmit power is most favored than its spectrum-consuming counterpart. Third, we capitalize on our second contribution to investigate cost-effective transmission schemes for cognitive MIMO decode-and-forward (DF) relaying systems employing transmit-antenna selection (TAS) along with maximum-ratio combining (MRC) at the transmitter and receiver sides, respectively. Driven by maximizing either the received signal-to-noise ratio (SNR) or signal-to-interference-plus-noise ratio (SINR), our newly derived outage performance results pertaining to both proposed TAS strategies are shown to entail an involved derivation roadmap yet demonstrate the optimality of the SINR-driven TAS against the detrimental effect of mutual interference in cognitive MIMO DF relay systems.